# IS EMBEDDING THE REACTOR BUILDING BELOW GRADE A COST-EFFECTIVE PROPOSITION?

By

Enrique Velez

Ingeniería Industrial Superior, Universidad Pontificia de Comillas (ICAI), 2012
Master's Degree in Numerical Simulation in Engineering with ANSYS, Universidad Politécnica de Madrid, 2018

Submitted to the Department of Nuclear Science and Engineering & the Department of Civil and Environmental Engineering in partial fulfillment of the requirements for the Degrees

of

Masters of Science in Nuclear Science and Engineering &
Masters of Engineering in Civil and Environmental Engineering

at the

Massachusetts Institute of Technology

February 2020



Signature of author: _____

Enrique Velez
Department of Nuclear Science and Engineering, MIT
Department of Civil and Environmental Engineering, MIT
Jan 15, 2020

Certified by: _____

Herbert Einstein
Professor of Civil and Environmental Engineering, MIT
Thesis Supervisor

Certified by: _____

Jacopo Buongiorno
TEPCO Professor of Nuclear Science and Engineering, MIT
Director, Center for Advanced Nuclear Energy Systems (CANES)
Thesis Supervisor

Accepted by: _____

Ju Li
Battelle Energy Alliance Professor of Nuclear Science and Engineering, MIT
Professor of Materials Science and Engineering, MIT
Chair, Department Committee on Graduate Students

Accepted by: _____

Colette L. Heald
Professor of Civil and Environmental Engineering
Chair, Graduate Program Committee

# IS EMBEDDING THE REACTOR BUILDING BELOW GRADE A COST-EFFECTIVE PROPOSITION?

by
Enrique Velez

Submitted to the Department of Nuclear Science and Engineering &
the Department of Civil and Environmental Engineering
on Jan 15, 2020, in partial fulfillment of the
requirements for the Degrees of
Masters of Science in Nuclear Science and Engineering &
Masters of Engineering in Civil and Environmental Engineering

## Abstract

The construction cost of reactor buildings has escalated substantially over time primarily for three reasons. First, new safety requirements, such as the post-9/11 airplane crash measures, have been imposed. Second, labor rates for construction workers and the cost of raw materials such as steel for rebar and cement for concrete have increased. Third, the deployment of new plant designs, such as AP1000 (Advanced Pressurized 1000 MWe Reactor) and EPR (European Pressurized Reactor), has been plagued by first-of-a-kind challenges and a general loss of construction know-how by the nuclear industry in the U.S and Western Europe. Embedding the reactor building below grade is a potential approach to reducing the construction cost of new plants, be they large LWRs (Light Water Reactors), SMRs (Small Modular Reactors) or Generation-IV designs. There are important trade-offs. Embedment of a reactor building requires a much larger excavation effort than is necessary for above-grade plants. However, embedded buildings have lower loads during an earthquake or an airplane crash, thus requiring a lot less reinforcement. The cost of the building itself can therefore be significantly lower. In this thesis we analyze various modularized, silo-type reactor buildings (i.e., the type used, for example, in GEH's (General Electric Hitachi) BWRX-300 (Boiling Water Reactor X-300) design) for a set of reference seismic loads at sites with both soil and rock stratigraphy. The comparison includes a completely embedded design, a partially-embedded design and an above-ground design. The level of reinforcement required is determined from FEM (Finite Element Method) analysis of the building, and the cost of constructing the buildings is estimated from productivity data, labor rates and materials costs obtained from industry sources. This leads to the finding that there are some building layouts and sites where there is a potential cost reduction in embedment.

Thesis Supervisor: Jacopo Buongiorno
TEPCO Professor of Nuclear Science and Engineering, MIT
Director, Center for Advanced Nuclear Energy Systems (CANES)

Thesis Supervisor: Herbert Einstein
Professor of Civil and Environmental Engineering, MIT

# 1. FRONT MATTER

## 1.1 ACKNOWLEDGEMENTS, DISCLAIMERS, AND CONTENTS

### 1.1.1 Acknowledgements

I would like to thank professor Einstein for his limitless support to all my undertakings, his care and his advice. I would particularly like to thank him and Nestor Sepulveda for putting me in touch with professor Buongiorno.

Special thanks to professor Buongiorno for accepting to supervise this thesis from the Nuclear side, his supportiveness, patience, and for including me in his group. His vision-driven stands towards what he does inspires me and others around him. I would also like to thank professor Shirvan for his support, trust and advice.

I would like to thank the rest of the group meeting weekly for discussing advanced, micro and small modular reactors issues: professor Baglietto, professor Driscoll, Dr Forsberg and William Robb Stewart.

Thanks to Kennard Johnston for his contribution to this work, and Electricité de France for the financial support.

To my parents and brother.

### 1.1.2 Disclaimer

The views expressed in this thesis are those of the author, and do not necessarily reflect the policy or position of any affiliated parties. And though great care has been taken to make the estimates presented herein as factual as possible, there is no explicit or implicit guarantee to their accuracy or suitability.

TABLE OF CONTENTS

### 1.1.4 List of Figures

### 1.1.3 List of Tables

### 1.1.4 Abbreviations

| | |
|---|---|
| ACI | American Concrete Institute |
| AG | Above Ground or Semi-embedded |
| AP1000 | Advanced Pressurized 1000 MWe Reactor |
| ASCE | American Society of Civil Engineers |
| BDC | Beyond Design Condition |
| BG | Below Ground or Embedded |
| BWR | Boiling Water Reactor |
| DBA | Design Basis Accident |
| ESBWR | Economic Simplified Boiling Water Reactor |
| EW | East-West |
| EPR | European Pressurized Reactor |
| FEM | Finite Element Method |
| FEA | Finite Element Analysis |
| FRS | Floor Response Spectra |
| FSI | Fluid Structure Interaction |
| KK | Kashiwazaki-Kariwa |
| LOCA | Loss Of Coolant Accident |
| LWR | Light Water Reactor |
| NEI | Nuclear Energy Institute |
| NOC | Normal Operation Condition |
| NPP | Nuclear Power Plant |
| OBE | Operational Basis Earthquake |
| RB | Reactor Building |
| SMR | Small Modular Reactor |
| PWR | Pressurized Water Reactor |
| SSE | Safety Shutdown Earthquake (Design Earthquake) |
| SSI | Soil Structure Interaction |
| UG | Under Ground or embedded |

## 2. INTRODUCTION

While nuclear energy contributes significantly to the reduction of carbon emissions in electricity production[1], the nuclear sector has been stagnating for almost a decade. The Fukushima accident in 2011 has tarnished the safety record of the nuclear industry. It has also resulted in additional regulatory requirements that have complicated and increased the cost of new reactor designs such as EPR and AP1000. In particular, civil works and site preparation costs have escalated due to (i) new safety requirements, such as the post-9/11 airplane crash measures, (ii) higher labor rates for construction workers and the cost of raw materials such as steel for rebar and cement for concrete, and (iii) the deployment of new plant designs, such as AP1000 and EPR, which has been plagued by first-of-a-kind challenges and a general loss of construction know-how by the nuclear industry in the U.S and Western Europe. Increased costs together with the public opposition to nuclear in some countries have hindered growth of the nuclear sector.

The small modular reactors (SMRs) have gained considerable attention in the recent decade, partly due to potential to address the mentioned issues with GW-sized reactors. SMRs generally require smaller construction teams and thus reduce the risk and potential delays in construction for the utilities. In this paper we explore the adoption of reactor building embedment as a way to reduce cost and increase robustness of future SMRs. Several NPPs were built underground in the past, e.g. Chooz, Halden, Agesta and Lucens. Lucens underwent a LOCA accident that resulted in a core meltdown without casualties[2], which is a clear example of fail-safe design. The porous concrete lining the reactor cavity, whose main function was groundwater drainage, created a gas distribution effect during the overpressure accident. Due to this condition, gas could flow gradually into the high-porosity and low-permeability rock. Consequently, filters placed before the porous concrete succeeded to provide the filtration of particulate contaminants. Siting NPPs underground affords several potential gains. They are better protected against sabotage. They are more resistant to airplane crashes and missiles. Their seismic response is generally more benign. There is an additional barrier between the containment and the atmosphere, reducing the likelihood of radiological release. On the other hand, the main drawbacks of underground NPPs have historically been the associated costs of excavation, site preparation, constraints on construction and operation.

There are three types of underground siting concepts: structures built at ground level and backfilled, cut and cover excavation, and deep in-rock siting[3]. Figure 1 illustrates these general concepts. The type of embedment herein studied is the second one, cut-and-cover, where the “cover” function is not performed by backfill soil, but rather a concrete shield. We assume that the top of the embedded reactor building is at grade level.

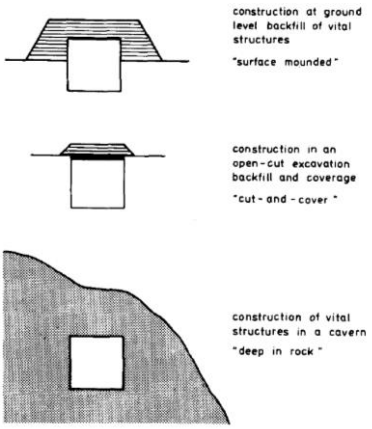


Figure 1. Underground siting types [3]

The goal of this study is to determine if there are sites where there is potential for a clear cost reduction through embedment. To that end, different designs at different sites are evaluated. Firstly, a notional reactor building design is produced, for a specific site in Japan, whose feasibility should be within reach of existing excavation technology, e.g., the Herrenknechkt vertical drilling machine. This building has its external wall sized for an

embedded and semi-embedded configuration. The difference in cost between both cases are evaluated. Then a building like the BWRX-300 [4] reactor building preliminary design, at generic rock and soil sites, has its external wall sized in embedded and semi-embedded configurations. As the BWRX-300 building is cylindrical, equivalent prismatic reactor buildings with equivalent perimeter or volume are assessed. Chapters 3 to 5 cover respectively the literature review, methodology and cost items identification for both, the BWRX-300 and the notional embedded reactor. Chapters 6 to 11 cover the design and cost comparison of the building for the reactor adapted to requirements, from now on, the building point design, i.e., the NuScale reactor. Chapters 12 to 16 cover the design and cost comparison for the BWRX-300 building. Chapter 17 states the conclusions.

## 2.1 BUILDING POINT DESIGN: NUSCALE

This reactor is to be sited in Kashiwazaki-Kariwa in Japan. The selection of a NPP technology is subordinated to the maximum excavation size that can be accomplished without escalating cost. This size has been estimated to be 18 meter in diameter, since the Herrenknechkt catalogue shows a maximum diameter of 16 m for its Vertical Shaft Sinking Machine[5]. As the size is the limiting factor, the reactor technology selected for this study is the Light Water Small Modular Reactor that is currently under development by NuScale [6]. Figure 2 shows the NuScale reactor vessel, its internals and its containment vessel. All the components of the primary system, including the core and the steam generator are inside the reactor vessel.

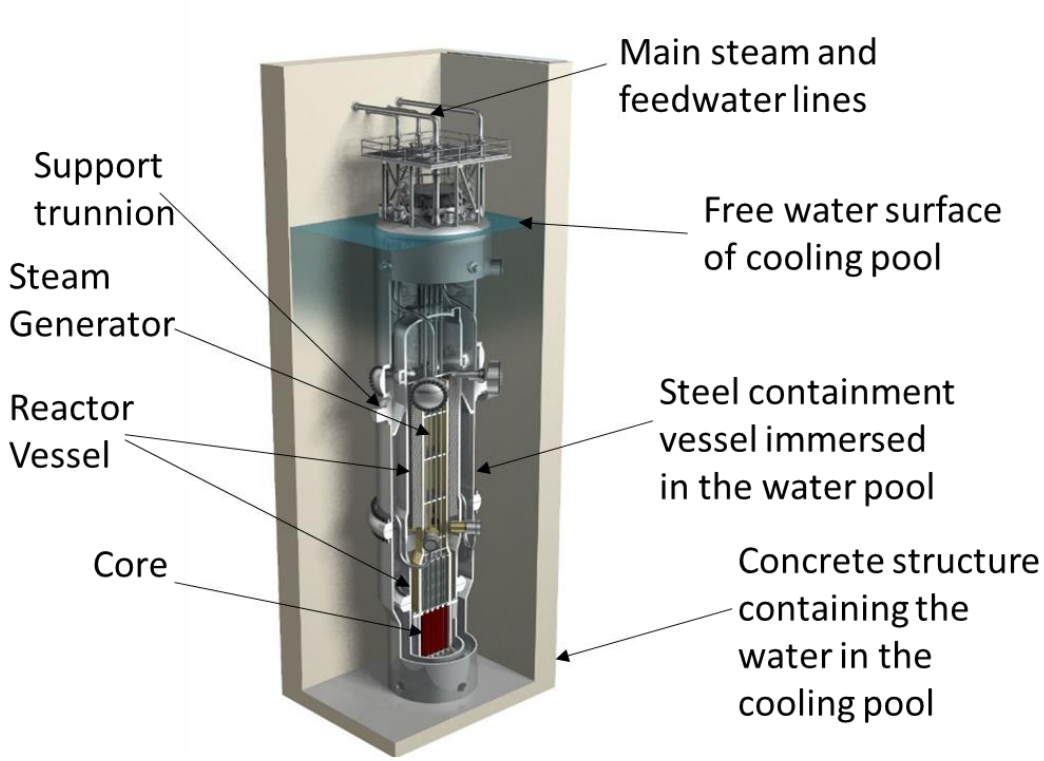


Figure 2. NuScale Reactor. Integral reactor submerged in a cooling pool.

Since the NuScale technology has an integrated steel containment vessel, the reactor building is expected to have lower design requirements regarding radiological release protection than traditional ones. However, given the high seismicity of the country wherein the reactor is to be installed, the ductility demand is high. Therefore, reinforced concrete is selected for the design of the reactor building. Although the functions of the reactor building do not correspond to those of a classical containment (it does not need to withstand pressure or prevent fission product release), from now on it will be referred to interchangeably as the “containment”, “partially/totally embedded containment” or “reactor building”. The steel boundary enveloping the reactor vessel, shown in Figure 2, will be referred to as the “containment vessel”.

Figure 3 shows both reactor buildings, the partially embedded one and the totally embedded one. The basic sizes of the reactor buildings are identical for both options: a cylindrical reinforced concrete structure enclosed by a hemispherical head above and by a flat basemat below. The reactor is inside a pool of water at atmospheric pressure that, in case of accident, removes the decay heat, reaching its boiling point [6]. An internal carbon steel liner provides leak tightness for keeping the water inside the building. The hemispherical head itself is a lid for introducing equipment and for long maintenance operations. It has a small entry inserted in it, for more recurrent operations. The reactor vessel and all the systems accounting for a significant portion of the equipment inside the building are supported on a series of concrete structures. These concrete structures are connected to the basemat. Pile foundations anchor the basemat to bedrock, 70 m below ground level.

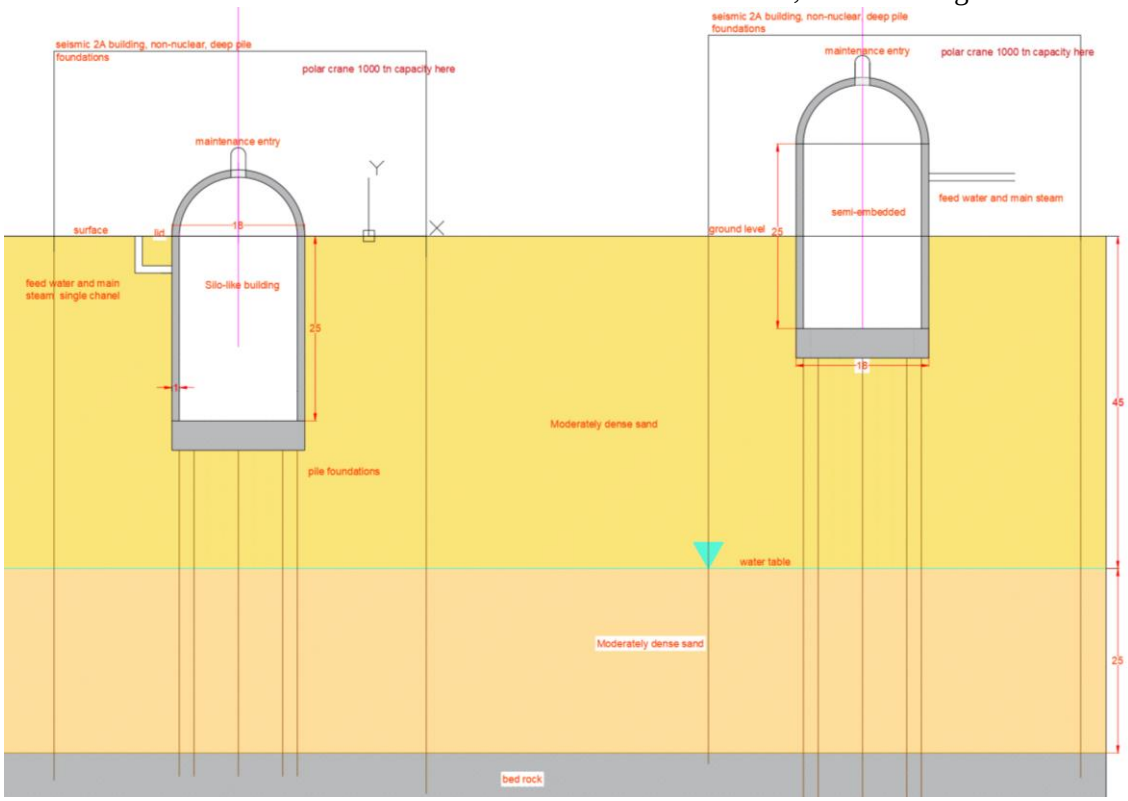


Figure 3. Reactor Building, left, embedded and right, semi-embedded

## 2.2 BWRX-300 AND PRISMATIC EQUIVALENT

The BWRX-300 is a SMR evolved from the ESBWR in design by General Electric Hitachi inc. A single reactor per building is envisioned. Figure 4 shows a preliminary representation of the reactor module and the maintenance building atop. In this work, we compare the construction cost of the external wall in this building at different degrees of embedment, for a rock and a soil site defined in the AP1000 design control document[7].

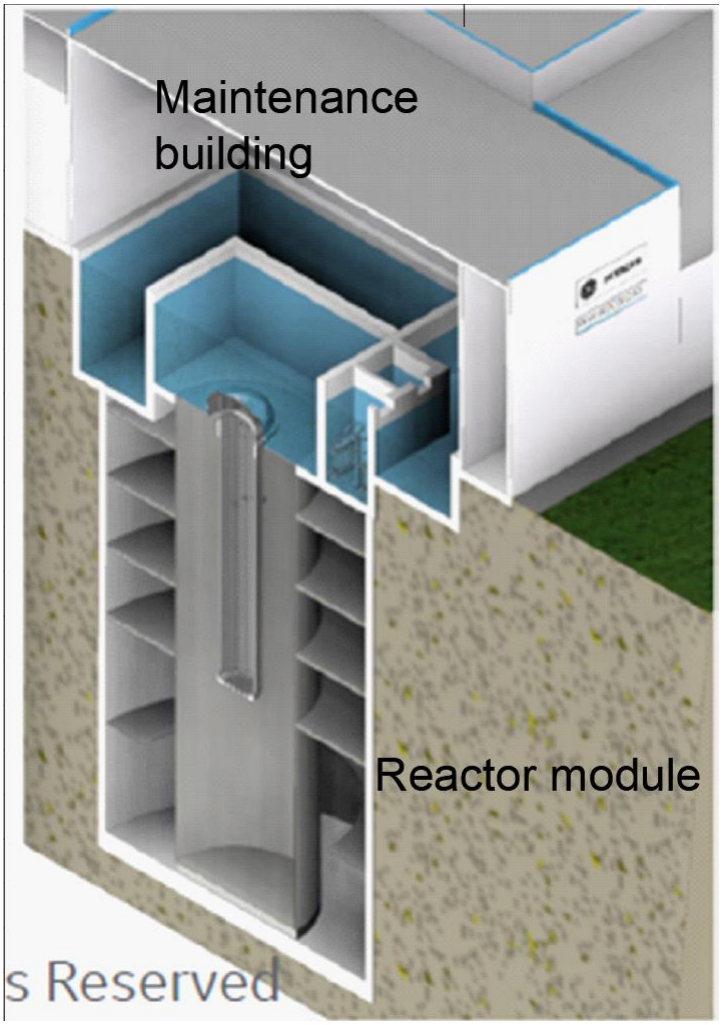


Figure 4. Reactor building BWRX-300, maintenance building on top and reactor module at the bottom**[4]**

This work relates the BWRX-300 building to a prismatic building with the same volume and a prismatic building with the same perimeter, which could host either a PWR or a BWR with similar power. The equal volume assumes components will fill the same space, but as the PWR vessels are smaller in diameter, another case where the equivalence is in perimeter, not in volume, is examined. Equal volume leads to a side of about 17.75m and equal perimeter to a side of about 15.75m. One is about 13% larger than the other.

On the other hand, it makes sense to compare the equal perimeter case, from a civil perspective, to have the same external surface area as that of the BWRX-300 building, so a higher minimum quantity of concrete is not imposed, since the same minimum thickness applies to all of them. The wall thickness is also limited to 0.4 m and no minimum concrete reinforcement is imposed.

# 3. LITERATURE REVIEW

## 3.1 IN-CAVERN SITING

The main projects completed thus far for civil (i.e., non-military) purposes are Halden in Norway, Agesta in Sweden, Lucens in Switzerland and Chooz in France. The Zheleznogorsk plant in Russia or the 816 Underground Nuclear Project in China, were conceived for military uses. The latter was not completed. Lucens underwent a core meltdown accident and it was decommissioned. Lucens brings about valuable lessons for conceiving future underground projects in a sensible manner. Other projects never advanced from the design phase, such as the Ontario Hydro, or the California Energy commission projects.

Table 1 compiles data from Halden in Norway, Agesta in Sweden, Lucens in Switzerland and Chooz in France [8] [2] [3]. It contains the rock type in which they were excavated, dimensions of the caverns, excavation volume, time to completion, civil works cost percentage, and design features concerning the interface. There are small discrepancies between the three sources of information Table 1 is based on, in some of the fields. The dimensions of the caverns vary slightly from one source to another.

Table 1. Characteristics of Chooz, Agesta, Lucens and Halden projects

| | | | | | | Dimensions (m) | | | | Power | | | |
|---|---|---|---|---|---|---|---|---|---|---|---|---|---|
| Year | Name | Country | Rock type | Rock Cover (m) | Water source | Reactor Cavern (m) | Other Caverns (m) | Excavation volume total/reactor cavern ($m^3$) | Time to first criticallity/ to completion of civil works (months) | MWe | MWth | civil engineering work cost (% of total cost) | Design |
| 1968 | Chooz | France | Schist (chalk and shale [8]) | 80 | Meuse | 18.5x41x42 | 15x42x49 | 85,000 / 36,000 | 56 / 36 | 305 | 905 | 20 | nuclear auxiliaries in caverns, steel liner, concrete back-filling |
| 1968 | Lucens | Switzerland | Molasse | about 20 | Brook | dia. 18 height 30 | 51x10x18 / 37.5x5.5x15 | ? / 6,300 | 52 / ? | 10 [2] | 30 | | two layers of concrete, foil and bitumen seal |
| 1964 | Halden | Norway | Granite (and Gneiss [8]) | about 50 | River | 10x30x26 | - | 8,900 / 5,600 | 43 / 23 | 6 | 20 [3] | 10.5 | 15-30 cm thick painted concrete lining |
| 1967 | Agesta | Sweden | Granite (and Gneiss [8]) | about 20 | Lake | 16.5x53x40 | - | 60,000 / 30,000 | 60 / 26 | 20 | 60 [3] | 17.5 | 4-8 mm steel plates for leak-tightness, concrete back filling |

The Halden cavern is not leak-tight. There are cracks between the reactor hall and the access tunnel caused by blasting during the excavation phase [8]. In this case, the width of the reactor cavern was limited by the quality of the rock wherein it was sited. There are fissures distributed along the rock, filled by stone powder and chloritic material, formed by the leaching of Gneiss [8]. Likewise, the rock quality limited the size of the Agesta reactor hall. This reactor was decommissioned in 1974 [8]. However, the Chooz reactor was not limited by the rock quality, but by the size of the equipment to be installed. It is deduced from Table 1 that the Chooz caverns were larger than the other three Nuclear Power Plant caverns. Figure 5 shows the Chooz caverns. Chooz was equipped with two drainage systems consisting of vertical channels and a collecting gallery for relieving hydrostatic pressure on the liner [8].

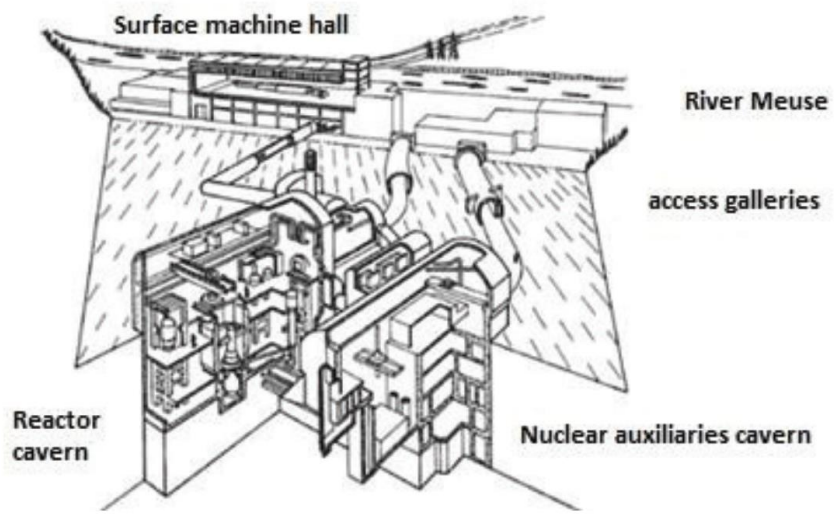


Figure 5. Chooz NPP [2]

From Table 1 it follows that there is not a strong relation between excavation size and time to completion [8]. There must be therefore other parameters, such as rock quality, type or project-specific issues, that contribute to define the time of excavation.

The four reactors, except Lucens, were sited inside crystalline rock [2]. Lucens, whose reactor cavern is shown in Figure 6, was sited in a clayey sedimentary sandstone strata. It was also the only cylindrically-shaped one among them [2]. All others had a rectangularly-shaped base [2]. The four designs are walled, separating the internal components from the rock in which the caverns sit.

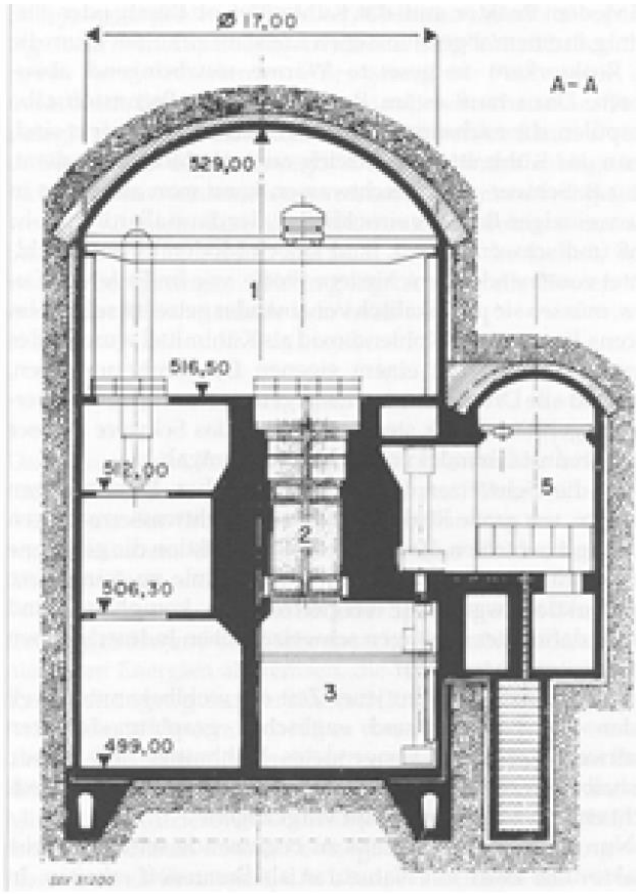


Figure 6. Lucens NPP reactor building, 1: crane hall, 2: reactor vessel cavity [9]

There are other projects on which less data are available, due to the fact that they were meant to serve military purposes. All of the nowadays publicly known ones were constructed around the 1960s. The Zheleznogorsk NPP in Russia was constructed in granite, and was completed in 1958 [2]. A section of its galleries and caverns, as well as its location in a granite mountain and the turbines room, are shown in Figure 7. The installation was kept secret for years, since in addition to heat and electric energy, it was producing weapon grade plutonium [2]. Likewise, a complex aimed at plutonium breeding, has been recently declassified in China [10]. It is sited under a mountain, in caves, in the Fuling in Sichuan province. The once-secret 816 Nuclear Military plant was never finished by the Chinese government, as due to its slow advancement, it was decided to give priority to other projects [10]. They stopped the project in 1984, with 85% of the civil works finished and 60 % of the equipment installed. It was declassified in 2003 and opened to the public for visiting in 2010 [10]. In Figure 8, the entrance and control room of the 816 Underground Nuclear Project are shown.

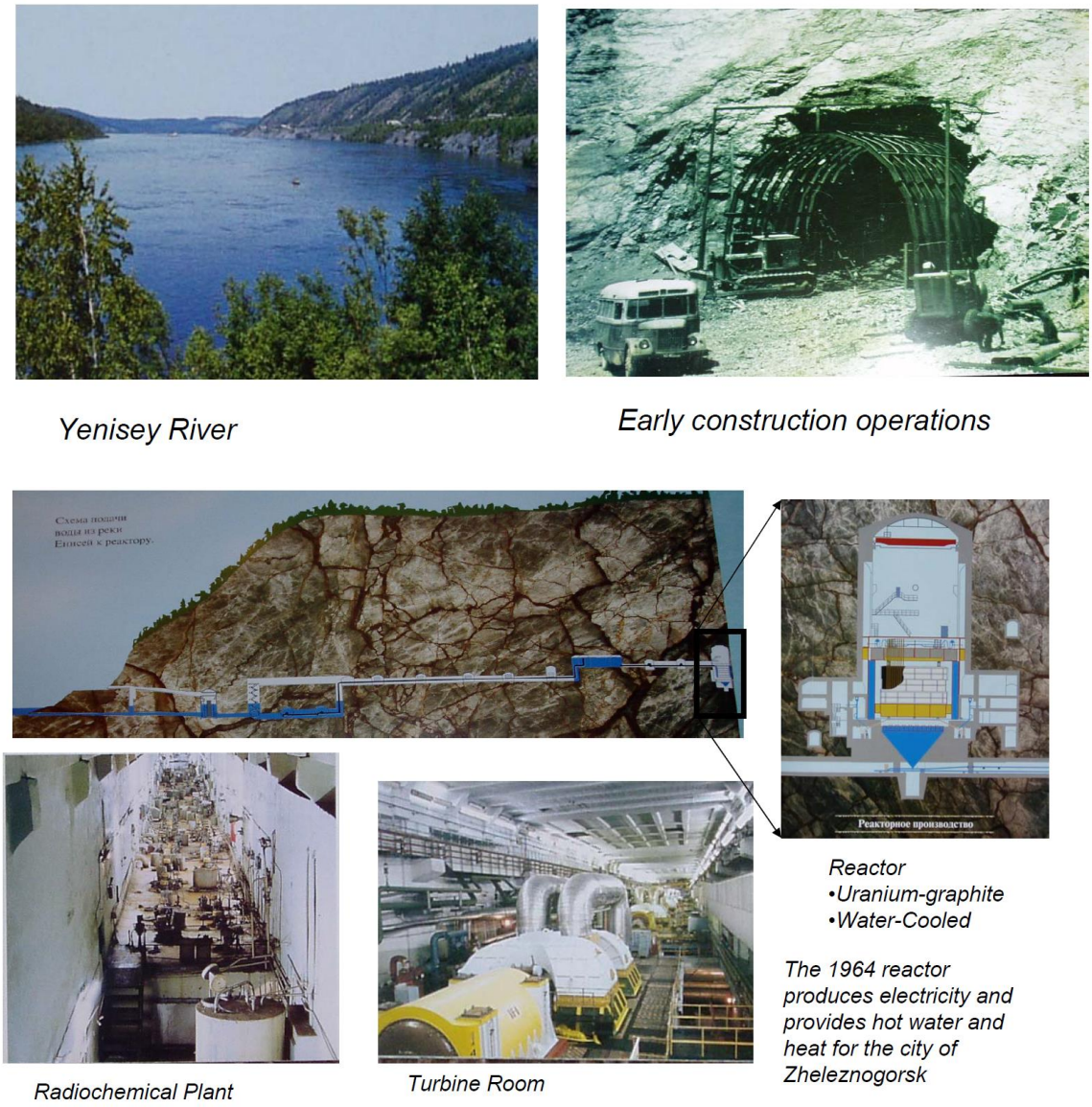


Figure 7. Zheleznogorsk NPP [11]

Figure 8. Left: entrance to nuclear complex “816 Underground Nuclear Project” Right: reactor control room [10]

### 3.1.1 The Lucens Incident

Lucens underwent a core meltdown, without casualties or environmental damage due to its siting being underground on Jan, 29 1969 [9]. It was subsequently shut down. This incident was discovered by the Swiss press 50 years later. Pinto [8] points out a very particular safety feature at this plant thanks, partly, to its underground design. The porous concrete lining the reactor cavity, whose main function was groundwater drainage, created a gas distribution effect during the overpressure accident. Due to this condition, gas could flow gradually into the high-porosity and low-permeability rock. Consequently, filters placed before the porous concrete succeeded to provide the filtration of particulate contaminants.

The decontamination of the plant was concluded in 1973. The decommissioning of Lucens suffered several difficulties. Some of them, derived from the decision of siting it underground. The increased cost of siting it underground was, intended to be mitigated by reducing space, which hindered the decommission activities [12]. Additionally, the floor loading capacity was too close to its design strength [12]. Consequently, the loading capacity of the floor was also an issue while dismantling the plant [12]. IAEA [12] lists measures for final decommissioning, to return the site to non-nuclear uses. They can be summarized as follows:

- filling with concrete to immobilize radioactivity and to ensure the mechanical stability of the bedrock (sandstone)
- construction of an additional drainage system around the caverns aimed at attracting groundwater from the bedrock, conducting it to a collection pond where it is monitored, and later to the nearby river
- transport to a waste repository of containers where the activated equipment was stored

### 3.1.2 Conceptual studies

Duffaut and Vaskou [2] list four models presented in the Hannover conference on Underground Nuclear Power Plants in 1981, collected from a paper written by another author. They were aimed at four locations: Canada, Germany, Japan and California. Each model took into consideration the characteristics of the landscape at the territory it was meant to be installed in. The Californian model, shown in Figure 9, was inside a granite mountain, and consisted on five or six caverns connected by 4 parallel lines. All caverns are big tunnels with flat sides and arched roofs, located at about 100 m depth.

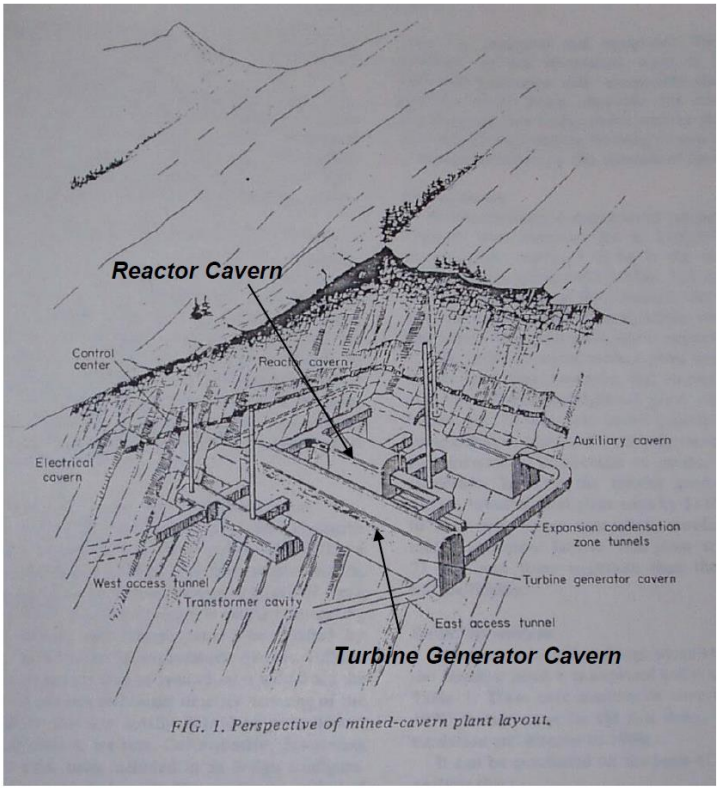


(after Finlayson, 1981)

Figure 9. California model [11]

The Canadian model, developed by Ontario Hydro, was meant to be installed deep in the Precambrian granite-gneiss basemat. It was deemed to be a rock mass sound enough to serve as the sole containment, even in the case of an explosion—presumably not a reactor explosion) — without concrete or steel lining[2]. It consisted of four 850 MW CANDU (CANada Deuterium Uranium) units. Figure 10 shows this NPP design.

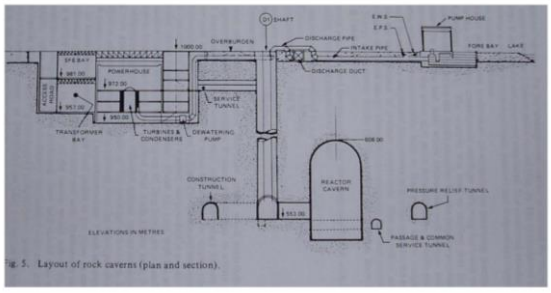

Figure 10. Canadian model [11]. Elevations in meters

The German model was a spherical 65 m diameter containment. The Japanese model was inside a rock insertion into the sea.

i. Cost penalty: Table *2* shows the expected cost penalty for each of the models with respect to the installation of their reference reactor above grade [11]. Ned Elkins [11] suggests that all them undergo a cost increase due to in-rock siting. On the other hand, the suggested increments, are different depending on contractor, location and project.

ii. Salt deposits as a promising option: Ned Elkins [11] defends salt as a promising option, not considered in the previously-mentioned studies. Mechanical, chemical and thermal properties of salt are well known, and salt has remarkable containment characteristics. Salt is used widely

for storing hydrocarbons and nuclear waste, claims Ned Elkins [11]. There is plenty of experience in machining salt, such as in drilling salt during oil and gas exploration and production operations, as well as in salt mining [11]. Massive salt beds can be big enough to host Nuclear Power Plants.

Ned Elkins [11] argues that in-salt-embedment has the potential of reducing costs with respect to above grade reactors by:

- reducing decommissioning costs through in-situ decommissioning and disposal,
- reducing transportation costs thru co-located storage/disposal facilities,
- eliminating the cost of a containment building,
- reducing site costs by eliminating the restriction in number of units at a single site due to space limitations,
- reducing reactor costs by installing several modular reactors together,
- lowering insurance costs by eliminating health and property risks.

Ned Elkins [11] presents these cost reduction features in Figure 12, which depicts the prototypical NPP in a salt deposit. In addition, Ned Elkins [11] estimates the excavation costs are about 4 times less in salt than in granite, as shown in Figure 11.

Table 2. Conceptual models studies summary [7]

| Study Sponsor | Rock Type | Depth (meters) | Construction Cost Penalty |
|---|---|---|---|
| California Energy Commission | Granite | 100 | 50-60% |
| Ontario Hydro | Granitic Gneiss | 450 | 31-36% |
| Swiss Federal Institute for Reactor Research | Rock Types in the Swiss Alps | -- | 11-15% |
| Japanese Ministry of Trade and Industry | Sedimentary | 150 | 20% |

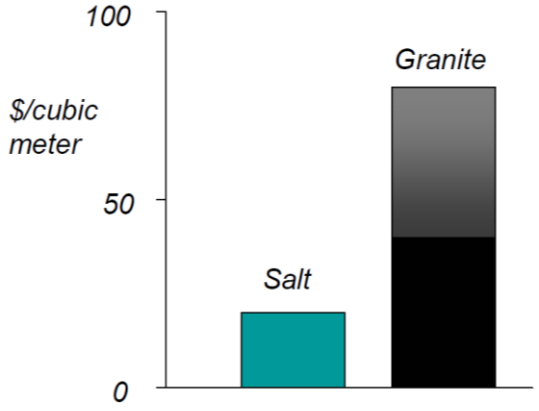


Figure 11. Range of excavation cost in salt versus excavation cost in granite [11]

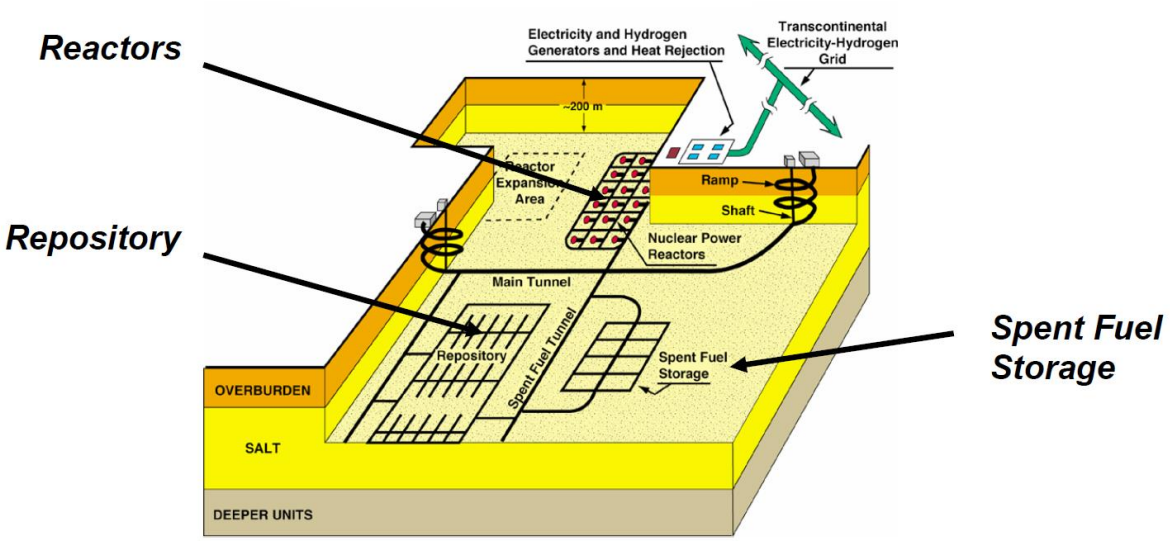


Figure 12. Prototypical salt NPP [11]

## 3.2 NPP SITING REGARDING EARTHQUAKES

Earthquake response of buildings sited on soil has been extensively studied by scholars. This topic is of particular interest, when these buildings host nuclear reactors, due to their relevance for safety of the installation, as well as for the general public. Earthquake response in nuclear reactor buildings is indisputably challenging, due to the difficulty added by the non-linear nature of Soil-Structure Interaction, to the already complex nature of those buildings.

Literature on total embedment in soil NPPs is scarce. However, every reactor sited on soil is embedded to some degree. The 10 MW High Temperature Gas Cooled Test Reactor (HTR-10) in China is an example of partial embedment of a relevant portion of the total height of the building. Wang et al. [13] compared the response spectra generated by means of a fixed-base FEM model, to the one obtained studying the SSI of the reactor building and the adjacent soil. The AP1000 is a generic reactor design developed by Westinghouse for a wide variety of sites. L. Tuñón-Sanjur [14] adopted a set of models to analyze the effect of soil-structure interactions in the floor response spectra (FRS) of the AP1000, as a function of an array of soil characteristics: soft rock, hard rock, soft soil, medium soil or hard soil. F. F. Tajirian [15] determined the FRS for a HTGR for three different sites, a rock site and two soil sites.

There is unanimous agreement among scholars on the fact that SSI may amplify the seismic response of the NPP's reactor building ([13] and [14]). F. F. Tajirian [15] concluded that embedment reduces the earthquake load at the chosen sites by reducing the amplification.

Furthermore, different strategies might be utilized to determine the FRS. Figure 13 shows a shells and beams model [13] dedicated to the HTR-10 analysis. Figure 14 depicts the SSI numerical model Tuñón-Sanjur et al. (2007) adopted for analyzing SSI at the AP1000 reactor, when sited on soil layer. F. F. Tajirian [15] modelled the flexibility of the exterior walls for computing the response spectra of the soil sites. However, as the rock site was assumed rigid, F. F. Tajirian [15] considered the reactor walls move rigidly with the adjacent rock. It is to note that in the vertical direction the shape of the responses was similar. In the horizontal direction the rock site resulted in the maximum acceleration at all frequencies higher than 1 Hz. The soil sites reduce the response from bedrock to the structure at all frequencies except around the resonant frequency.

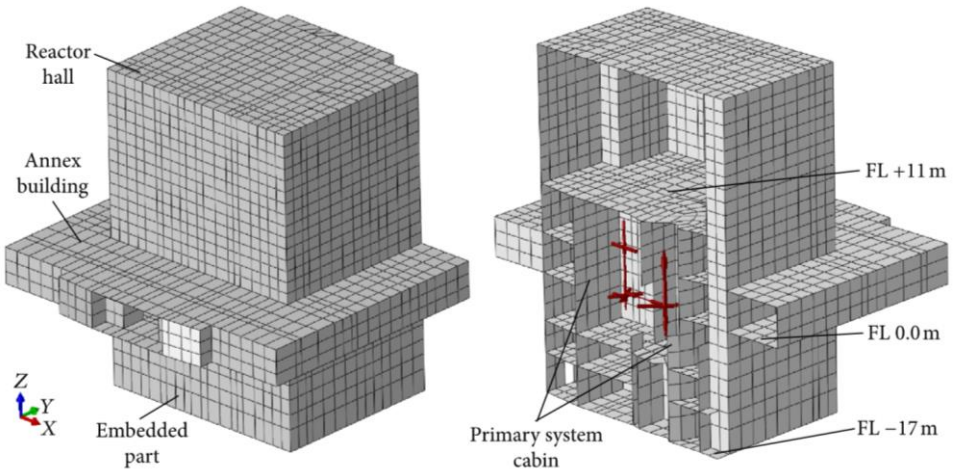


Figure 13. FEM model of the HTR-10[13]

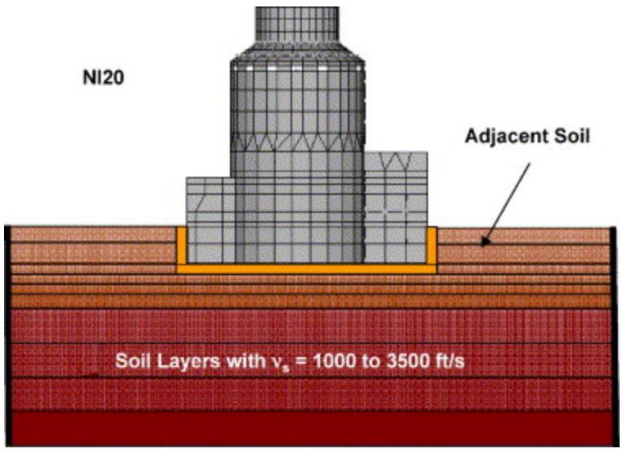


Figure 14. SSI model of the AP1000 [14], reporting also the speed of shear waves in the ground.

## 3.3 REINFORCED CONCRETE CONTAINMENT DESIGN

### 3.3.1 Containment types

There are two basic types of concrete containments: reinforced concrete containments and prestressed concrete containments. Additionally, containments can be single wall (with a steel liner on the inner surface), or double walled. When they are double walled they are categorized as primary and secondary containment. In double walled containments, the internal (primary) one can be either a steel containment or a concrete containment, cylindrical or spherical, as shown Figure 15[16]. Figure 16 shows the configuration of a single walled prestressed concrete containment for a typical PWR Nuclear Power Plant.

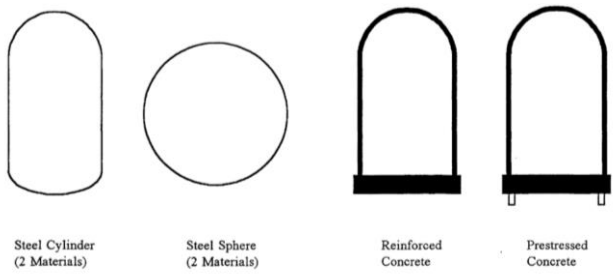


Figure 15. types of containment. [16]

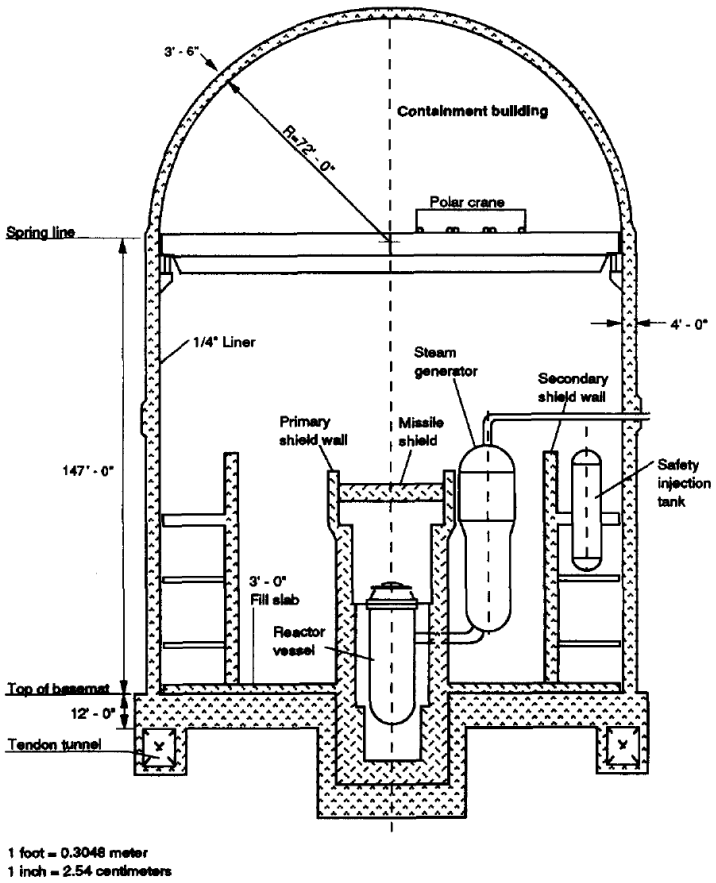


Fig. 1. Cross-section through a typical PWR prestressed concrete containment.

Figure 16. Prototype containment [17]

### 3.3.2 Loads and their effects in shear

The amount and type of reinforcement is driven mainly by the loads a containment needs to prove structural integrity against. The most relevant ones are summarized hereinafter:

- Normal operation temperature and accidental temperature: $T_o$ and $T_a$ [18]
- Normal operation condition pressure and overpressures: $P_o$ and $P_a$ [18]
- Earthquake and wind loads: SSE and OBE [18], W[16]
- Pipe breaks and jet impingements: R[16]
- Dead loads and live loads: D and L [16]

Klamerus [12] identifies 15 factored load combinations contained in ASME III, Table CC-3230-1. The loading conditions that according to Uciferro [18] determine the design are:

Abnormal: D+1.5$P_a$+$T_a$
Severe environmental: D+1.25$P_a$+$T_a$+1.25OBE
Extreme environmental: D+$P_a$+$T_a$+SSE+R

However, prudence dictates that even in preliminary sizings, the other types of loads be considered. Additionally, it is important to note that these loadings, as defined before, do not include live loads or prestressing loads, which are mandatory in agreement with ASME III Div. II CC (2013) Table CC-3230-1 [19].
All these loads bring about the need for steel hoop and meridional reinforcements, since the concrete shear capacity is generally not enough to provide the shear resistance demanded. Meridional, hoop and diagonal reinforcement resist membrane forces, among which tangential shear is one (see Figure 17 top). Some tangential shear, the one typically coming from wind and earthquake loads, can be resisted by meridional and hoop tendons meant to resist, primarily, tensile stresses. Nevertheless, diagonal reinforcement reduces the deformation of the structure [20]. Figure 18 shows meridional, hoop and diagonal reinforcement tendons.

The way in which temperature loads due to the difference in temperature between the liner and the concrete produce shear is like the way in which the pressure loads cause it: radial shear, also known as out-of-plane shear (see Figure 17). The thermal gradient along the concrete wall can cause shear in planes perpendicular to the hoop direction. Punching shear (peripheral), is a particular case of radial shear, that is caused by point loads perpendicular to the wall. Punching shear (see Figure 23) can occur around penetrations due to large forces exerted caused by pipe breaks [18]. Transverse reinforcement (see Figure 18) resists general radial and peripheral shear. There is a fourth type of shear: torsional shear, which is the result of externally applied moments about an axis perpendicular to the wall, or other element [19].

More generally, shear can also be classified as in-plane shear and out-of-plane shear. Radial shear and punching shear are out-of-plane types of shear. Tangential shear is an in-plane type of shear. Torsional shear in containment buildings normally refers to in-plane-shear. Figure 17 illustrates in-plane-shear on the top, and out of plane shear at the bottom.

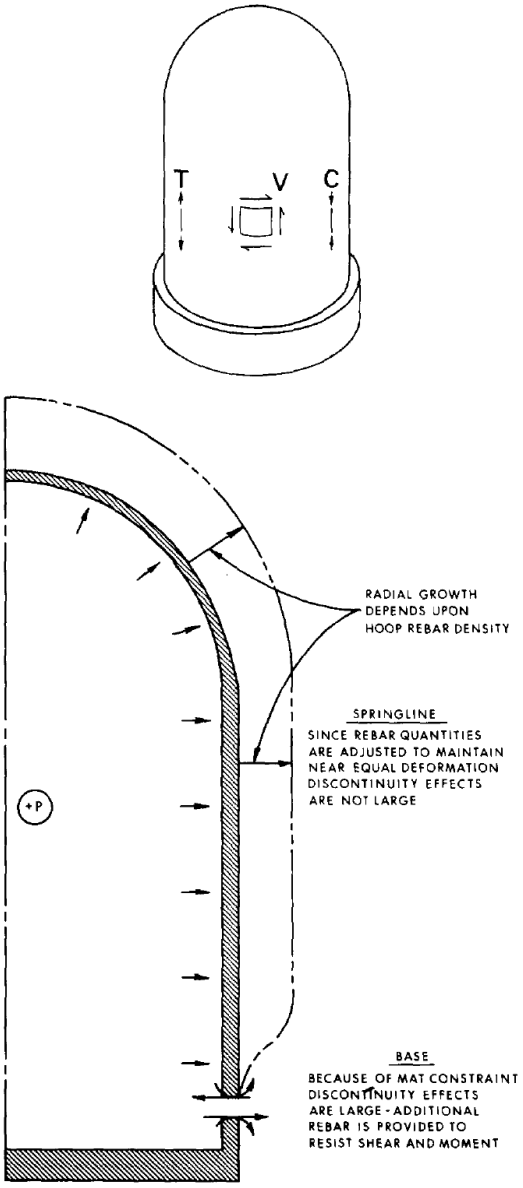


Figure 17. Types of shear [18]. Top: meridional (C & T) and in-plane (or tangential) shear (V) loads due to earthquake. Bottom: Radial (also known as out-of-plane) shear next to basemat constraint due to pressure

### 3.3.3 Prestressed versus Reinforced Concrete

Figure 18 shows the reinforcement close to the base of the cylinder of a reinforced concrete containment. The conservativeness of the design codes leads to congestion in that area due to the need for hoop and meridional bars, added to the diagonal reinforcement. This makes their placement, the grouting and the quality assurance of the system extremely difficult. Positioning of radial shear and peripheral shear reinforcement is especially complex around openings and at the base of the cylinder. In some instances, a scale model is needed during the design phase to visualize its placement [18].

Figure 19 shows the reinforcement around an equipment hatch. The placement of transversal shear in this region is challenging, since the tension reinforcement bends around the opening [18]. There are other openings

where a similar phenomenon occurs. These are the personnel air lock, the mainstream, springline and feedwater penetrations and the equipment hatch.

Both reinforced and prestressed concrete are commonly used. While the first has the advantage of leading to a thinner wall and dome, for not requiring so much shear reinforcement, it needs more precision in construction [20].

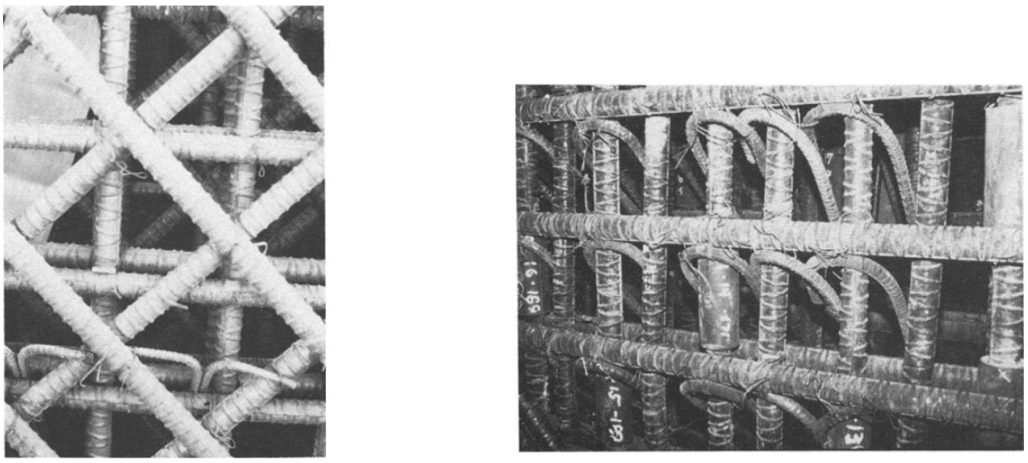

Figure 18. Left: meridional, hoop and diagonal reinforcement. Right: Stirrups (transverse reinforcement) fixed to meridional and hoop reinforcement to absorb radial shear [18].

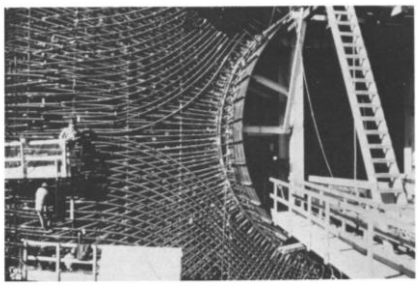

Figure 19. Reinforcement around equipment hatch [18]

### 3.3.4 Shear reinforcement

#### 3.3.4.1 Reinforcement around the base

Klamerus [12] carried out an analysis of membrane loads caused by earthquakes by means of Roark's formulae. The discontinuity shear determines the amount of radial shear reinforcement required near the base of the cylinder. Figure 20 shows the accelerations utilized in the analysis, the shear resistance demand along the wall height and the junction between cylindrical wall and base slab. Figure 21 shows the typical radial stirrups absorbing shear at the junction with the base mat.

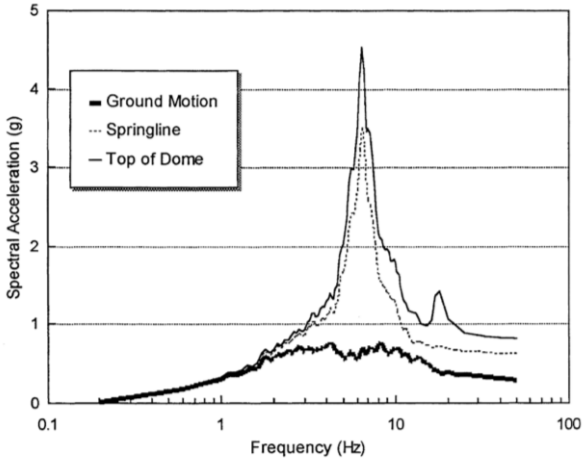


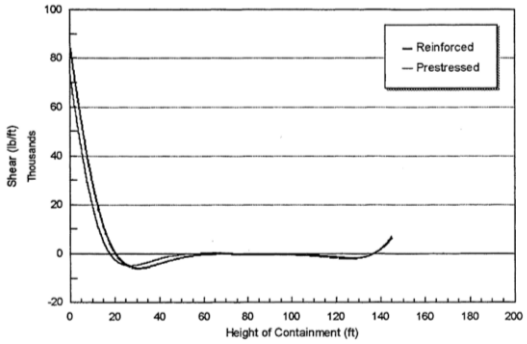


Figure 4.8 Overpressure Discontinuity Moments and Shears for Reinforced and Prestressed Concrete Containments, Moment (top) and Shear (bottom).

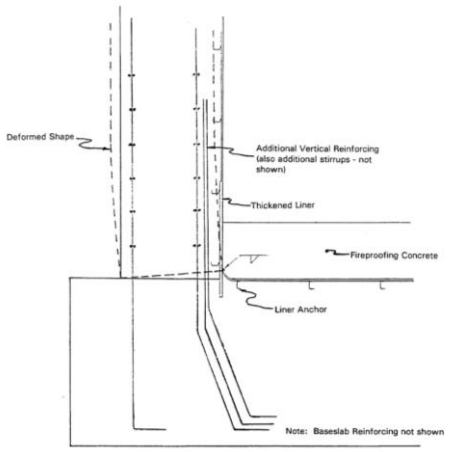


Figure 20. Earthquake induced shear around basemat [16]

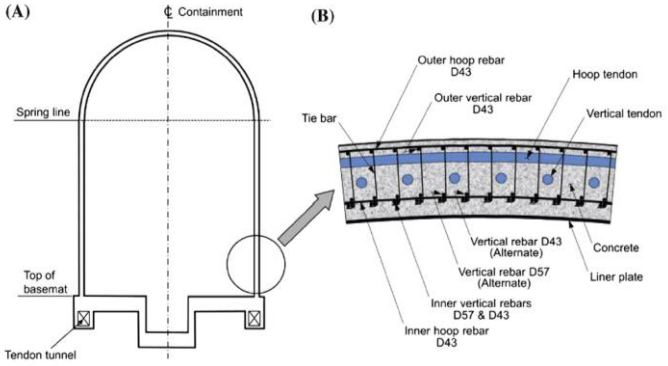


Fig. 1 – Wall reinforcement. (A) PCCV. (B) Reinforcing bars. PCCV, prestressed concrete containment vessel.

Figure 21. Radial reinforcement(Choun and Park, 2015)

#### 3.3.4.2 Reinforcement far from discontinuities

During pressure tests, the concrete in the containment typically cracks, and shear is resisted by other mechanisms than the concrete's own shear capacity. These cracks are expected to reopen during an over-pressurization accident. Sometimes there is no radial reinforcement or inclined bars contributing to the shear resistance of the concrete. In these cases, the concrete together with the meridional and circumferential reinforcement have some shear capacity due to dowel action and aggregates interlock, which are meant to resist shear [22]. Figure 22 shows the layout of meridional and circumferential (hoop) tendons.

The presence of shear dedicated reinforcement, i.e., inclined bars and radial reinforcement, is driven by the shear resistance demand. Buyukozturk et al. [22] point out that design codes allow only for a certain amount of tangential shear stress to be transmitted by the cracked concrete. If there is an excess beyond this amount of tangential shear, reinforcement must be included in the design to address it. This shear resistance demand depends on design-loads and geometry, and consequently unique for each project.

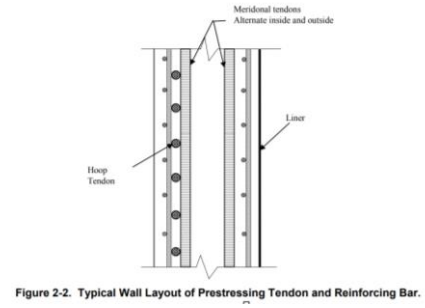


Figure 22. Reinforcement far from discontinuities [23]

#### 3.3.4.3 Reinforcement around equipment hatch, air locks and penetrations

At the spring line penetration, the discontinuity effects are small due to the similarity between deformations at dome and cylindrical shell. Transverse shear reinforcement is provided around it to cope with transverse shear. On the other hand, large openings, such as equipment hatches and personnel air locks, induce large load concentrations because of the interruption of hoop and meridional reinforcement. Further, the pressure on their lids results in a punching load radial to the cylinder in the perimeter of the opening, which results in flexural and radial shear, local to the openings. The concrete section is usually thickened around these areas to accommodate the extra reinforcement to cope with these loads, increasing the discontinuity effect and thus inducing additional shear and moments.

Pipe breaks or jet impingements at the main steam and feedwater penetrations are responsible for radial forces that occur without membrane tension. These forces are resisted by the transverse shear reinforcement in regions where allowable shear stresses are exceeded [18].

### 3.3.5 Failure modes

Klamerus [12] discusses several types of failure modes on concrete containments, some of them more related to shear than others. Klamerus [12] lists 8 typical containment overpressure failures. Those are:

1. Wall-basemat junction flexure
2. Wall-basemat junction shear

3. Basemat flexure
4. Cylinder hoop membrane (tension)
5. Dome meridional membrane (tension)
6. Cylinder meridional membrane (tension)
7. Personnel airlock door
8. Emergency airlock door

According to Klamerus [12], the wall-basemat junction flexure and wall-basemat junction shear failure modes derive from the formation of a hinge. This leads to the radial deformation of the containment to be controlled by the hoop strain in the steel. The steel liner adds resistance against this failure mode, and if the containment structure is deeply embedded, the soil pressure contributes to impede this type of failure. The type of shear acting predominantly on this failure mode is radial shear [20].

Klamerus [12] mentions a set of possible failure modes in major hatches, which are typically the equipment hatch, and personnel and emergency airlocks. Among the failure modes Klamerus [12] describes for major hatches, loss of the sleeve concrete shear anchor is the one most directly related to shear reinforcement. Additionally, Klamerus [12] describes deformation induced failure modes, as those coming from

- adjacent structures punching shear, shown in Figure 23, and
- pipe penetrations rigidly attached to concrete wall, upstream or downstream failures, which typically consist of pressure boundary buckling or support failure from pipes.

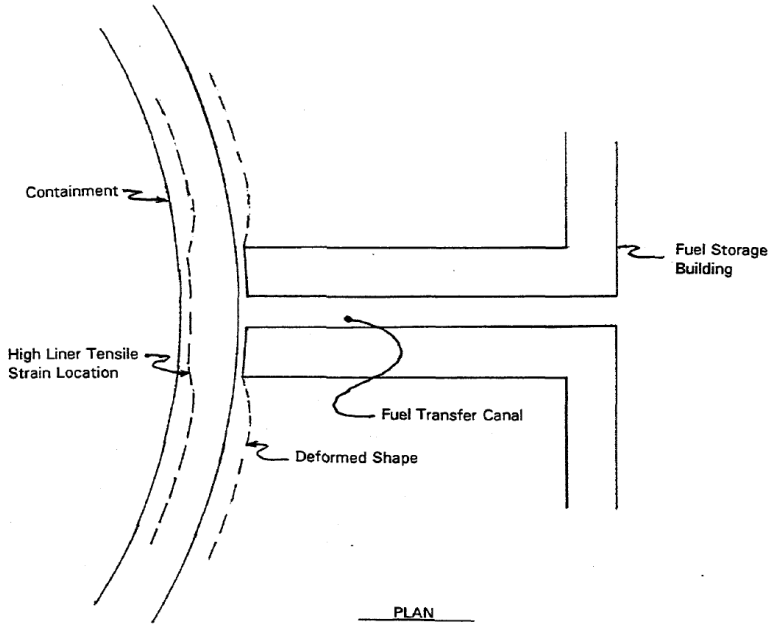


Figure 3.14 Possible Punching Shear Failure Location

Figure 23. Punching shear caused by adjacent structure [16]

# 4. METHODOLOGY

Two designs are generated for the cost comparison, one embedded and the other semi-embedded. These designs are generated according to Nuclear design rules ( ASME III Division II CC (2013)[19] and ASCE 4-98[24]). The difference in direct capital cost of these two designs are compared by assessing the material, labor and construction cost. MIT graduate student Patrick A. Champlin [25] analyzed the cost of the AP1000, which include the material, labor and construction cost, deriving from the material cost per unit volume, labor rates per discipline (e.g., ironworker), and labor time per volume of material and discipline (e.g., ironworker: rebar). These are condensed into cost in dollars per cubic meter of concrete and steel, which encompass all the material, and labor construction cost. Each design's cost comes from multiplying the volumes of steel and concrete obtained in the design with the unit cost figures condensed. These cost items are then compared to determine the potential savings from one design option to the other.

## 4.1 DESIGN METHODOLOGY OF NUSCALE

The first aspects to consider for conducting the design of a reactor building are 1) which nuclear technology does it contain and 2) where will it be sited. The functions that the reactor building need to satisfy derive from these two aspects. The building's functions, the nuclear technology and the location lead to design constrains that ultimately lead to sizes and configurations. Design constraints include all the boundary conditions that affect the design. These are subdivided in loads and site characteristics. The site characterization and the technology selection are therefore the first step, in designing the reactor building.

The designs generated in this work are meant to serve the only purpose of comparing cost. For this reason, complete designs are not generated. The parts that are deemed to be negligible in the final cost comparison are excluded. The methodology for sizing the cylindrical walls is composed of the following steps:

1. A basic sizing of the building is generated based on its functional requirements.
2. Design loads are defined in the same way for the AG and BG designs, from ASME III divII CC (2013)[19] (which contains the same provisions as ACI 359). The only "beyond design basis" load considered is airplane crash [26], [27].
3. Wall thicknesses and material properties are assumed: 1 meter, standard concrete and steel material properties.
4. Internal loads demand (i.e. stresses in compression in the case of concrete and shear/tension in the case of rebar) are determined in agreement with ACI 359 [19] for these dimensions, properties and loads defined in previous steps, by means of FEA.
5. Based on the results for internal load demands, rebar densities and thicknesses of walls are redefined.
6. Based on these new sizes, the loads are reevaluated, applied onto the building and steps 4 and 5 repeated, until convergence.

Note that the earthquake loads depend on the sizing since as the walls get thicker, mass and stiffness properties change, and consequently the natural frequencies of the building. These frequencies will result in a higher or lower response of the building. Figure 24 illustrates the iterative process described herein. A modal analysis for estimating the natural frequencies of the building is conducted in each iteration, from which the seismic loads are defined.

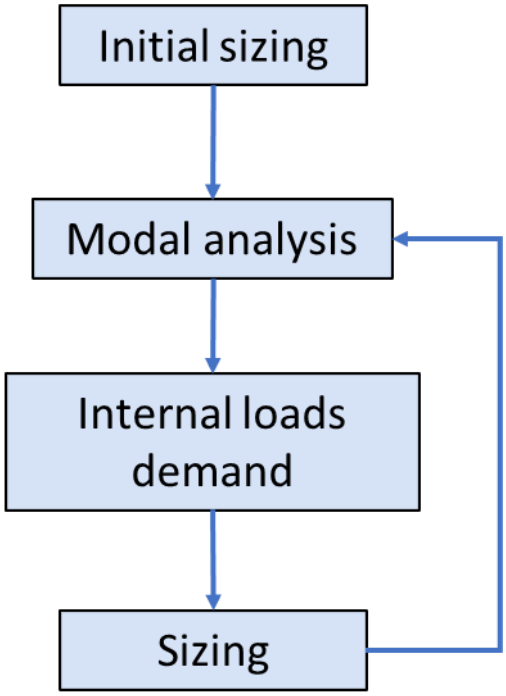


Figure 24. Iterative sizing process schematic

Once the cylindrical walls are designed, the foundations are designed for the AG and BG cases. The design process for the piles is not iterative. It is defined based on the loads that these need to withstand as a result of the design of the cylindrical walls.

## 1. SITE CHARACTERIZATION

The Kashiwazaki-Kariwa site in Japan is selected as the location to consider for the comparison. Site response to the Niigata-ken Chuetsu-Oki Earthquake in 2007 at the Service Hall vertical array [28] and horizontal earthquake response accelerations at basemats of units 1 and 7 [29] characterize the site for the earthquake loads definition. The soil strata data and the location of the water table complete the site characterization. The location of the Hall is shown in Figure 25. The soil properties [28] are utilized for determining the loads that the portion of the building underground need to withstand.

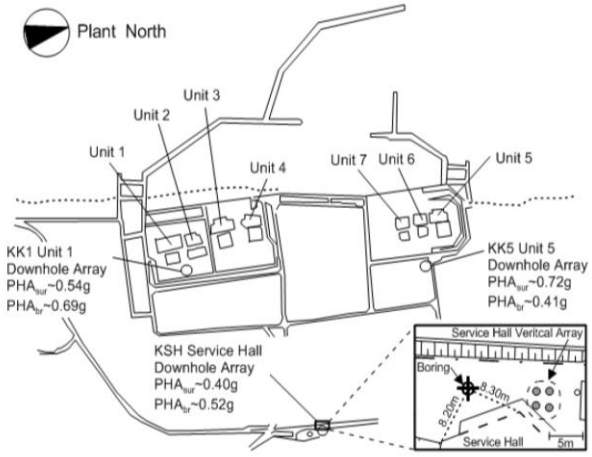


**Figure 1.2 Map of Kashiwazaki-Kariwa nuclear power plant showing locations of downhole arrays and geometric mean peak accelerations from 2007 Niigata-ken Chuetsu-oki earthquake. Peak accelerations are shown for surface ('sur') and bedrock ('br') conditions.**

Figure 25. KK site in Japan

Data on the design tornado is extracted from RG_1.76[30]. Annual precipitation, design tsunami and changes of temperature are not considered in the study.

## 2. TECHNOLOGY SELECTION

The technology is selected based on the maximum size for the excavation to be cost-effective. Eighteen meters is set as the maximum diameter for the excavation. Two meters gap margin are left for the civil works, i.e., the boundary between the nuclear systems and the soil at the site. This leaves 14 m as the maximum diameter that the Building's internals can occupy. Based on these data, the NuScale reactor is selected as the technology for the reactor building (see Figure 2).

## 3. FUNCTIONS DEFINITION

From the technology selection, the functions that the RB must perform are derived. A basic sizing stems from these functions.

## 4. LOADS DEFINITION

Internal and external design loads are defined as described by ASME III divII CC (2013) [19].

- All internal loads except those coming from earthquake accelerations on pipes are equal for the AG and BG options.
- The design earthquake floor response spectra at the Reactor Building are derived from both, the design floor response spectra at the basemats of units 1 and 7, before the Chuetsu-Oki earthquake in 2007 took place, and the response spectra of the Chuetsu-OKI earthquake [29].
- Airplane crash loads are defined as prescribed by NEI [27].

## 5. ANALYSIS

Different parts of the building are analyzed separately. Several assumptions simplify the analysis. These assumptions are made at different stages of the design.

### Cylindrical wall

Regarding the cylindrical wall, once all the loads are defined or estimated, the loading combinations as per ASME III divII CC (2013) that constrain the design at each region are identified. As described before, the design is iterated for finding convergence between seismic loads and design. Modal and structural integrity analyses are conducted in ANSYS V19.2[31].

Stresses in the dominating loading cases are computed by means of several FEA models. Absence of crushing of concrete is verified assuming a square biaxial interaction failure law and adding all the loads in each loading that cause relevant compression. The compression in each direction is limited to 0.3Fc in service load combinations and to 0.6Fc in factored load combinations. Fc is the uniaxial compressive stress of concrete.

Out-of-plane, in-plane shear, hoop and meridional membrane tensile stresses are retrieved from the results and combined to generate reinforcement area needs in accordance to the ASME III divII CC (2013) expressions:

$$A_{sh} + A_{si} = \frac{N_h + ({N_{hl}}^2 + {V_u}^2)^{1/2}}{0.9 f_y}$$

$$A_{sm} + A_{si} = \frac{N_m + ({N_{ml}}^2 + {V_u}^2)^{1/2}}{0.9 f_y}$$

where

- $A_{sh}$ = area of bonded reinforcement in the hoop direction
- $A_{si}$ = area of bonded reinforcement in one direction of inclined bars at 45 deg to horizontal. Inclined reinforcement shall be provided in both directions.
- $A_{sm}$ = area of bonded reinforcement in the meridional direction
- $N_h \; and \; N_m$ = membrane force in the hoop and meridional directions respectively due to pressure, prestress, and dead load. The prestress force shall be the effective value. $N_h \; and \; N_m$ are positive when tension and negative when compression.
- $N_{hl} \; and \; N_{ml}$ = membrane force in the hoop and meridional direction, respectively, from lateral load such as wind, tornado or earthquake loading. When considering earthquake loading, this force is based on the square root of sum of squares of the components of the two horizontal and vertical earthquakes. The force is always considered as positive.
- $V_u$ = the peak membrane tangential shear resulting from lateral load such as earthquake, wind, tornado loading. When considering earthquake loading, this force is based on the square root of sum of squares of the components of the two horizontal and vertical earthquakes. The shear force shall be always considered as positive.

These areas are computed in the four different zones indicated in Figure 26. Afterwards, based on these areas, the total volumes of steel are computed. Based on these volumes, the thickness of the cylindrical wall is iterated until finding a sensible combination of steel and concrete volumes. The criterion for conducting this iteration is that the typical steel to total (steel plus concrete) volume in reinforced concrete walls in NPPs is in the order of 6-7%.

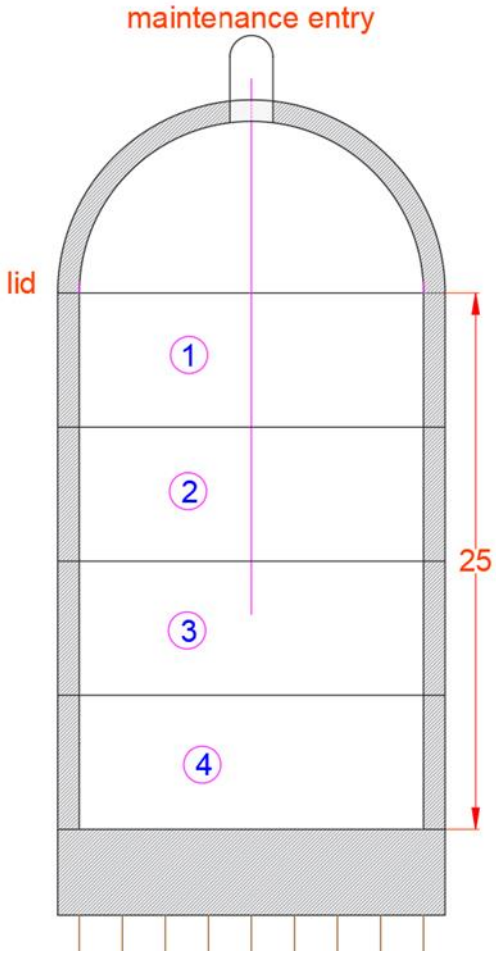


Figure 26. sizing zones in cylindrical walls

Foundations

Basemat and piles are designed by means of a simplified 2D OptumG2 models for a load case, from which later on, the size of the relevant parts (piles and/or basemat) are extracted. A preliminary hand calculation serves as a means for presizing the piles. The basemat is assumed rigid throughout the whole process [32].

## 4.2 DESIGN METHODOLOGY OF BWRX-300 AND PRISMATIC EQUIVALENT BUILDING

The other analysis carried out in this work is the embedment of the BWRX-300 reactor. A cylindrical building configuration and a prismatic one are analyzed. In the case of the BWRX-300 and its prismatic counterpart there is no need to select a technology and size a building based on their functions, since the approach is different from what was defined before for the analysis of NuScale. The selection of NuScale as a reactor stems from constraints in the maximum space for rooms inside the building: 14 meters in diameter of excavation. In the BWRX-300 case, instead of using a technology that adapts to a certain excavation and building limits, a nuclear reactor building where a preliminary sizing has been already conducted is used as a reference, and the cost of embedding it assessed.

Unlike in the NuScale case, in the case of the BWRX-300 and its equivalent prismatic counterpart the external walls can have a totally different reinforcement in hoop and vertical directions, and thickness of concrete. This stems from the possibility of using each of the floor slabs as a location where to anchor the vertical

reinforcement. The density of vertical rebar thus can vary through the height of the building. Naturally, the analysis of this building takes each space between floors as a sizing zone, similarly to how the NuScale case is subdivided as shown in Figure 26.

As there are no precise dimensions of the building available, an artificial building that serves as an artifact is defined. The space between floors is defined based on the apparent dimensions in Figure 4, the fact that the building is 20 m in diameter and 15,500 $m^3$ total volume [4].

The iterative process for defining the areas of reinforcement and thicknesses of concrete is the same as in NuScale. The criterion for conducting this iteration is that the maximum steel to total (steel plus concrete) volume in reinforced concrete does not go beyond 8-10 %.

The site considered is defined in the AP1000 design control report [7]. This document does not define the soil layers below the reactor, only gives general soil types, hence foundations are not evaluated.

## 4.3 COST COMPARISON METHODOLOGY

The parts whose cost is expected to differ significantly in embedded and semi-embedded reactors are evaluated and then their cost compared. The cost is simplified to three items: concrete, steel and excavation. As the only purpose of this study is to determine whether an embedded design can be cheaper than a non-embedded design, the cost assessment only includes direct cost. Indirect cost and contingencies, assumed to be proportional to direct cost, thus are excluded from the assessment [25]. The direct cost assessment is rather simple. Every cost item is condensed into material volumes, i.e., concrete, steel rebar, and amount of soil to excavate, and includes excavation and material cost, but also labor cost.

Regarding concrete and steel cost; equipment, logistics cost and design cost are not included in the analysis. The cost of the labor time in hauling sand during the excavation, for instance, is included in the labor excavation cost, which ultimately is included in the condensed excavation cost. There are aspects of the direct costs that are not considered in the analysis as their effect on the total cost is negligible. Champlin [25] established that the direct transportation cost was overall between one and two orders of magnitude below the direct cost of labor and materials. Therefore, the transportation cost associated with steel rebar and concrete is not included in the assessment. As one of the premises of the study is that the external diameters and total heights of the AG and BG options are equal, the cost of formwork, and all the aspects that derive from it are not accounted for in the assessment. Likewise, the cost of tasks that are meant to be equal after simplifications of the study are not included. Welding, pipe fitting and wiring are among these cost items. The design of the penetrations and their surroundings are deemed alike for the AG and BG designs, therefore they are excluded from the evaluated parts.

Nevertheless, there are other cost items excluded as well from the assessment, that might have a relevant effect on the cost difference between options. For instance, the cost of machinery utilization/amortization corresponding to concrete and steel rebar, which might be higher for the BG option than the AG one is not included. Other complexities such as the increment in design cost derived from the necessity of making a model for planning the assembly sequence of the reinforcement or the use of complex validation procedures for assuring integrity against “beyond design” conditions are also not considered in the analysis.

To summarize, the condensed cost of steel includes the cost of purchased rebar per cubic meter and the cost of labor for installing that rebar per cubic meter. The same applies to the condensed cost of concrete. The cost of excavation, however, includes labor cost, formwork and machinery cost. The following formula summarizes the cost evaluation:

$$\text{Cost}[\$] = \text{steel}[m^3]*UC\_steel[\$/m^3] + \text{Concrete}[m^3]*UC\_concrete[\$/m^3] + \text{Excavation}[m^3]*UC\_excavation[\$/m^3]$$

# 5. COST ITEMS

As mentioned before, integrated cost items corresponding to materials are used for the cost assessment as opposed to cost sorted by activities. Volumes of concrete and steel are multiplied by the unit costs. Unit direct costs stemming from Champlin2018 [25] are shown in Table 3.

Table 3. Unit direct cost

| | Labor demand (man-hr/ m³) | Labor rate ($/man-hr) | Labor ($/m³) | Material ($/m³) | Labor + Material ($/m³) |
|---|---|---|---|---|---|
| Concrete | 9.18 | 36.10 | 331 | 318 | 649 |
| Steel Rebar | 420.24 | 52.8 | 22,189 | 13,773 | 35,962 |

Champlin [25] utilized in his model excavation data from different projects conducted in the 60s and 70s to build integrated excavation cost figures, 50 ($/man·h) and 0.1 (man·h/ft³). These are combined to obtain 176.6 ($/m³). Champlin [25] argues that as these costs are not affecting significantly the outcome of his study, their validity did not need verification with more recent data. Champlin [25] did not distinguish whether these figures were extracted from excavation in soil or in rock and what excavation method they corresponded to. Here data from different sources are combined, in order to devise sensible unit excavation cost, for the current study.

An extensive literature review was conducted yielding Table 4. Timo's estimations [33]range from a low $130/m³ to a much higher $1700/m³. Ball's rate is 1700 $/m³ [4], which we assume to only entail excavation related costs. The prediction for a 20m diameter drilled shaft are approximately $1200/m³ and $1700/ m³ respectively. Although these rates are for different years, excavation techniques, type of rock, project types, and certainly different magnitudes, it follows that the they are all between about $130/m³ and $1700/m³.

These figures are different by an order of magnitude. This difference is due to specificities of each project. The O'Neill [34] factor indicates that dry drilling in rock is 8x more than in dry soil. This scalable figure is very important if the reactor location is in rock because it means that it will be 8x more expensive if TBM or boring techniques are used instead of blast/dig. Rock type and rock quality also influence excavation cost. Assuming all those variables are set favorably so cost of excavation in rock is driven down, the cost will be at the lower end of the spectrum. Since Champlin's data, roughly $175/m³, is at the lower end of the spectrum, it is chosen as the reference excavation cost in rock in this thesis. As the rock quality, type, excavation technique and other variables come into play, the cost can raise to the order of $1000/m³ or $1500/m³ with the potential to exceed these rates.

This analysis suggests that the unit excavation costs shown in Table 10 are reasonable for a close to ideal rock site. In a soil site, half this unit cost seems within the right order of magnitude.

Table 4. Excavation cost from different sources and for different conditions in dollars per cubic meter

| Excavation Data | Costs | Source (date) | Data Process | Soil/Rock Type | Soil/Rock Quality | Excavation Techinque | Project Type (Nuclear/Non-nuclear) | Comments |
|---|---|---|---|---|---|---|---|---|
| GE BWR-300 | $1700/m$^3$ | 2018 [4] | Volume and costs given | Rock | Unspecified | Conventional blast/dig/pour | Nuclear | Estimation for presentation, total costs |
| Drill Shaft (dry rock) | $230/m$^3$-$330/m$^3$ | 1987 [34] | Rate given | Piedmont Region Rock (schists, amphibolite, gneiss, migmatites, and granite) | moderate-to-high-grade | Drilling | Non-nuclear (shaft foundation) | specified rock type, unspeficied volume |
| Drill Shaft (dry soil) | 1/8 of Drill Shaft Rock | 1987 [34] | "O'Neill Factor" applied | Soil | Good | Drilling | Non-nuclear (shaft foundation) | "O'Neill factor" for dry soil is 8x less |
| Timo Nuclear (benchmark) | 120€/m$^3$-300€/m$^3$ | 2019 [33] | Estimation | Finish Granite | Good | Drill and blast | Nuclear (repository) | overnight costs, expert estimation |
| Timo Non-Nuclear | 50% benchmark | 2019 [33] | Estimation | Finish Granite | Good | Drill and blast | Non-nuclear | overnight costs, expert estimation |
| Timo Nuclear - Bad Rock | 150% benchmark | 2019 [33] | Estimation | Finish Granite | Bad | Drill and blast | Nuclear/non-nuclear | overnight costs, expert estimation |
| Timo Nuclear - TBM or Shaft | 300%-500% benchmark | 2019 [33] | Estimation | Finish Granite | Good or Bad | TBM or Vertical Shaft Sinking | Nuclear | overnight costs, expert estimation |
| Shaft Sinking Extrapolation (ø20m x 30m) | 1196.59/m$^3$ | 1987 [34] | Linear regression | Soil (assumed) | Unspecified | Conventional Shaft Sinking | Non-nuclear | Regression estimation |
| Shaft Sinking Extrapolation (ø20m x 15m) | 1708.14/m$^3$ | 1987 [34] | Linear regression | Soil (assumed) | Unspecified | Conventional Shaft Sinking | Non-nuclear | Regression estimation |
| Champlin's Figures | $176.57/m$^3$ | 1970, 1986, 2001 [25] | Extrapolated | Rock (gneiss, granite, chalk, and shale) and/or earth (soil) | Good/ Varies | Conventional blast/dig/pour | Nuclear | $/manh multiplied by manh/ft$^3$, $/ft$^3$ convert to $/m$^3$ |
| RSMeans | excavation in rock ≈ 2x to 8x excavation in soil | 2017 [35] | Cost components built | Rock (unspecified type) and Soil (unspecified type) | Unspecified | Soil Unspecified/ Rock Blasting | Non-nuclear | Includes Overhead for a generic city in the US: $/ft$^3$ convert to $/m$^3$ |

It follows that 50% of the excavation cost rate used in an ideal case, $176.6/m³/2 = 83.3$/m³ appears as moderately conservative and reasonable excavation cost in soil. Hence, it is taken as the excavation cost in soil in this work.

The values in Table 3 do not provide reference information on pile foundations. The cost of bored and driven large piles, in length and diameter, was estimated using RSMeans [35], coming up with cost rate of the order of $12,000-18,000 /m³ for steel. This cost is similar in order of magnitude to the cost of steel from Table 3. Additionally, it was concluded from Table 4 that excavation costs in the Nuclear industry are higher than in other industries, giving a reference value of a factor 2x, due to additional inspections and hardware requirements. Given those figures, it appears as a suitable initial guess to assign the piles foundations the same unit costs for steel and excavation, as to the rest of the reactor.

One example of excavation technology in soil is the Vertical Shaft Sinking Machine from Herrenknecht, claiming to be capable of removing up to 35,000 ft³ (≈1000 m³) of material per 8 hour shift[25]. This could reduce significantly the excavation labor cost in soil. However, setup of the machine would still likely cost $1-2M, which would likely make it economically unattractive for small excavations as the ones considered in this work.

# 6. ASSUMPTIONS, CONSIDERATIONS AND HYPOTHESES OF THE STUDY ON NUSCALE

The different general assumptions at each stage of the cost assessment and considerations made are listed hereinafter. There are three important groups of general assumptions and simplifications: those on how an artificial set of loads that shape the design are created, those on how these loads lead to a design, and those on the cost evaluation of this design. The assumptions and simplifications on how the defined loads lead to a design are listed after the loads definition, in chapter 8.

General

- The building's internals, and the external areas in the AG and BG designs are identical.
- The analysis is conservative regarding BG, since the goal of this work is to yield a cost comparison, not a cost assessment. Hence the supports of the internals, and the extra costs in the AG design with respect to the BG one for making internals earthquake resistant are not accounted for in the cost assessment.

Design

- It is possible to detach foundations and building above the RB from the maintenance building, and have a polar crane in it that does the required operations on the reactor from outside the RB.
- The maintenance building, enclosing the RB can be categorized as seismic 2A.
- The duct where the main steam and feed water pipes are hosted that extends from the external wall of the embedded building (BG) to the surface, can be engineered in such a way that the pipes inside keep the required flexibility to absorb the relative displacements imposed by every design loading, fulfilling the pertinent structural integrity requirements and without producing a relevant cost increment compared to the cylindrical wall cost, or the basemat.

Loads definition

- The same site and design earthquake accelerations at the buildings' basemats are considered.

Earthquake loads

- The earthquake load is defined based on the design response spectra before the Chuetsu-Oki earthquake and the spectral response of the Chuetsu-OKI earthquake at the basemat of units 1 and 7 in the current KK plant[29]. This definition entails the following underlying assumptions:
    - The Soil Structure Interaction is similar for the units already installed on the site
    - The Chuetsu-OKI earthquake and the FRS before 2007 are representative of how the design earthquake would look like today.
    - It is assumed that "beyond design" earthquake requirements for proving absence of a cliff edge effect do not affect the design.
- Combination of responses in different directions is simplified. Three earthquake scenarios are considered:
    - **The average FRS** at the basemat considers no directional combination, since the structure is axisymmetric. This scenario is also named lower bound, or LB.

    - **Horizontal enveloping** takes the maximum at unit 1 (from the 2007 Chuetsu-Oki earthquake and the design response before it), envelops it in accordance to ASCE 4-98[24] (extending 15% in frequency the peaks) and then applies a factor of 1.4 to account for bidirectionality.
    - **Increased FRS** is basically the average FRS multiplied by 7. This scenario is also named upper bound, or UB.
- The EW response spectra[29] are representative of the horizontal response spectra in every direction.

Cost items

- The costing data do not consider the fact that building embedded structures is more complex (and hence more expensive) than building them above ground, especially, with respect to what relates to the penetrations and lines that are placed below ground. Therefore, this study does not consider that extra difficulty in the final cost.

Site

- $\rho$(rock)= 20KN/m³≈2000 kg/m³ (reasonable value)
- $\rho$ (sand under the buildings)= 17KN/m³≈1700 kg/m³
- $\rho$ (sand at the same elevation as the buildings)= 15KN/m³≈1500 kg/m³

# 7. INPUT DATA IN NUSCALE

## 7.1 SITE CHARACTERIZATION

The site characteristics at the location of the entry hall are described herein. Figure 27 shows the standard penetration test results on the site, the relative densities derived from the SPT and the P-wave and S-wave velocities.

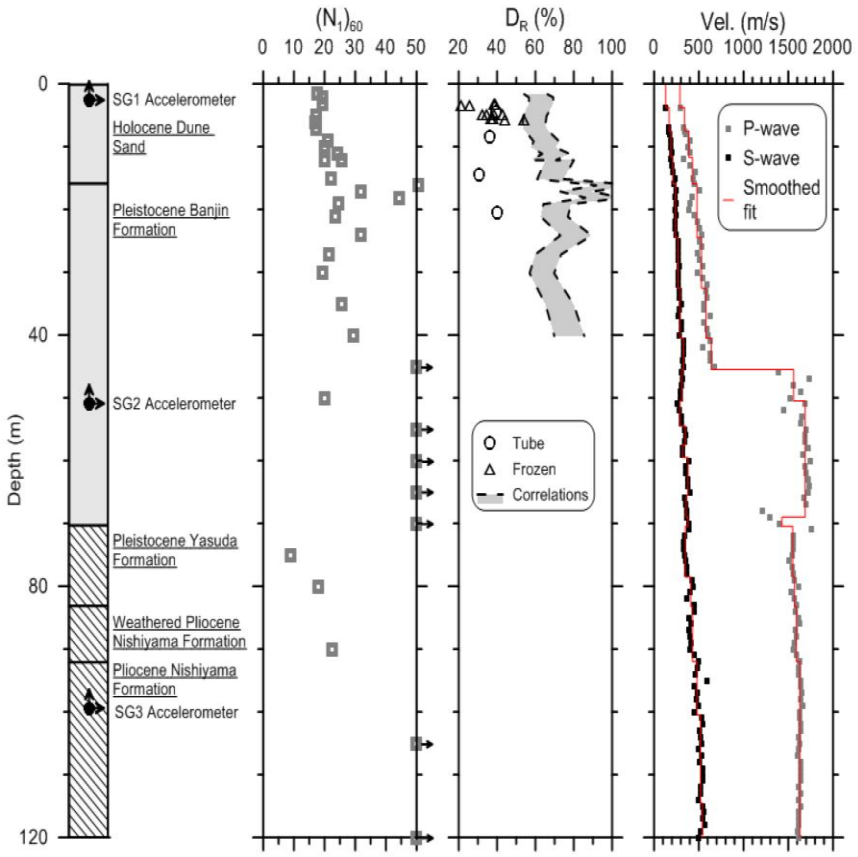


Figure 27. Vertical position of accelerometers that measured the 2007 earthquake SPT blow count, relative densities from test and [28]

Table 5 shows the soil properties extracted from laboratory tests. From left to right, these properties are vertical compressive stress ($\sigma_c$), dry specific weight ($\gamma_{dry}$), water content (w), Liquid limit (LL), Plasticity Index (PI), void ratio (e), friction angle ($\Phi$), maximum shear modulus ($D_{max}$), minimum damping ($D_{min}$) and pseudo reference strain($\gamma_r$).

Table 5. Summary of solid index tests triaxial compression shear strength test, and resonant-column torsional shear test for dynamic soil properties [28]

| Sample | | | | | | | | | Triaxial | | RCTS | |
|---|---|---|---|---|---|---|---|---|---|---|---|---|
| Depth | $\sigma_c$ | $\gamma_{dry}$ | w | LL | PI | e | $e_{min}$ | $e_{max}$ | $\phi$ | $G_{max}$ | $D_{min}$ | $\gamma_r$ |
| (m) | (kPa) | (kN/m$^3$) | (%) | | | | | | (°) | (MPa) | (%) | (%) |
| 4-5$^P$ | 81 | 14.95 | 19.9 | | NP | 0.794 | | | 39.4 | 50 | 1.3 | 0.057 |
| 8-9$^P$ | 153 | 14.23 | 15.0 | | NP | 0.886 | | | 36.4 | 74 | 0.9 | 0.1 |
| 14-15$^P$ | 256 | 14.42 | 23.3 | | NP | 0.859 | | | 38.7 | 88 | 1.7 | 0.15 |
| 20-21$^P$ | 361 | 14.18 | 11.9 | | NP | 0.899 | | | 35.9 | 112 | 0.8 | 0.163 |
| Bulk (sand) $^S$ | | | 16.6 | | NP | | 0.538 | 0.930 | | | | |
| 75.15$^S$ | | | | 69 | 33 | | | | | | | |
| 80.15$^S$ | | | | 65 | 22 | | | | | | | |
| 90.15$^S$ | | | | 69 | 22 | | | | | | | |

P – Pitcher sample
S – SPT samples

- Soil data [28]:
  - γ=14-15 KN/m³ (we take 15 KN/m³ conservatively)
  - Moderately dense sand, with Dr ranging from 0.4 to 0.65
  - G= 70-120 MPa (triaxial test data),
  - Vp≈400m/s and
  - Vs≈200m/s
  - Φ≈36°
  - Water table[28]: 45 m under the surface
- Joint sets:: Conjugate joint sets striking 34° and dipping 54° NW and 36 ° SE [28].

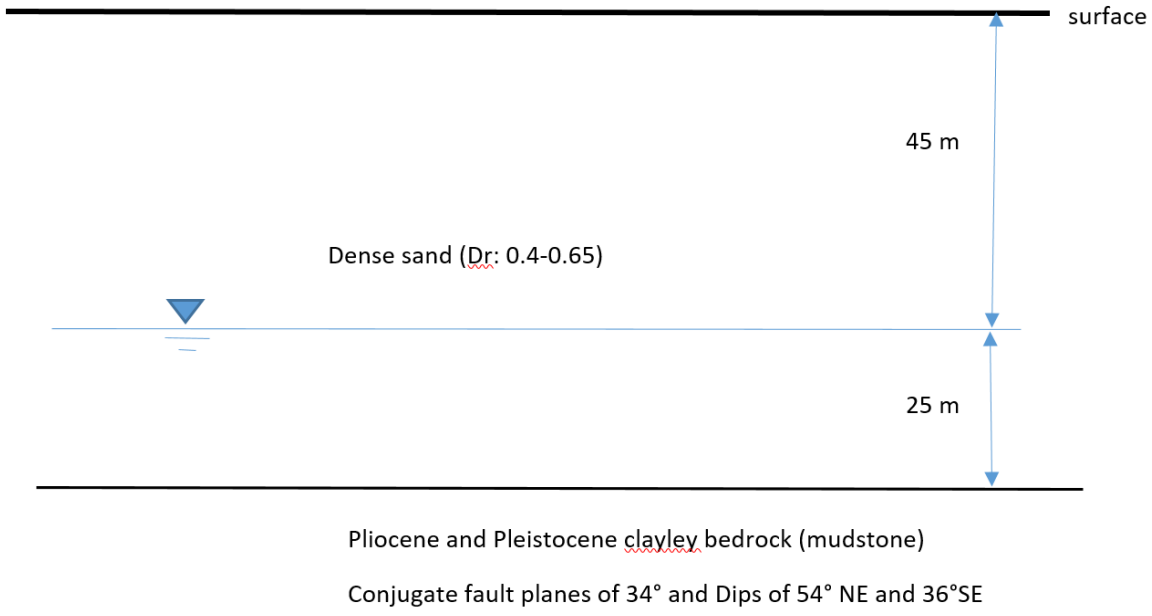


Figure 28. Soil strata at the KK site

- Rock S-Wave velocity: 500 m/s [28]
- Rock P-Wave velocity: 1600 m/s [28]
- Rock type: Clayey mudstone [28]
- Depth of bedrock: the interface between bedrock and soil starts at 70 m under the surface [28]

### 7.1.1 Estimated site characteristics

#### 7.1.1.1 Fs, G and $\nu$ in sand

Despite the fact that there are data available on G coming from a triaxial test, G is double checked by means of the relations proposed by [36]. From them, it follows that:

$$\frac{Vp}{Vs} = \sqrt{\frac{2(1-\nu)}{1-2\nu}} = \frac{400}{200} = 2 \rightarrow \nu = .33$$

$$G = \rho V_s^2 = 80MPa\ (coherent\ with\ triaxial\ test\ data)$$

The friction coefficient between piles and sand is estimated as: fs(Dr≈.5) = 4 kPa [37]

#### 7.1.1.2 E and v in rock

From $E = 2(1+\nu)\rho V_s^2$ and $E = \frac{(1-2\nu)(1+\nu)}{1-\nu}\rho V_p^2$ [38] one gets:

$$\frac{Vp}{Vs} = \sqrt{\frac{2(1-\nu)}{1-2\nu}} = \frac{1600}{500} = 3.2 \rightarrow \nu = .45$$

$E = 2(1+\nu)\rho V_s^2 = 2 \times 1.45 \times\ 2000\ \times\ 500^2 = 1{,}450\ MPa$

The Poisson's ratio obtained, .45, doesn't go by very far off the range proposed for claystone by Gercek in 2007, in accordance to the OptumG2 users guide (2018) [39]: between 0.25 and 0.4.

#### 7.1.1.3 Failure criterion

The failure criterion chosen for the rock is the Hoek-Brown criterion [40]. The Hoek-Brown yield function is given by:

$$F = -(\sigma_1 - \sigma_3) - \sigma_{ci}\left(-m_b\frac{\sigma_3}{\sigma_{ci}} + s\right)^a$$

$$m_b = m_i exp\left(\frac{GSI - 100}{28 - 14D}\right)$$

$$s = exp\left(\frac{GSI - 100}{9 - 3D}\right)$$

$$a = \frac{1}{2} + \frac{1}{6}\left(e^{\frac{-GSI}{15}} - e^{\frac{-20}{3}}\right)$$

where the input parameters are:

- GSI: Geological Strength Index

- $\sigma_{ci}$: Uniaxial compression strength
- $m_i$: Intact rock parameter
- $D$: Disturbance factor

The Disturbance factor describes the damage on the rock caused by the excavation method. It ranges between 0 and 1, where 1 corresponds to the highest damage, caused for instance by poor blasting, and 0 to the lowest. Figure 29 shows orientating values of D, for different excavation methods.

| Appearance of rock mass | Description of rock mass | Suggested value of D |
|---|---|---|
| 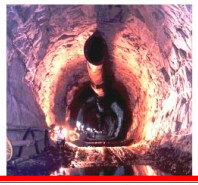 | Excellent quality controlled blasting or excavation by Tunnel Boring Machine results in minimal disturbance to the confined rock mass surrounding a tunnel. | D = 0 |
| 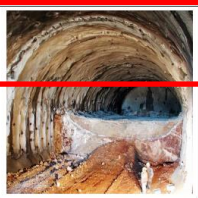 | Mechanical or hand excavation in poor quality rock masses (no blasting) results in minimal disturbance to the surrounding rock mass.<br><br>Where squeezing problems result in significant floor heave, disturbance can be severe unless a temporary invert, as shown in the photograph, is placed. | D = 0<br><br>D = 0.5<br>No invert |
| 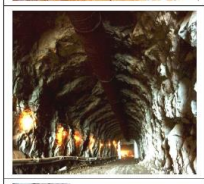 | Very poor quality blasting in a hard rock tunnel results in severe local damage, extending 2 or 3 m, in the surrounding rock mass. | D = 0.8 |
|  | Small scale blasting in civil engineering slopes results in modest rock mass damage, particularly if controlled blasting is used as shown on the left hand side of the photograph. However, stress relief results in some disturbance. | D = 0.7<br>Good blasting<br><br>D = 1.0<br>Poor blasting |
|  | Very large open pit mine slopes suffer significant disturbance due to heavy production blasting and also due to stress relief from overburden removal.<br><br>In some softer rocks excavation can be carried out by ripping and dozing and the degree of damage to the slopes is less. | D = 1.0<br>Production blasting<br><br>D = 0.7<br>Mechanical excavation |

Figure 29. Guides for estimating the disturbance factor D **[40]**

The adopted design: bored piles, is meant to cause minimal disturbance on the rock. Drilling is a type of mechanical excavation, for that reason, the factor D is set to 0.

The rock type in the site is mudstone. Consequently, conservatively, the minimum uniaxial compressive strength corresponding to claystone and siltstone in Figure 30 is selected: 25 MPa.

| Grade | Term | Uniaxial Compressive Strength (MPa) | Field estimate of strength | Examples |
|---|---|---|---|---|
| R6 | Extremely strong | > 250 | Specimen can be chipped with a geological hammer | Fresh basalt, chert, diabase, gneiss, granite quartzite |
| R5 | Very strong | 100 – 250 | Specimen requires many blows of a geological hammer to fracture it | Amphibolite, sandstone, basalt, gabbro, gneiss, granodiorite, limestone, marble, rhyolite, tuff |
| R4 | Strong | 50 – 100 | Specimen requires more than one blow of a geological hammer to fracture it | Limitstone, marble phyllite, sandstone schist, shale |
| R3 | Medium strong | 25 – 50 | Cannot be scraped or peeled with a pocket knife, specimen can be fractured with a single blow from a geological hammer | Claystone, coal, concrete schist, shale, siltstone |
| R2 | Weak | 5 – 25 | Can be peeled with a pocket knife with difficulty, shallow indentation made by firm blow with point of a geological hammer | Chalk, rocksalt, potash |
| R1 | Very weak | 1 – 5 | Crumbles under firm blows with point of a geological hammer, can be peeled by a pocket knife. | Highly weathered or altered rock |
| R0 | Extremely weak | 0.25 – 1 | Indented by thumbnail | Stiff fault gouge |

Figure 30. Field estimates of unconfined compressive stress σci **[40]**

In Figure 31 the intact rock parameter recommended for siltstone is 9 and for claystone 4. We select a value of 4. Beside the fact that the mudstone in the site is clayey, selecting a low value for this parameter is conservative, since the lower $m_i$ is, the lower $m_b$ will get, and therefore the smaller F will be for a certain stress state when using the Hoek-Brown criterion.

| Rock type | Class | Group | Texture | | | |
|---|---|---|---|---|---|---|
| | | | Coarse | Medium | Fine | Very Fine |
| SEDIMENTARY | Clastic | | Conglomerate (20) | Sandstone 19 | Siltstone 9 | Claystone 4 |
| | | | | Greywacke (18) | | |
| | Non-Clastic | Organic | | Chalk 7 | | |
| | | | | Coal (8-21) | | |
| | | Carbonate | Breccia (22) | Sparitic Limestone (10) | Micritic Limestone 8 | |
| | | Chemical | | Gypstone 16 | Anhydrite 13 | |
| METAMORPHIC | Non-Foliated | | Marble 9 | Hornfels (19) | Quartzite 24 | |
| | Slightly Foliated | | Migmatite (30) | Amphibolite (25-31) | Mylonites (6) | |
| | Foliated | | Gneiss 33 | Schists (4-8) | Phyllites (10) | Slate 9 |
| IGNEOUS | Light | | Granite 33 | | Rhyolite (16) | |
| | | | Granodiorite (30) | | Dacite (17) | |
| | | | Diorite (28) | | Andesite 19 | |
| | Dark | | Gabbro 27 | Dolerite (19) | Basalt (17) | |
| | | | Norite 22 | | | |
| | Extrusive Pyroclastic Type | | Agglomerate (20) | Breccia (18) | Tuff (15) | |

Figure 31. Values of constant mi by rock group **[40]**.

In the following paragraph, the Geological Strength Index is defined based on the information available on joint sets and the empirical relationships between Rock mass modulus and GSI measured by Hoek and Diederichs (2006) [41], using in situ measurements from China and Taiwan.

The fact that the joint sets are described as conjugate, dipping 54° NW and 36 ° SE, suggests that the structure of the block is neither intact nor excessively disturbed. Likewise, there are no direct data on the rock surface conditions. However, the site is next to the sea and highly seismic, having undergone recently relatively intense earthquakes [28], the rock is below groundwater level and it is close to the interface with soft soil. Given these considerations, the rock's structure is expectably blocky, with poor to very poor surface conditions. These correspond to a GSI of 50 to 25 in Figure 32.

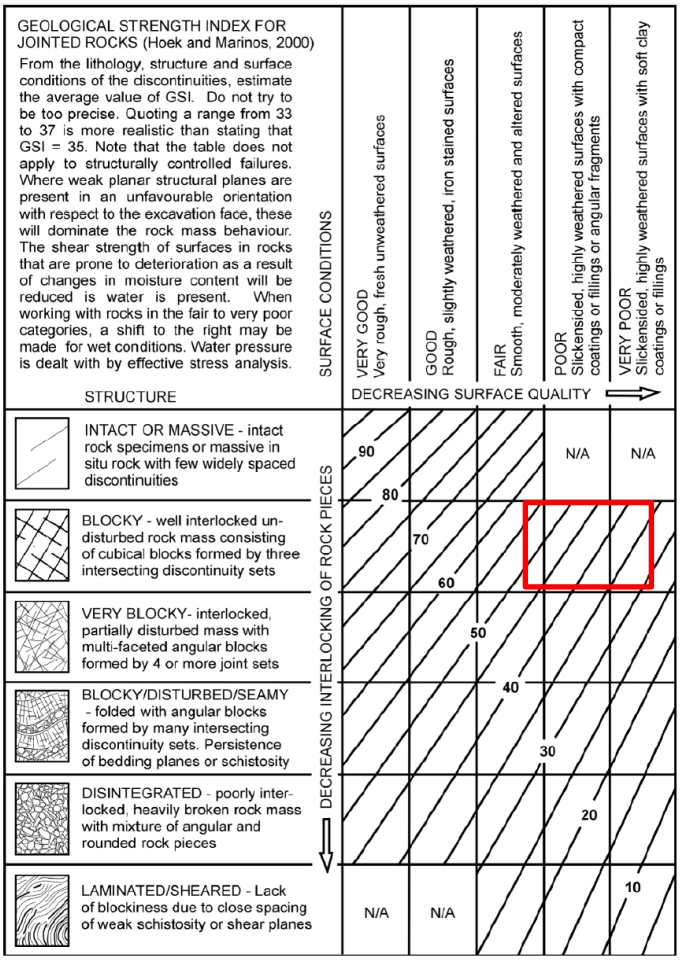


Figure 32. GSI for blocky rock masses on the basis of interlocking and joint conditions **[40]**

On the other hand, having defined the Young's modulus based on $V_p$ and $V_s$ it is possible to backcheck the value of GSI from empirical correlations. Figure 33 and Figure 34 show relations between GSI, D and E, from where GSI is deduced, and checked that it is in the order we have estimated.

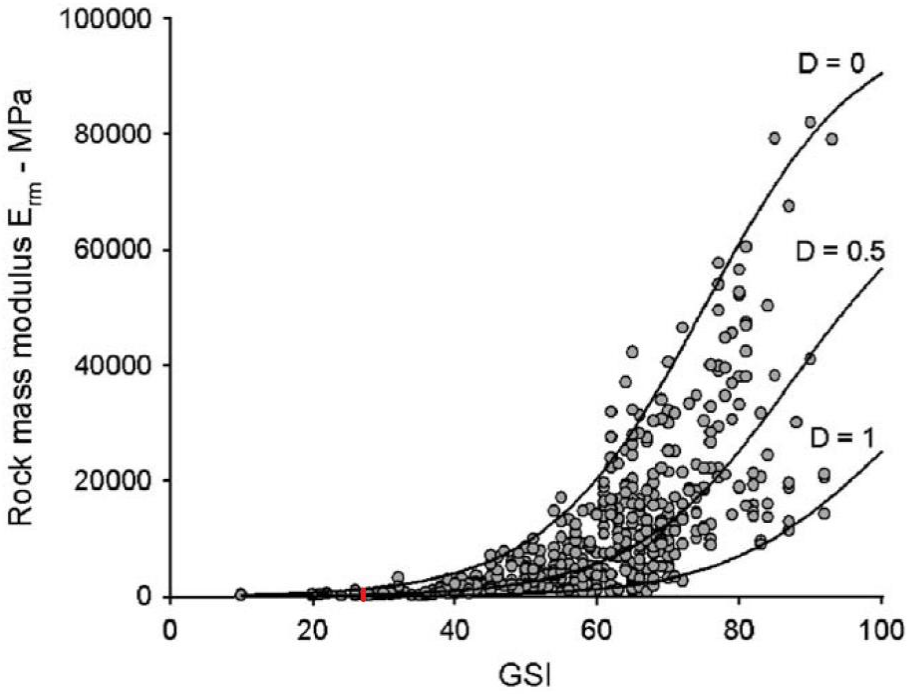


Figure 33. Plot of Simplified Hoek and Diederichs equation for Chinese and Taiwanese data **[41]**

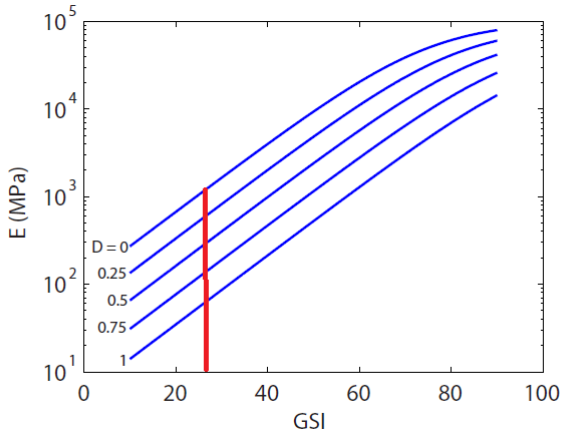


Figure 34. Variation of E with GSI according to OptumG2 users guide (allegedly coming from **[40]**)

Figure 34 and Figure 33 probably come from the same data source. Having checked GSI in both of them and obtained very similar values, between 25 and 30, increases the confidence in them. GSI is conservatively set to 25.

The FE software OptumG2 offers the possibility of setting the flow rule as associated or non-associated. When the flow rule is set as non-associated, a Coulomb plastic potential is defined best-fitting the Hoek-Brown failure surface and adding a tension cutoff. To have the Hoek-Brown surface, both as yield surface and plastic potential, an associated flow rule is defined.

#### 7.1.1.4 Fs in rock

A good approximation of the friction angle in rock would be the friction angle of a Coulomb failure surface that is the best fit to the Hoek-Brown that characterizes this rock. Figure 35 shows an example of such a fit.

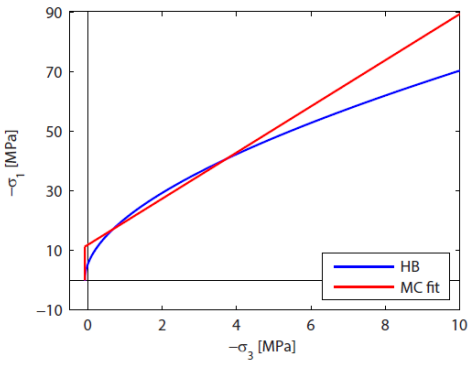


Figure 35. Coulomb fit into a Hoek-Brown surface **[39]**

However, since only one maximum frictional axial load per meter can be introduced due to the limitations of the model, this procedure doesn't need to be undertaken for the following logic. The maximum shear between piles and sand was defined as 4 KPa in the model. The undisturbed vertical stress at the top of the bedrock mass is in the order of (70m x 20 KPa/m) = 1.4 MPa. This means that the friction angle we are considering implicitly in rock is about $\varphi=\text{atan}(4/1400) = 0.16^{o}$, which is very low compared to what a fit of a Coulomb failure surface into a Hoek-Brown would result in. Consequently, setting a maximum axial shear of 4 kPa at the rock is conservative.

## 7.2 TECHNOLOGY SELECTION

The SMR NuScale [42] is selected as the technology to accommodate within the 18 m maximum diameter for an excavation to be cost effective.

## 7.3 REACTOR BUILDING FUNCTIONS AND BASIC SIZING

The reactor building functions based on the technology selected, can be summarized as follows:

- Since the NuScale reactor has its own steel containment integrated [42], the reactor building does not need to serve as a fission product barrier.
- The reactor building must mitigate a radiation release form the containment.
- The reactor building must allow transfer of its internals; permit inspection, maintenance and reshuffling operations; and ensure easy access for personnel.
- The reactor building must accommodate feed water and main steam penetrations [6].
- The reactor building must contain the emergency cooling water that surrounds the containment vessel ensuring a moderate leak rate [6].
- The reactor building must allow venting of the emergency cooling water surrounding the steel container.
- The reactor building serves as link in the support load path of the equipment inside.

Figure 36 shows the basic sizing of the reactor buildings conducted for this project on the KK site soil profile and an indication of the reactor surroundings. This basic sizing comes from the functions the building must perform (i.e. its design specification). In both cases, AG and BG, the reactor building consists of a moderately thick basemat, connected to bedrock via eight piles of 2 m diameter evenly distributed in the azimuthal direction at the edge of the basemat, as shown in Figure 37. The need to use pile foundations is justified in Appendix A, where it was calculated that the vertical settlement without them would reach about 6 cm. Since

the vertical earthquake loads are similar to the dead weight of the building, the settlement due to earthquake loads would be excessive without the implementation of a displacement reduction strategy. An initial cylindrical wall thickness of 1 m is defined. The basemat is set at 4 m thickness. An internal carbon steel liner provides leak tightness for keeping the water inside the building. The hemispherical head itself is a lid for introducing equipment and long maintenance operations. It has a small entry inserted in it, for more recurrent operations. The reactor vessel and all the systems accounting for a significant portion of the equipment mass inside the building are supported on a series of concrete or/and steel structures. These structures are anchored at the basemat. Feed water and main steam lines penetrate the reactor building below the elevation of the hemispherical lid. Four penetrations are on the liner and through the concrete wall for the feed water and main steam lines. A steel binding system accommodates and anchors one end of the vertical rebar. This binding system consists on evenly spaced shear keys with a small screw to prevent uplift. The plates where those screws lay allow certain differential radial expansion. The plates present discontinuities in the azimuthal directions to allow a robot or human arm to screw-unscrew a nut on the inside part of the plates. The shear keys present discontinuities as well on the azimuthal direction to allow the vapor inside the building, in an accidental condition when the emergency water boils, to vent out. A venting penetration is thus not needed. Figure 38 shows a conceptual vertical cross section of the binding system. The binding system and internal concrete structures of the building are designed as appropriate for preventing excessive neutron radiation to escape the building by means of concrete pieces inserted in steel casings when the emergency water boils off. In normal operation, the emergency water also functions as additional shielding for neutrons.

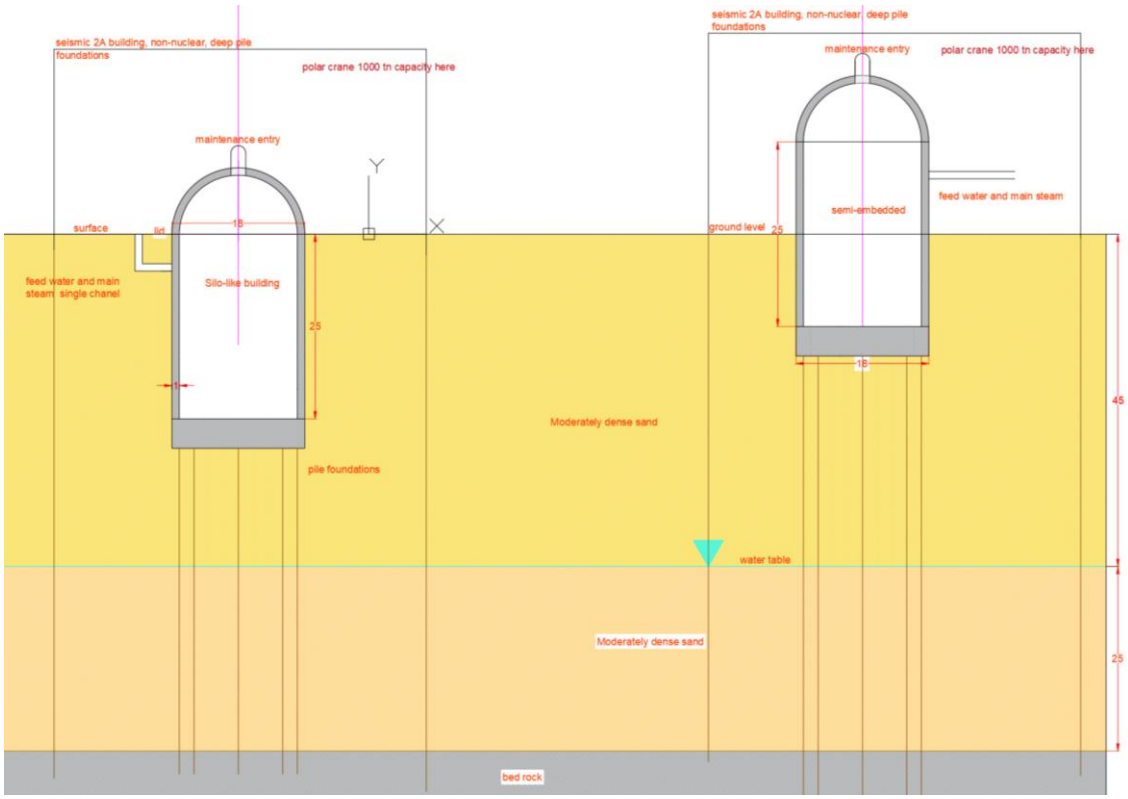


Figure 36. On the left: embedded design (BG), on the right: semi-embedded design (AG)

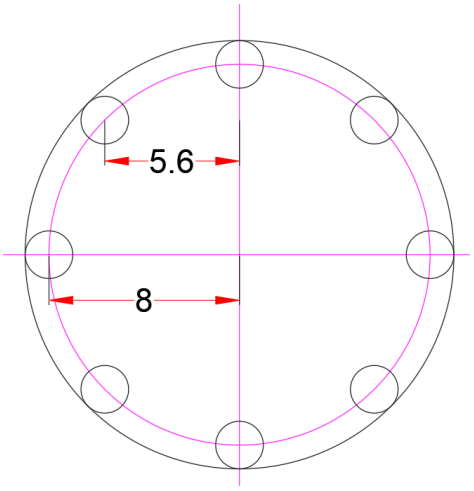


Figure 37. Basemat footprint

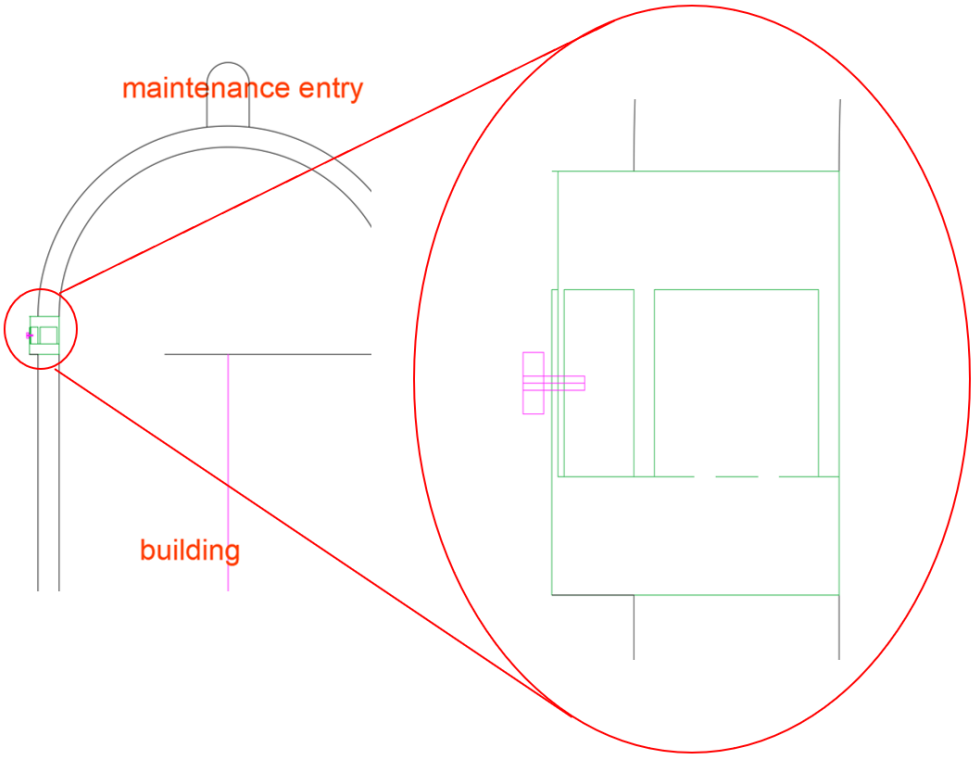


Figure 38. Reactor Building lid binding system: a screw (pink) connects two plates(green) that prevent uplift but allow relative radial displacements

## 7.4 LOADS DEFINITION

The different loads to consider as imposed in ASME III divII CC (2013) Table CC-3230-1 [19] are summarized herein.

### 7.4.1 Internal loads

- Dead loads D

The hydrostatic column of water in contact with the building plus the self-weight of the reinforced concrete and the liner. Figure 2 shows the level of the water free column relative to the containment vessel. This level coincides with the elevation of the lid bindings, i.e., the cylinder to hemisphere transition.

- Live loads L

  Live loads occur only during maintenance operations. Thus, no live load is considered.

- Loads resulting from prestress F

  No prestress load is considered.

- Loads resulting from relief valve opening G

  No loads from relief valve opening are considered.

- Thermal effects: NOC and accident To and Ta

  To is the room temperature and Ta the boiling temperature of water at 1 atm, 100 $^{o}$C.

- Pipe reactions: NOC and accident condition Ro and Ra

  Loads at the penetrations are not considered. It is assumed that a penetration type such as the one in Figure 39 can relieve the walls from thermal expansion and seismic loads, and can be installed.

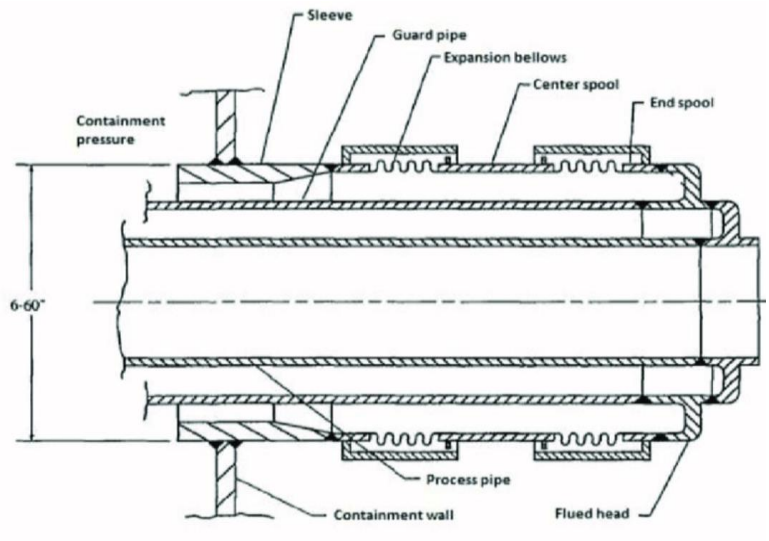


Figure 39. Example of bellows-sleeve system

- Accidental pressure $P_a$

  As the RB does not have a containment function, no accidental pressure is considered.

- Hydrostatic pressure $H_a$

  The containment vessel is flooded permanently during NOC. Thus this load is included as a dead load.

### 7.4.2 External loads

- Earthquake loads

  i. Earthquake loads are different for the AG and BG options. Only SSE is considered in both cases. OBE is assumed to be small enough to be covered by SSE.

  ii. Figure 40 shows the SSE accelerations at the basemats of units 1 and 7 at the Kashiwazaki-Kariwa NPP, and records from the 2007 earthquake [29]. The horizontal response spectra utilized in this work are based on those accelerations.

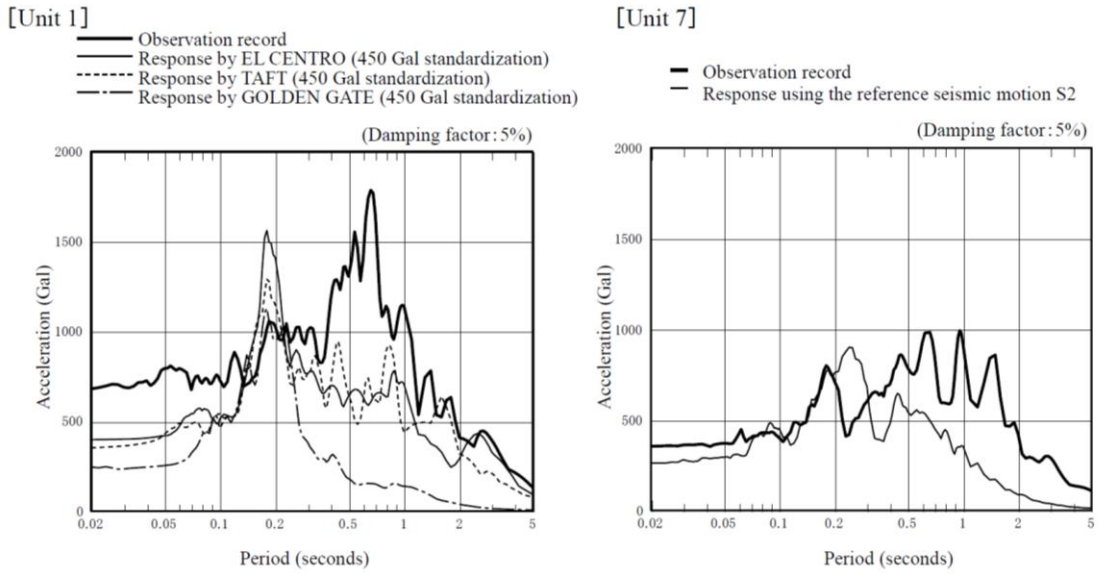


Figure 40. Comparison of observed records and design basis (EW direction) for the base mat of reactor buildings (units 1 and 7, see Figure 25 for orientation in map)[29]

a) The **upper bound (or increased FRS)** is defined as the average of these floor response spectra multiplied by 7.

b) The **lower bound (or average FRS)** is defined as the average of these response spectra.

c) The **Horizontal Enveloping FRS** is defined as the maximum response in unit 1(between the before 2007 design horizontal response spectrum and the corresponding to the Chuetsu-Oki earthquake) enveloped. The peaks are enveloped in accordance to ASCE 4-98 [24] (extending 15% in frequency the peaks) and then a factor of 1.4 is applied to account for bidirectionality (SRSS and 100-40-40, given the axisymmetric nature of the structure, RG_1.92[43] would yield the same result).

The horizontal response spectra for the three cases described above are shown in Figure 41. Horizontal earthquake accelerations are introduced in a single direction. Consequently, the accelerations in Figure 41 include the horizontal directional combination implemented. Equivalently, the average base mat FRS implicitly assumes that no directional combination is necessary. Since the structure can be assumed as axisymmetric for the analyses conducted, the Horizontal enveloping FRS includes directional combination and the increased FRS represents a scenario of a much larger design earthquake than the design FRS before 2007, such that the building needs to be so robust, achieved by increasing sections and hence stiffness, that the site natural modes of vibration define the vibration of the system.

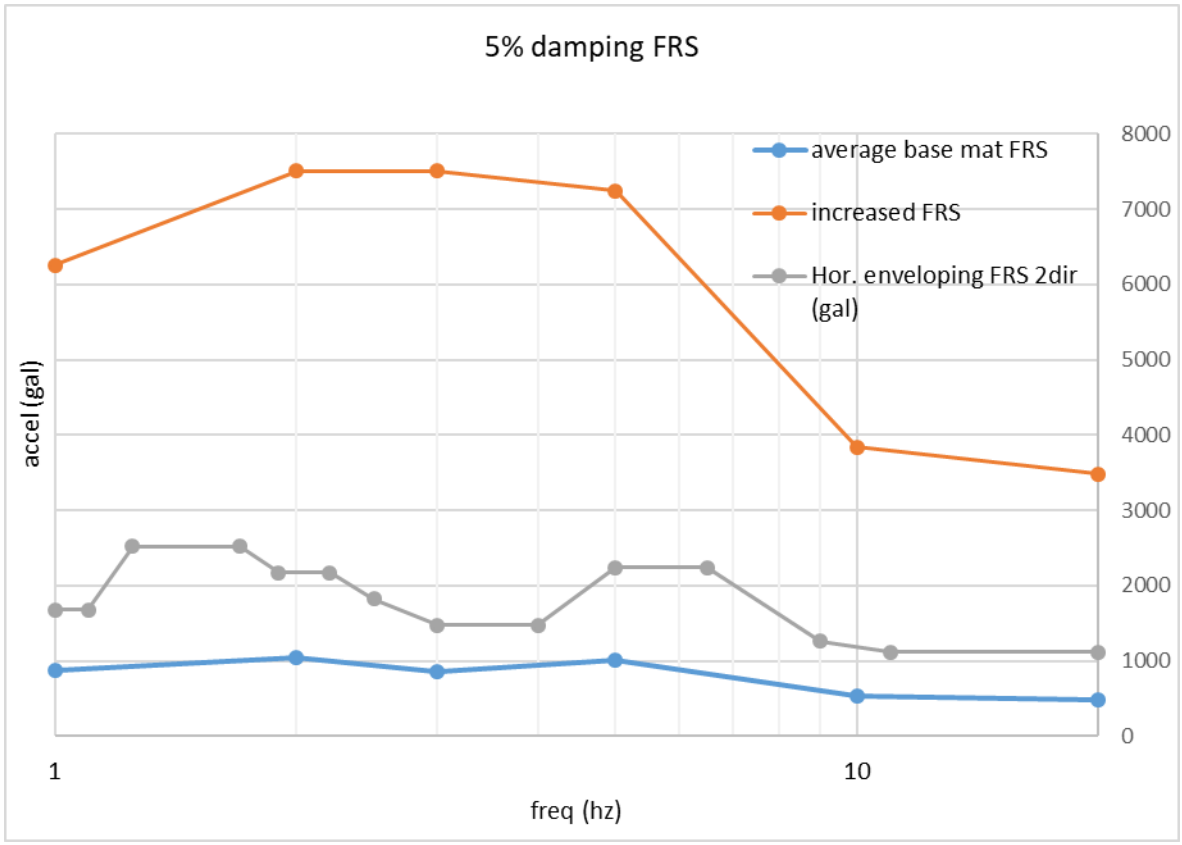


Figure 41. 5% damping FRS

iii. The whole fluid contribution to the FSI is considered impulsive. The convective natural period for a radius of 8.5 m and a fluid height of 25 m is about 4 seconds, which corresponds to a frequency of 0.25 Hz[44]. The accelerations corresponding to this frequency are lower in every case than for any frequency beyond 0.25 Hz (see Figure 40, period equal to 4 seconds). Assuming the steel containment and its surroundings resemble a cylindrical concentric obstacle, assessing the convective natural frequency of the system neglecting the obstacle has very little error[45]. Subsequently, assuming the whole response as impulsive is conservative.

iv. The SSI and the RB response are accounted for as follows. Based on ASCE 4-98[24], the static accelerations in the horizontal direction in the center of gravity, to be considered for the design of the RB wall, are obtained as follows:

a) The vibration frequencies assuming a rigid structure supported on springs representing the soil supporting medium is obtained.

b) The vibration frequencies of the AG building and BG building are obtained from a modal analysis by clamping them up to the surface minus 6 meters.

**Upper bound**

c) The CoG acceleration is the one at point ii)a above corresponding to the frequency that is the average value between point iv)a and point iv)b in the BG case. Both AG and BG cases are assumed to have the same acceleration at the center of gravity to represent the fact that the response is highly dependent on the site. This frequency is calculated at the first iteration and kept constant through the analysis.

**Lower bound and Horizontal Enveloping FRS**

d) The CoG acceleration is the one at point ii)b and point ii)c corresponding to the vibration frequency obtained at iv)a.

v. The accelerations at the center of gravity in the vertical direction are disregarded in the cylindrical part.

a) The building, the soil and the pile foundations are assumed stiff enough in the vertical direction to make the amplification negligible in the vertical direction.

b) The loads caused by the vertical accelerations are negligible compared to the stresses caused by loads in the horizontal direction.

c) The wall's mass over which the earthquake accelerations is applied in the vertical direction is lower than the mass over which the horizontal accelerations are applied, since no water added mass is taken into account in the vertical direction. The whole mass of the water contained in the building is applied in the horizontal direction.

vi. The accelerations at the center of gravity in the vertical direction are 1.1 g, included in the design of the foundations.

- External pressure loads resulting from pressure variations Pv

No external pressure variation is considered. It is assumed that the water table raise will not reach the level of the lid.

- Wind loads: design wind and tornadoes

The prescriptions on tornado loads in RG_1.76[30], and the loading combination to which it applies are included by airplane crash and earthquake load. Hence wind and tornado loads are not considered in the study.

- Earth pressure

A Passive condition is considered all-over the embedded portion of the building. Since the friction angle is 36º (Table 5), Kp=(1+sin(Φ))/(1-sin(Φ))= 3.85. Then the maximum horizontal stress t the bottom is given by:

$$\sigma_h = 3.85\sigma_v = 3.85 * 15\ KPa/m$$

- Airplane crash

Despite not being categorized as a design load, and not included in ASME III divII CC (2013) Table CC-3230-1 [19], airplane crash shall be taken into account in the design of new NPPs. A Boeing 767 crash is taken into account [46]. Local and global effects if the crash are discussed [27].

# 8. BUILDINGS DESIGN ASSUMPTIONS AND SIMPLIFICATIONS IN THE NUSCALE CALCULATIONS

The following set of building design assumptions were made:

- Tension cracks appear on the surrounding soil during earthquake. Half of the sand envelope resist in passive condition as illustrated in Figure 42. The rest is taken by the piles.

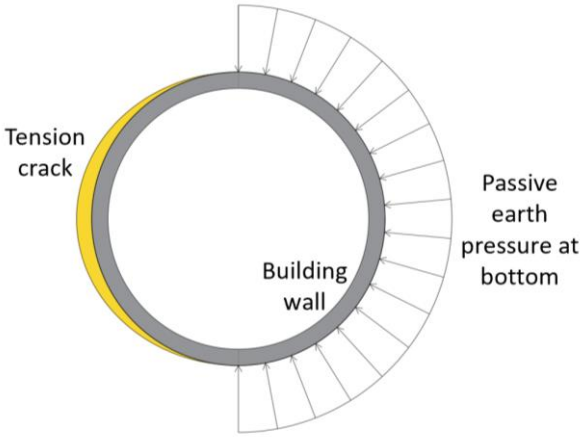


Figure 42. Pressures on wall during earthquake

- The vibration frequencies of the cylindrical wall are assumed decoupled from the containment vessel and its support.

- The lateral vibration mode of the cylindrical wall during earthquake rotates around the basemat: this is not exactly true, especially in the AG case, where the soil fails on the sides of the building, thus it fails at lower lateral bearing loads. This failure load depends on the vertical compressive stress on the soil, and the depth of the of embedment. Overall, this effect results in larger flexibilities of the AG design, larger rotating arms, larger moments and consequently the need of a sturdier foundation design, which is costlier than the BG one. Subsequently, it is conservative, in the current study, to proceed considering that both AG and BG cases rotate around the basemat.

- Loads at the penetrations are not considered. It is assumed that a penetration type such as the one in Figure 39 can relieve the walls from thermal expansion and seismic loads and can be installed. The analysis of the cylindrical wall is simplified by not considering the extra reinforcement that penetrations might need around the walls.

- The soil around the building is assumed to be competent in that it can take bearing pressures even though the soil stiffness is low. General geotechnical engineering good practice and Nuclear Codes,

such as ASCE4-98[24] discourage considering the weak soil around the building to take bearing pressures.

- The dynamic degradation of soil properties is not considered in the analysis.

- Radial shear demand is neglected since it is assumed to be only relevant in discontinuities, therefore, will be assumed to not have a major impact on final cost.

- Stresses at the discontinuities, such as penetrations, can be mitigated by local thickening, hence, their effect in cost is negligible.

- In the design of the cylindrical walls, the vertical earthquake is not considered. This simplification is based on the following:

    - No water added mass need to be considered in the cylindrical wall in the vertical direction. On the other hand, in the cylindrical wall, the whole mass of water is considered as added mass in the horizontal direction.

    - The building is much stiffer in the vertical direction than in the horizontal one and the vertical accelerations within the same order of magnitude as the horizontal accelerations[28].

- Convective effects due to sloshing are ruled out based on the logic exposed in 7.4.2.

- Effect of steel containment (quasi-cylindrical concentric obstacles) in FSI is neglected since gap between liner and obstacles is large[47] [48].

- Despite the fact that the Reactor Building of the NuScale reactor does not have the safety functions of a Containment, it is conservatively designed following the provisions for concrete containments set forth in ACI 359 [19]. The NuScale Reactor Building serves as support to the carbon steel liner, which has the function of preventing the water, that extracts the decay heat from the containment vessel, from leaking into the atmosphere. Since this is a safety function that normally is guaranteed by containments, it follows as prudent to base the design on ACI 359 [19] instead of on ACI 349 [49].

- Basemats are the same for AG and BG, since their amount of material is determined by the vertical earthquake load. The amount of water and concrete above the basemat, outside what remains atop the circumference of piles, shown in Figure 37, is the same for the AG and the BG designs.

- Shear is absorbed by hoop and meridional rebars.

## 8.1 LOADING CONDITIONS

ASME III code [19] indicates the load combinations to prove structural integrity against in the design of a Concrete containment. The load combination that drives the design of the cylindrical wall of the Reactor Building is considered the Abnormal/extreme environmental, marked in red in Table 6.

Table 6. ASME BPV CODE SECTION III, DIV 2, SUBSECTION CC LOAD COMBINATIONS AND LOAD FACTORS

| Category | $D$ | $L$ [Note (1)] | $F$ | $P_t$ | $G$ | $P_a$ | $T_t$ | $T_o$ | $T_a$ | $E_o$ | $E_s$ | $W$ | $W_t$ | $R_o$ | $R_a$ | $R_r$ | $P_v$ | $H_a$ |
|---|---|---|---|---|---|---|---|---|---|---|---|---|---|---|---|---|---|---|
| Service | | | | | | | | | | | | | | | | | | |
| Test | 1.0 | 1.0 | 1.0 | 1.0 | — | — | 1.0 | — | — | — | — | — | — | — | — | — | — | — |
| Construction | 1.0 | 1.0 | 1.0 | — | — | — | — | 1.0 | — | — | — | 1.0 | — | — | — | — | — | — |
| Normal | 1.0 | 1.0 | 1.0 | — | 1.0 | — | — | 1.0 | — | — | — | — | — | 1.0 | — | — | 1.0 | — |
| Factored | | | | | | | | | | | | | | | | | | |
| Severe environmental | 1.0 | 1.3 | 1.0 | — | 1.0 | — | — | 1.0 | — | 1.5 | — | — | — | 1.0 | — | — | 1.0 | — |
| | 1.0 | 1.3 | 1.0 | — | 1.0 | — | — | 1.0 | — | — | — | 1.5 | — | 1.0 | — | — | 1.0 | — |
| Extreme environmental | 1.0 | 1.0 | 1.0 | — | 1.0 | — | — | 1.0 | — | — | 1.0 | — | — | 1.0 | — | — | 1.0 | — |
| | 1.0 | 1.0 | 1.0 | — | 1.0 | — | — | 1.0 | — | — | — | — | 1.0 | 1.0 | — | — | 1.0 | — |
| Abnormal | 1.0 | 1.0 | 1.0 | — | 1.0 | 1.5 | — | — | 1.0 | — | — | — | — | — | 1.0 | — | — | — |
| | 1.0 | 1.0 | 1.0 | — | 1.0 | 1.0 | — | — | 1.0 | — | — | — | — | — | 1.25 | — | — | — |
| | 1.0 | 1.0 | 1.0 | — | 1.25 | 1.25 | — | — | 1.0 | — | — | — | — | — | 1.0 | — | — | — |
| Abnormal/severe environmental | 1.0 | 1.0 | 1.0 | — | 1.0 | 1.25 | — | — | 1.0 | 1.25 | — | — | — | — | 1.0 | — | — | — |
| | 1.0 | 1.0 | 1.0 | — | 1.0 | 1.25 | — | — | 1.0 | — | — | 1.25 | — | — | 1.0 | — | — | — |
| | 1.0 | 1.0 | 1.0 | — | 1.0 | — | — | 1.0 | — | 1.0 | — | — | — | — | — | — | — | 1.0 |
| | 1.0 | 1.0 | 1.0 | — | 1.0 | — | — | 1.0 | — | — | — | 1.0 | — | — | — | — | — | 1.0 |
| Abnormal/extreme environmental | 1.0 | 1.0 | 1.0 | — | 1.0 | 1.0 | — | — | 1.0 | — | 1.0 | — | — | — | 1.0 | 1.0 | — | — |

where:
D= dead loads, including hydrostatic and permanent equipment loads
L= live loads, including any moveable equipment loads and other loads that vary with intensity and occurrence, such as soil pressures
F= loads resulting from the application of prestress
G = loads resulting from relief valve or other high-energy device actuation
To = thermal effects and loads during normal operating or shutdown conditions, based on the most critical transient or steady state condition
Ro = pipe reactions during normal operating or shutdown conditions, based on the most critical or steady state conditions
Pv = external pressure loads resulting from pressure variations either inside or outside the containment
Pt=pressure during the structural integrity and leakage rate test
Tt=thermal effects and loading during test
W = loads generated by the design wind specific for the plant site
Eo = loads generated by the operating basis earthquake (only the actual dead load and existing live loads need to be considered in evaluating seismic response force)
Es = loads generated by the safe shutdown earthquake; weights considered shall be the same as for Eo
Wt = tornado loading including the effects of missile impact
Pa = design pressure load within the containment generated by the DBA
Ta = thermal effects and loads generated by the DBA including To
Ra = pipe reaction including thermal conditions generated by DBA, including Ro
Rr = local effects on the containment from DBA
Ha = loads resulting from flooding of containment following a DBA.

From the loads' definition, it follows that there is no L, F, G, $P_t$, $T_t$, $P_a$, $T_o$ and Ha to include. Also, from previously stated assumptions, Ra and Ro are ruled out. Tornado load (Wt) is included by earthquake and airplane crash loads, and the wind design load (W) by tornado load. It is assumed that $E_o$ is so small compared to Es, that the loading cases that contain Es include $E_o$. External pressure variation ($P_v$) is neglected. Therefore, the only design loads to consider at the design, are D, $E_s$, and $T_a$. Consequently, as Abnormal/extreme environmental load combination is the only one including the three of them, it is the only one analyzed in sizing the reactor building.

# 9. SIZING OF CYLINDRICAL WALL FOR NUSCALE BUILDING

In the first iteration, only the average basemat FRS (lower bound) and the increased FRS are considered. The sizing to include in the second iteration for the enveloping FRS is extrapolated from the first iteration's results. A 1 m thickness of concrete is considered for the walls of the reactor buildings, both in the embedded and semi-embedded case in the first iteration. The concrete wall thicknesses are redefined after the first iteration (see Table 7). The second iteration is conducted using these new thicknesses. Convergence is reached at the second iteration.

The material properties considered are as follows:

- The density considered in the structural parts is around 2300 kg/m³. This accounts for rebar and concrete. The density of steel is 3 to 4 times this of concrete, and the volume of reinforcing steel is limited to 10 %. This means that the maximum error regarding density of the structural parts is 28% underestimation, which is conservative, as are the most in need of reinforcement designs are the AG ones. This error is diminished by the increment of density in the cylindrical walls to account the added mass of water.

- The Young's modulus E, is assumed to be 30GPa, which again, neglects the contribution of steel. The contribution of steel, being limited to 8% in the densest direction, results in a maximum directional increment in Young's modulus of about +50%. The range of change, from +0 to +50% Young's modulus does not constitute a relevant change, since the most crowded walls will be the most underestimated, as it happens with density, and the loads defining the design are primary loads. This is, loads that cause stresses that are only Young's modulus dependent at structural discontinuities. Far from structural discontinuities primary loads are not Young's modulus dependent.

- The total Poisson's ratio considered, neglecting reinforcing steel is 0.18. The rebar has a yield limit of 410 MPa. The concrete has an uniaxial compressive strength of 35 MPa.

## 9.1 MODAL ANALYSES

The modal analyses are conducted by means of 3D shell FEM models representative in mass and stiffness. They have nodal displacements constrained in the 3 directions at the lower edge and in the radial direction on the cylindrical wall, up to 6m below the surface, as detailed in 7.4.2. Figure 43 indicates the constrains applied in each model.

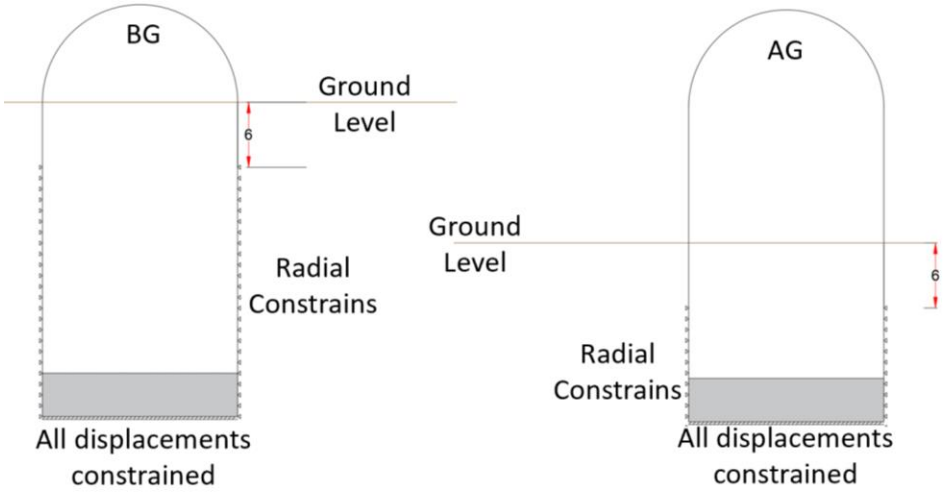


Figure 43. Constrains applied in each of the models for assessing natural frequencies

Flexible building-rigid soil

The modal shape of the first mode of vibration in the horizontal direction and its natural frequency for the BG case-1st iteration case are shown in Figure 44.

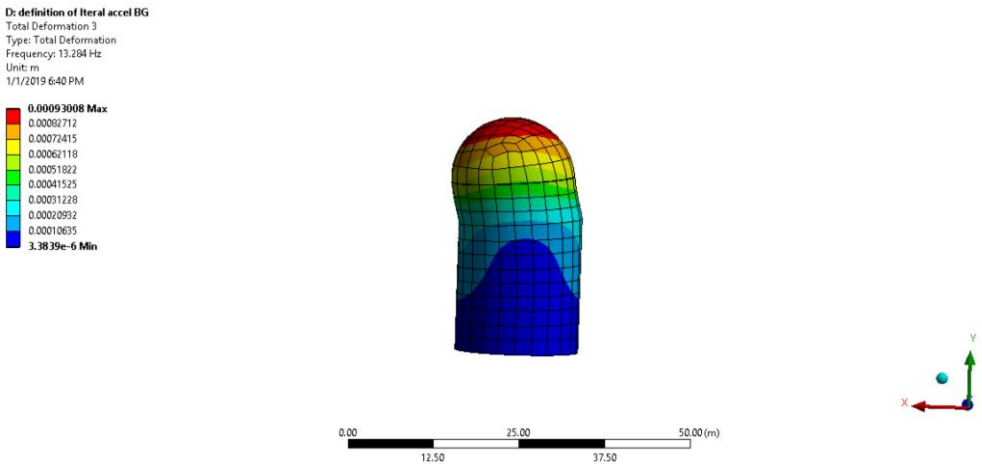


Figure 44. Modal analysis BG-1st iteration

Flexible soil-rigid building

$$Kx = \frac{32(1-\nu)GR}{7-8\nu} = 2882\ MN/m$$

The total mass of the building is estimated in 13,000 Tn, then the horizontal vibration frequency is:

$$f = 1/(2\pi)\sqrt{\frac{Kx}{m}} = 2.3\ Hz$$

Subsequently, the frequency considered for estimating the acceleration at the center of gravity for the "Increased FRS" cases is (2.2+13.2)/2 =15.5/2=7.75 Hz.

Using the same models as in the first iteration, varying the wall thicknesses and densities to represent the new size and water added mass as per Table 7, modal analyses were carried out. Then the newly computed accelerations were introduced statically in the structural models, with the wall thicknesses and densities modified.

Table 7. Variation of cylindrical wall concrete density to represent added mass for each of the earthquake cases, "average base mat FRS", "Enveloping FRS" and "Increased FRS"; and degrees of embedment, BG and AG.

| cylindrical wall thickness (m) | ρ factor | ρ model (kg/m3) | FEM model (2nd iteration) | FEM model (1st iteration) |
|---|---|---|---|---|
| 0.5 | 4 (approx) | 11500 | Avg basemat FRS (both) and Enveloping FRS (BG) | |
| 1 | 2.5 | 5750 | Enveloping FRS (AG) | all |
| 1.5 | 2 | 4600 | Increased FRS (BG) | |
| 3 | 1.5 | 3450 | Increased FRS (AG) | |

Table 8 describes the response accelerations introduced in the second iteration. They are marked in Figure 45. The response accelerations computed are approximated with a precision of 0.1 g. The frequencies in Table 8 stem from the modal analysis with the thicknesses and densities of the walls updated as per Table 7.

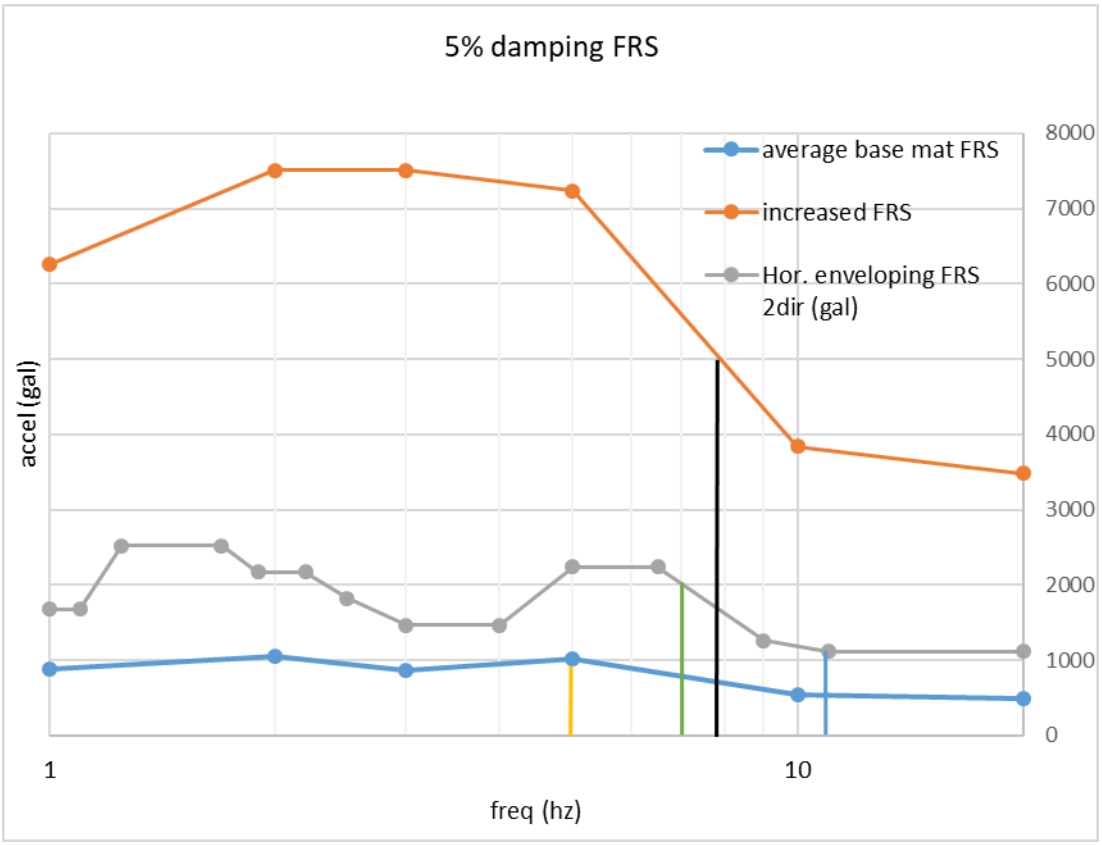


Figure 45. Response accelerations-second iteration

Table 8. static accelerations-input for the stress analysis

| | | Avg basemat FRS | Hor. enveloping FRS | Increased FRS |
|---|---|---|---|---|
| AG | color in figure intersection | yellow-blue | green-gray | black-orange |
| | freq (hz) | 5.5 | 7 | 7.75(site&building BG) |
| | accel (g) | 1 | 2 | 5 |
| | Assumptions | building decoupled 1dir | building decoupled 2dir | Follow ASCE 4-98 and make simplificaitons |
| | Key data source | Chuetsu-OKI + before 2007 FRS @ u1 & u7 | Chuetsu-OKI + before 2007 FRS @ u1 | Avg Basemat FRS |
| BG | color in figure intersection | blue-blue | blue-gray | black-orange |
| | freq (hz) | 11 | 11 | 7.75(site&building BG) |
| | accel (g) | 0.5 | 1 | 5 |
| | Assumptions | building decoupled 1dir | building decoupled 2dir | Follow ASCE 4-98 and make simplificaitons |
| | Key data source | Chuetsu-OKI + before 2007 FRS @ u1 & u7 | Chuetsu-OKI + before 2007 FRS @ u1 | Avg Basemat FRS |

## 9.2 SIZING OF THE CYLINDRICAL WALL AND COST ESTIMATION

### 9.2.1 FE models

Three FEA models in ANSYS are developed to compute the stresses in the cylindrical part of the building that affect the volumes of steel and concrete in the cylindrical wall. These models are a 3D shell model for computing the seismic stresses and two axisymmetric models, one for computing stresses caused by Ta, and the other for computing the stresses caused by D loads (gravity acceleration + water pressure) plus earth pressures. Figure 46 shows the FE models.

The 3D shell model includes the effect of the sand preventing the movement of the building in the horizontal direction, in passive failure state of stresses. The lower edge has its 3 displacements ($u_x$, $u_y$ and $u_z$) constrained. The models shown in Figure 46 correspond to the BG case-increased FRS case. The models for the AG average base mat FRS and increased FRS are analogous, except for the fact that the earth pressures in the former are not in the passive state when the total moment about the lower edge reverts the direction caused by earthquake. In these cases, a constant lateral pressure is applied such that moments are balanced.

In the Ta model it is assumed that the lower edge is constrained only in the vertical direction, whereas in the pressure model (hydrostatic of water inside the building + earth pressure at passive failure), both directions $u_r$ and $u_z$) are constrained.

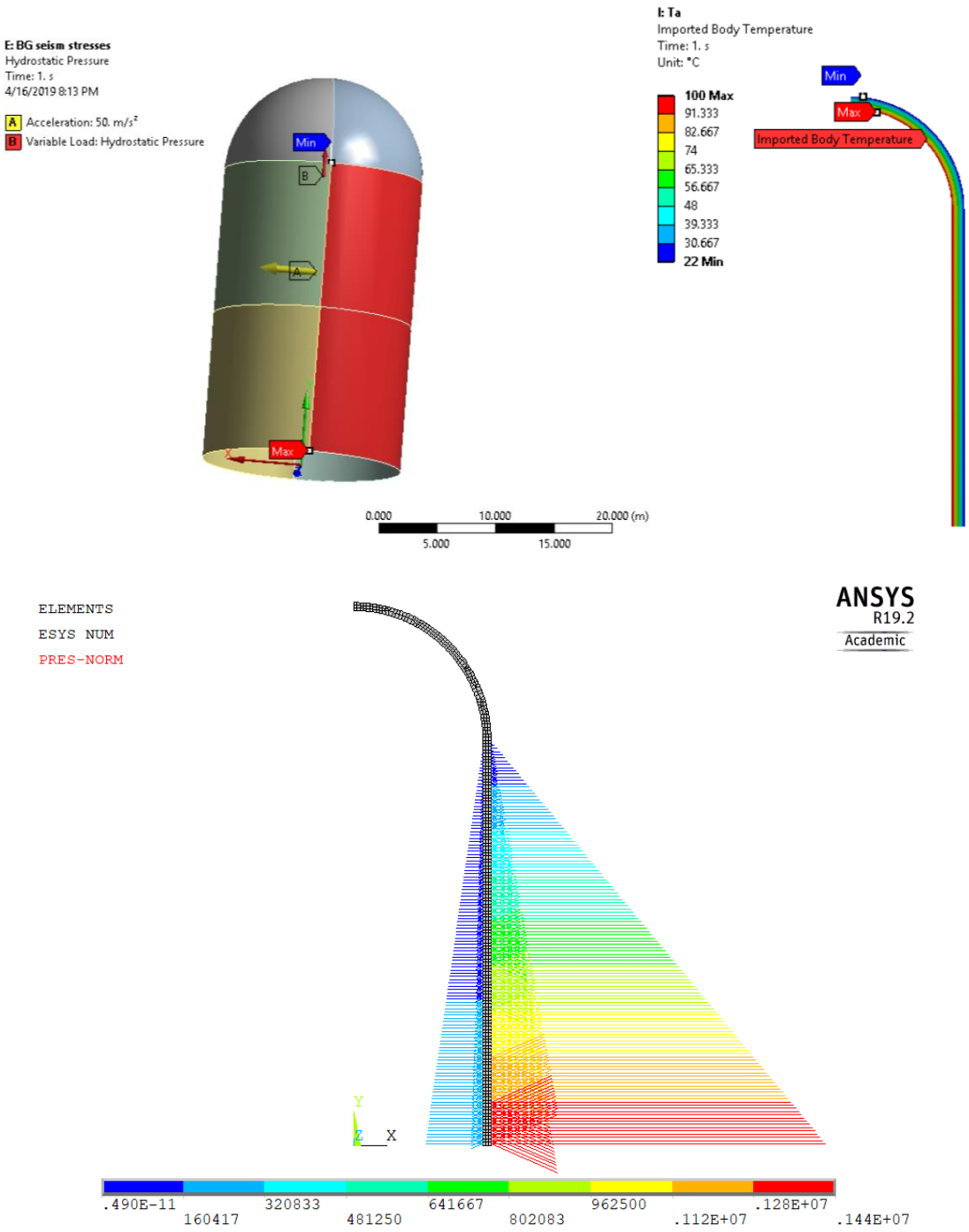


Figure 46. FE models. Top left: Seismic stresses model, in red the surface affected by earth pressures. Top right: Accidental temperature model. Bottom: Load D, pressure from the water inside the building and the soil in passive failure state.

### 9.2.2 Results

From the analyses carried out it follows that:

- Crushing of the concrete is strongly dependent on the dead load case in the BG design (earth pressures).

- , $T_a$ causes tensile stresses that can hardly be absorbed by adding steel reinforcement. However, as they are thermal stresses they are self-relaxing. They will make the concrete crack locally and the steel yield, but that doesn't compromise the structural integrity of the system or its proper function[49].

- Hoop and vertical tension; and shears are driven by the earthquake loads in both cases.

The airplane crash is not a dominating load. The engines are assumed to be 100 inches (2.5 m) diameter and 4000 lb (about 2 metric tons). Local effects are ruled out by means of the NEI formulas[27], assuming 500 ft/s velocity at impact. The resulting required depth to avoid perforation is 0.9 m, and as long as there is a liner, scabbing can be ruled out, since the liner prevents concrete chunks from detaching from the internal wall. Consequently, if the internal structures supporting the containment vessel (assumedly 0.4 m thick) are lined to avoid scabbing, the minimum thickness the cylindrical wall needs to have is 0.5 m. This minimum thickness is already included as such in the study for coping with earth pressures. Regarding global effects, the peak of a force time history [46] scaled with a dynamic factor of 2 (that includes all the dynamic factors [50]) results in a load at the base about 4 times this of horizontal earthquake in the lowest acceleration scenario (BG, Avg basemat FRS). However, as this is a "beyond design" load, the material properties can be considered up to the limit, therefore the extra margin provided by the ultimate to yield strength of the steel reinforcement added to the tensile strength of the concrete (about 1/10 the compressive strength) make this load included by earthquake even for the weakest of the designs.

All the AG models mobilize the full passive resistance of the soil for coping with the design earthquake. Among the BG cases, only the one corresponding to the increased FRS scenario does mobilize the full passive resistance of the soil. In the BG case, the minimum concrete thickness is determined by the earth pressures (in compression), to about 0.5 m. In this case, both, the compression resistance of the concrete and that of the hoop reinforcement are mobilized. Figure 47 shows the hoop compressive stress due to earth pressures in the BG case, 0.5 m thickness, up to a maximum compressive stress of 17.9 MPa. At the bottom of the element, in the part that represents the junction with the base mat, we can appreciate a local effect. This is an example of location where by increasing the thickness locally, we would manage to relieve these local effects:

- Some of them are self-relieving, the concrete will crack locally, the steel reinforcement elongates, and the stresses will relax.

- The ones where relaxation cannot happen by cracking do not require large volume of concrete and reinforcement for reducing them to acceptable limits. This happens because their locations are limited to the areas around penetrations, and the junction with the basemat, which are much smaller in surface than the areas far from discontinuities subsequently their effect on cost is negligible.

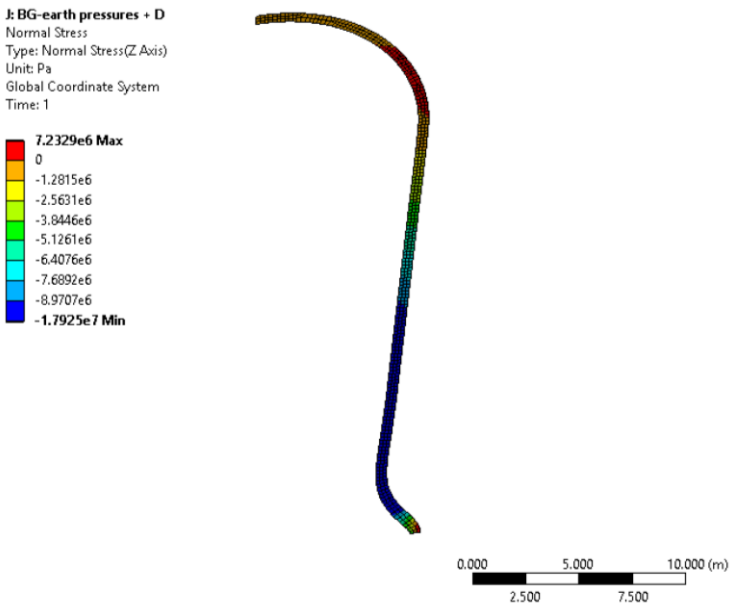


Figure 47. Hoop stress due to earth pressures (scaled deformed shape)

In Table 9 The results are expressed in the form of load/area as opposed to stresses, because the results of the analyses are not stresses directly in the reinforced building. Tensile loads are transmitted by the steel reinforcement, and hence the result is expressed in terms of load absorption in the steel reinforcement, per square meter of concrete. In Table 9 , $A_{sh}$ + $A_{si}$ and $A_{sm}$ + $A_{si}$ stand for density of reinforcement needed to cope with loads in the meridional or horizontal directions. Number of bars/m² gives an idea of how many # 11 stirrups, (1.41 in² each (0.00091 m²)) are necessary to fulfill the reinforcement areas requirements. It is to note that the number of bars and reinforcement areas in Table 9, are referred to needs. Given the fact that the vertical rebars are anchored at the ring hosting the shear keys that connect the lid and the cylindrical wall (section 7.4), the vertical rebars need to be continuous along the entire height of the cylindrical wall. For this reason, when computing the cost addition caused by the vertical rebars, the highest density in the 4 sectors is considered, i.e., the rebars in the building corresponds to rebar of the region where the rebar density is the highest.

In accordance to ASCE 4-98, radial stresses require reinforcement whenever there is no tension or compression stresses, above a threshold of 1.7 MPa. The threshold value varies whenever there is tension or compression stresses. In the AG models the radial shear (out-of-plane) is in the order of a few MPa around the junction with the base mat and close to 0 elsewhere. The radial shear (out-of-plane) is generally higher in in the BG models than in the AG ones (Table 9). Radial reinforcement would be thus needed in the BG cases. However, to simplify the study, it is not provided. The cases in which radial shear reinforcement would be clearly needed are marked in Table 9 with a question mark.

We can deem that convergence is reached in this iteration. The “increased FRS” reinforcement densities and the “enveloping FRS” AG density are above the 6% target established. At the increased FRS, both have similar reinforcement, therefore they are coherent. For targeting 6% reinforcement, the AG would need to increase thickness more than the BG one, hence it is conservative in determining whether embedment is worthy. The same logic applies to the AG “enveloping FRS” with respect to the BG one. The “average base mat FRS” AG case has a steel reinforcement density of about 6%. The remaining BG cases have a density way below the target 6%, but as they are dominated by crushing, and it is more efficient (and cheap) to resist compressive stresses with concrete than with rebar steel, they can be considered to have converged as well.

# Table 9. Reinforcement and cost evaluation in the 2nd iteration

| Load/Area (MN/(1 m circ)*th) units=MPa | | | | | Reinforcement areas (m²/m²) | | | Number of # 11 bars/m² | | Volume fraction | | Volume gross | Volume steel | Volume | Cost |
|---|---|---|---|---|---|---|---|---|---|---|---|---|---|---|---|
| region | out of plane | in-plane | hoop | meridional | Ash+Asi | Asm+Asi | Ar | i+h | m+i | horizontal | meridional | (m³) | (m³) | concrete (m³) | (labor+material) |
| 2nd iteration: **average base mat FRS** | | | | | | | | | | | | | | | |
| Semi-Embedded (AG) (seismic accel= 1 g **th = .5 m**) | | | | | | | | | | | | | | | |
| 1 | 0 | 1 | 2.2 | 1 | **0.012** | **0.006** | - | 14 | 8 | 0.012 | 0.039 | 172 | 9 | 163 | |
| 2 | 0 | 2 | 2.7 | 2 | **0.016** | **0.013** | - | 18 | 15 | 0.016 | 0.039 | 172 | 10 | 162 | |
| 3 | 0.1 | 3 | 2.5 | 4 | **0.017** | **0.024** | - | 19 | 27 | 0.017 | 0.039 | 172 | 10 | 162 | |
| 4 | 3 | 3 | 3.5 | 7 | **0.022** | **0.039** | ? | 24 | 44 | 0.022 | 0.039 | 172 | 11 | 161 | |
| Embedded (BG) (seismic accel=.5 g **th = .5m**) | | | | | | | | | | | total AG | 687 | 39 | 649 | $ 1,811,622 |
| 1 | 0.4 | 1 | 1 | 1.25 | **0.006** | **0.008** | - | 8 | 9 | 0.006 | 0.018 | 172 | 4 | 168 | |
| 2 | 0.4 | 1 | 1.5 | 1.25 | **0.009** | **0.008** | - | 10 | 9 | 0.009 | 0.018 | 172 | 5 | 167 | |
| 3 | 0.4 | 2 | 2.5 | 0.75 | **0.015** | **0.008** | - | 17 | 9 | 0.015 | 0.018 | 172 | 6 | 166 | |
| 4 | 4 | 4 | 3.5 | 2.2 | **0.024** | **0.018** | ? | 27 | 21 | 0.024 | 0.018 | 172 | 7 | 165 | |
| | | | | | | | | | | | total BG | 687 | 22 | 665 | $ 1,218,143 |

| Load/Area (MN/(1 m circ)*th) units=MPa | | | | | Reinforcement areas (m²/m²) | | | Number of # 11 bars/m² | | Volume fraction | | Volume gross | Volume steel | Volume | Cost |
|---|---|---|---|---|---|---|---|---|---|---|---|---|---|---|---|
| region | out of plane | in-plane | hoop | meridional | Ash+Asi | Asm+Asi | Ar | i+h | m+i | horizontal | meridional | (m³) | (m³) | concrete (m³) | (labor+material) |
| 2nd iteration: **Enveloping FRS** | | | | | | | | | | | | | | | |
| Semi-Embedded (AG) (seismic accel=2g **th = 1 m**) | | | | | | | | | | | | | | | |
| 1 | 0 | 1 | 1.2 | 1 | **0.007** | **0.006** | - | 9 | 8 | 0.007 | 0.061 | 334 | 23 | 311 | |
| 2 | 0 | 2 | 1.2 | 3 | **0.010** | **0.018** | - | 11 | 20 | 0.010 | 0.061 | 334 | 24 | 310 | |
| 3 | 0.1 | 4 | 1.2 | 6 | **0.014** | **0.036** | - | 16 | 40 | 0.014 | 0.061 | 334 | 25 | 309 | |
| 4 | 1 | 4 | 1.2 | 11 | **0.014** | **0.061** | ? | 16 | 68 | 0.014 | 0.061 | 334 | 25 | 309 | |
| Embedded (BG) (seismic accel=1 g **th = .5m**) | | | | | | | | | | | total AG | 1335 | 97 | 1238 | $ 4,287,478 |
| 1 | 0.8 | 1 | 1 | 2.5 | **0.006** | **0.014** | - | 8 | 16 | 0.006 | 0.028 | 172 | 6 | 166 | |
| 2 | 0.8 | 1 | 1.5 | 2.5 | **0.009** | **0.014** | - | 10 | 16 | 0.009 | 0.028 | 172 | 6 | 165 | |
| 3 | 0.8 | 2 | 2.5 | 1.5 | **0.015** | **0.011** | - | 17 | 12 | 0.015 | 0.028 | 172 | 7 | 164 | |
| 4 | 4 | 4 | 3.5 | 4.5 | **0.024** | **0.028** | ? | 27 | 32 | 0.024 | 0.028 | 172 | 9 | 163 | |
| | | | | | | | | | | | total BG | 687 | 29 | 658 | $ 1,463,346 |

| Load/Area (MN/(1 m circ)*th) units=MPa | | | | | Reinforcement areas (m²/m²) | | | Number of # 11 bars/m² | | Volume fraction | | Volume gross | Volume steel | Volume | Cost |
|---|---|---|---|---|---|---|---|---|---|---|---|---|---|---|---|
| region | out of plane | in-plane | hoop | meridional | Ash+Asi | Asm+Asi | Ar | i+h | m+i | horizontal | meridional | (m³) | (m³) | concrete (m³) | (labor+material) |
| 2nd iteration: **increased FRS** | | | | | | | | | | | | | | | |
| Semi-Embedded (AG) (seismic accel= 5 g **th = 3 m**) | | | | | | | | | | | | | | | |
| 1 | 0 | 2 | 1.5 | 1 | **0.011** | **0.009** | - | 12 | 10 | 0.011 | 0.080 | 884 | 80 | 804 | |
| 2 | 0 | 4 | 1.5 | 4 | **0.016** | **0.026** | - | 18 | 29 | 0.016 | 0.080 | 884 | 84 | 799 | |
| 3 | 0.1 | 6 | 1 | 8 | **0.019** | **0.048** | - | 21 | 54 | 0.019 | 0.080 | 884 | 87 | 796 | |
| 4 | 1 | 7 | 2.5 | 14 | **0.027** | **0.080** | ? | 30 | 88 | 0.027 | 0.080 | 884 | 94 | 789 | |
| Embedded (BG) (seismic accel=5 g **th = 1.5m**) | | | | | | | | | | | total AG | 3534 | 346 | 3189 | $ 14,499,722 |
| 1 | 1 | 2 | 1.5 | 1 | **0.011** | **0.009** | - | 12 | 10 | 0.011 | 0.078 | 486 | 43 | 443 | |
| 2 | 1 | 4.5 | 1.5 | 5 | **0.017** | **0.032** | - | 19 | 35 | 0.017 | 0.078 | 486 | 46 | 440 | |
| 3 | 1 | 5 | 1 | 8 | **0.016** | **0.047** | - | 19 | 52 | 0.016 | 0.078 | 486 | 46 | 440 | |
| 4 | 1.6 | 5.5 | 2.5 | 14 | **0.023** | **0.078** | ? | 26 | 86 | 0.023 | 0.078 | 486 | 49 | 437 | |
| | | | | | | | | | | | total BG | 1944 | 184 | 1759 | $ 7,774,141 |

# 10. FOUNDATIONS DESIGN IN THE NUSCALE CALCULATIONS

The foundations are designed based on FEA. The FE analyses are not representative of the actual physical properties of the Foundations for their sizing, however, they are conducted in a manner as to be possible to extrapolate to the actual building. The type of foundation selected is a pile foundation, which is how the ones at the NPPs at KK are designed currently. The solution devised herein is not necessarily the optimal solution, but one among the many that probably are feasible.

Two-meter diameter drilled reinforced concrete piles are modelled to represent the piles foundations depicted in Figure 37. This does not exclude employing a different geometry and/or type of pile, still based on the results from this analysis.

Up to this point, it has been checked that earthquake together with dead weight loads define the design. The loads at basemat stem from the soil structure interaction. In the vertical direction, they come from dead weight plus/minus the vertical earthquake load defined in section 7.4.2. In the horizontal direction, both shear and moment loads on the basemat, come mainly from the reactions that the soil around the cylindrical wall is not able to absorb due to reaching failure condition, i.e., remanent loads. These horizontal loads are indicated in Figure 48.

Lower Bound:

Semi-Embedded:

- Shear=41MN
- Tilting moment= 1185MN·m

Embedded:

- Shear= 0 MN
- Tilting moment= 0 MN·m

Upper Bound:

Semi-Embedded:

- Shear=581.25 MN
- Tilting moment= 7935 MN·m

Embedded:

- Shear= 285 MN
- Tilting moment= 1260 MN·m

Enveloping FRS

Semi-Embedded:

- Shear= 161 MN
- Tilting moment= 2685 MN·m

Embedded:

- Shear= 0 MN
- Tilting moment= 0 MN·m

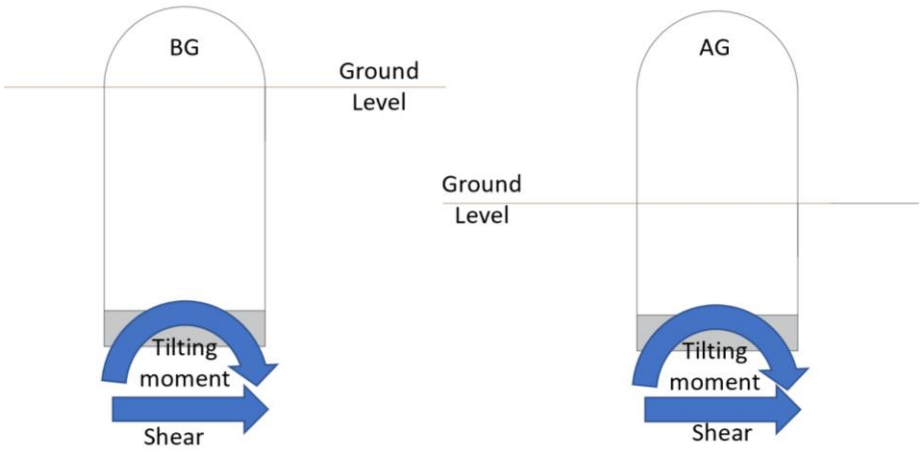


Figure 48. Loads at the piles

## 10.1 PRELIMINARY SIZING OF FOUNDATIONS

The piles reach the bedrock layer to prevent excessive settlements to occur. Provided they are robust enough, they will have no problem in taking the moment and lateral loads via lateral reactions from the sand that surrounds them. The friction coefficient between piles and soil is so low that requires a large surface to absorb the uplift forces (friction force is 4 kPa). From 7.4.2 it follows that the total uplift forces are 14 MN. Since the friction between piles and soil is capped at 4 kPa (see section 7.1.1.1), a total pile area of 3500 m² is required to absorb the uplift load. Dividing 3500 m² over 8 piles of diameter 2 meter, gives roughly 70 m (3500/(2πRn)=69.6 m). Based on the previous logic, 70 m is the length of piles required both for the AG and the BG designs.

## 10.2 FE MODEL OF FOUNDAITONS

A FE model is developed in OPTUM G2 for assessing the structural integrity of the piles and ensuring that the displacements caused by the earthquake are not excessive. Since the purpose of this analysis is to size the piles, the basemat is modelled as rigid, which is an acceptable representation for assessing loads on the piles.

For saving modeling and computational time, a plane-strain model is adopted, that represents conservatively the piles-basemat-soil-rock interaction regarding the piles. It is based on assumptions that preserve the contributions to area and moment of inertia, of piles and basemat, in a conservative manner for sizing the piles. For meeting this purpose, the next set of relations need to be true. First, the contributions to area and to moment of inertia of the basemat and the piles at the conservative equivalent system, shall be lower than those at the real system, so total load and moments are higher on the piles. Second, the relation of contributions of a real to any equivalent system, shall be lower at the basemat than at the piles, for both the area and moment of inertia. So the proportions of loads and moments absorbed by the piles is higher in the equivalent system than in the real system. These relations are expressed mathematically in the next lines:

$$I_{basemat} \geq I_{basemat,eq}$$
$$A_{basemat} \geq A_{basemat,eq}$$

$$I_{piles} \geq I_{piles,eq}$$
$$A_{piles} \geq A_{piles,eq}$$
$$\frac{I_{piles,eq}}{I_{piles}} \geq \frac{I_{basemat,eq}}{I_{basemat}}$$
$$\frac{A_{piles,eq}}{A_{piles}} \geq \frac{A_{basemat,eq}}{A_{basemat}}$$

The following layout complies with the 6 previous relations:

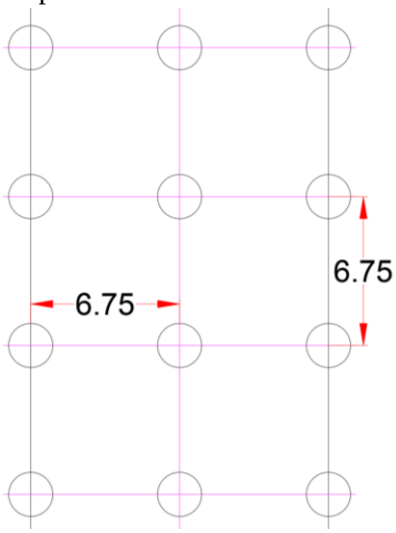


Figure 49. Equivalent system

Note that the equivalent contributions are written in terms of a distance of 18 m (the diameter of the basemat) in the direction perpendicular to the modeling plane. The set of relationships from before are verified below. $A_p$ represents the cross section of a single pile:

$$I_{basemat} \geq I_{basemat,eq} \rightarrow \frac{1}{16}\frac{1}{4}18^4\pi \geq \frac{1}{12}18^4(6/8)^3$$
$$A_{basemat} \geq A_{basemat,eq} \rightarrow \frac{18^2\pi}{4} \geq 18^2(6/8)$$
$$I_{piles} \geq I_{piles,eq} \rightarrow 4A_p 8^2 \geq 5.33A_p(18 \times 3/8)^2$$
$$A_{piles} \geq A_{piles,eq} \rightarrow 8A_p = 8A_p$$
$$\frac{I_{piles,eq}}{I_{piles}} \geq \frac{I_{basemat,eq}}{I_{basemat}} \rightarrow \frac{5.33A_p(18 \times 3/8)^2}{4A_p 8^2} \geq \frac{\frac{1}{12}18^4(6/8)^3}{\frac{1}{16}\frac{1}{4}18^4\pi}$$
$$\frac{A_{piles,eq}}{A_{piles}} \geq \frac{A_{basemat,eq}}{A_{basemat}} \rightarrow \frac{8A_p}{8A_p} \geq \frac{18^2(6/8)}{\frac{18^2\pi}{4}}$$

An elastoplastic analysis using second order triangular elements is carried out. Two models are generated, one for the semi-embedded design (AG), and another for the totally embedded one(BG). Both have the same length of piles (70 m) but different sand layer thicknesses, based on the distance to the rock layer. Figure 50 shows their meshes:

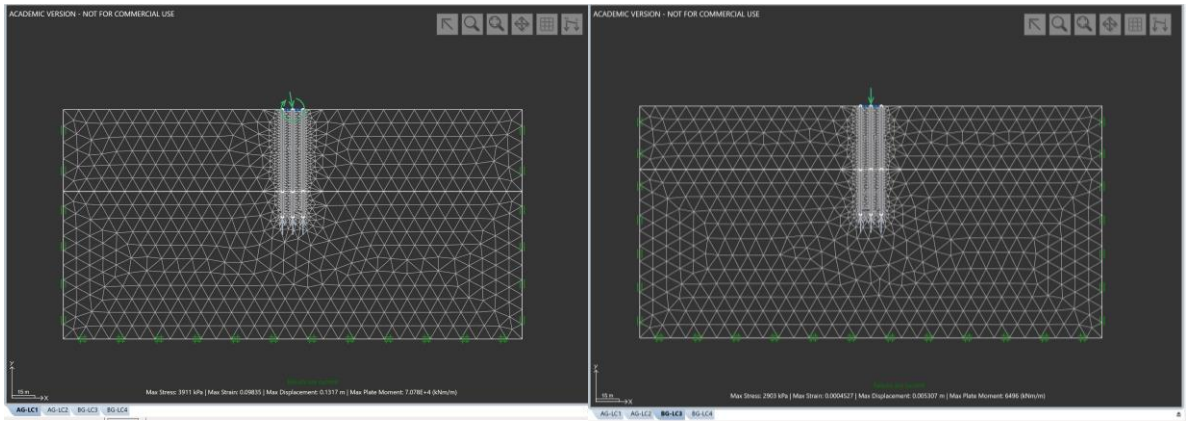


Figure 50 mesh, right, BG and left, AG

Based on the assumptions and material characterization undertaken thus far, the material properties selected for rock (Hoek-Brown model[39]) and sand (Mohr-Coulomb model) are depicted in Figure 51.

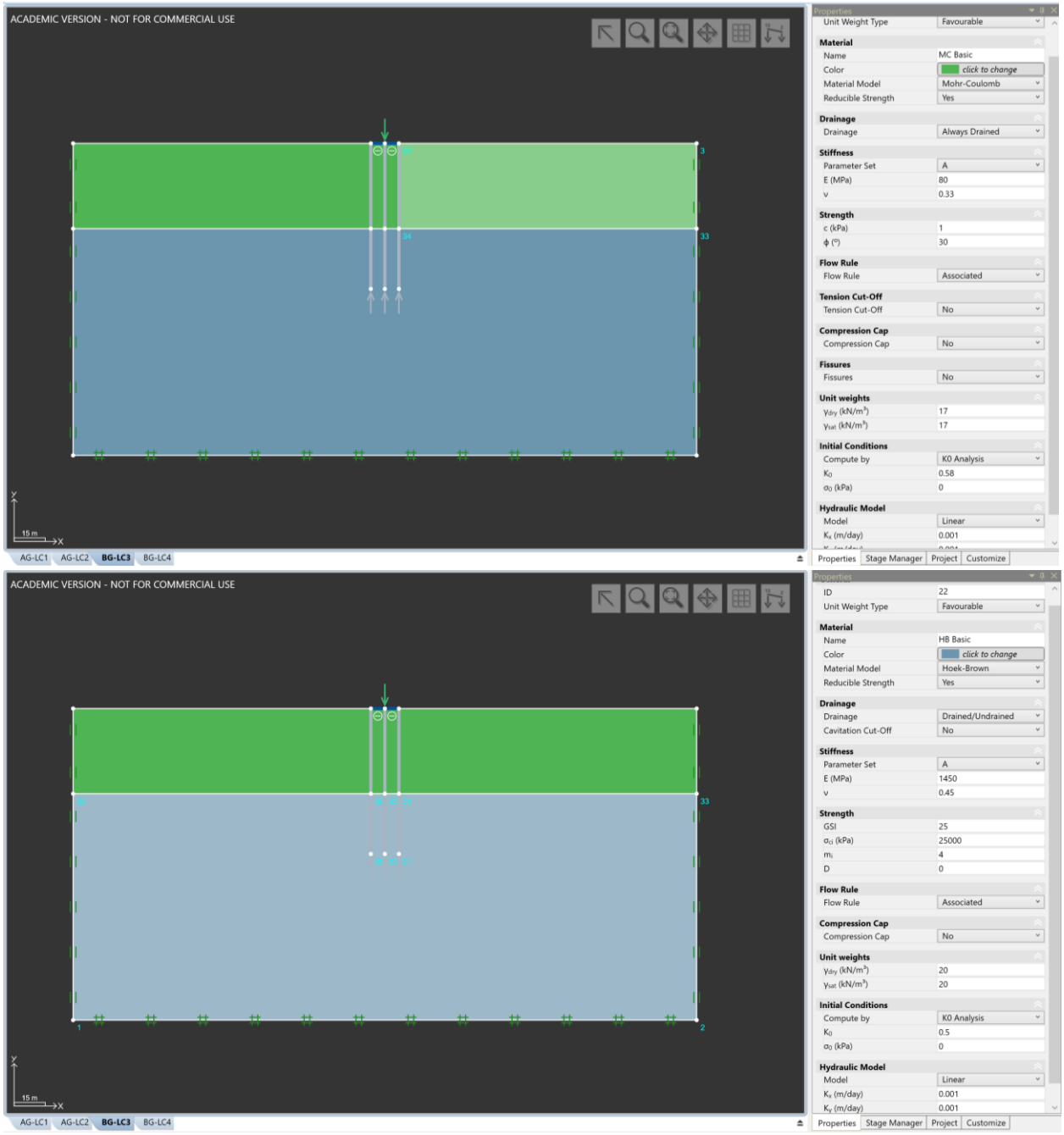


Figure 51. Materials properties (at the left of the figures). Top: sand, bottom: rock

## 10.3 LOAD COMBINATIONS FOR FOUNDATION DESIGN

Two loadings are analyzed on the AG configuration and two loadings on the BG, stemming from the Lower Bound case (at the beginning of this chapter), for enveloping the worst loading conditions a pile can be subjected to in each configuration. Loads are reduced to the plain-strain equivalent system:

AG
Vertical:
Downwards: (21x14) MN/18 m = 16.33 MN/m
Upwards: 14MN/18 m = .77 MN/m
Horizontal: 41MN/18 m = 2.27 MN
Moment: 1185MN·m/18 m = 65.83 MN·m/m
BG
Vertical:
Downwards: (21x14) MN/18 m = 16.33 MN/m
Upwards: 14MN/18 m = .77 MN/m

Figure 52 shows the 4 loading conditions that come from the loads before.

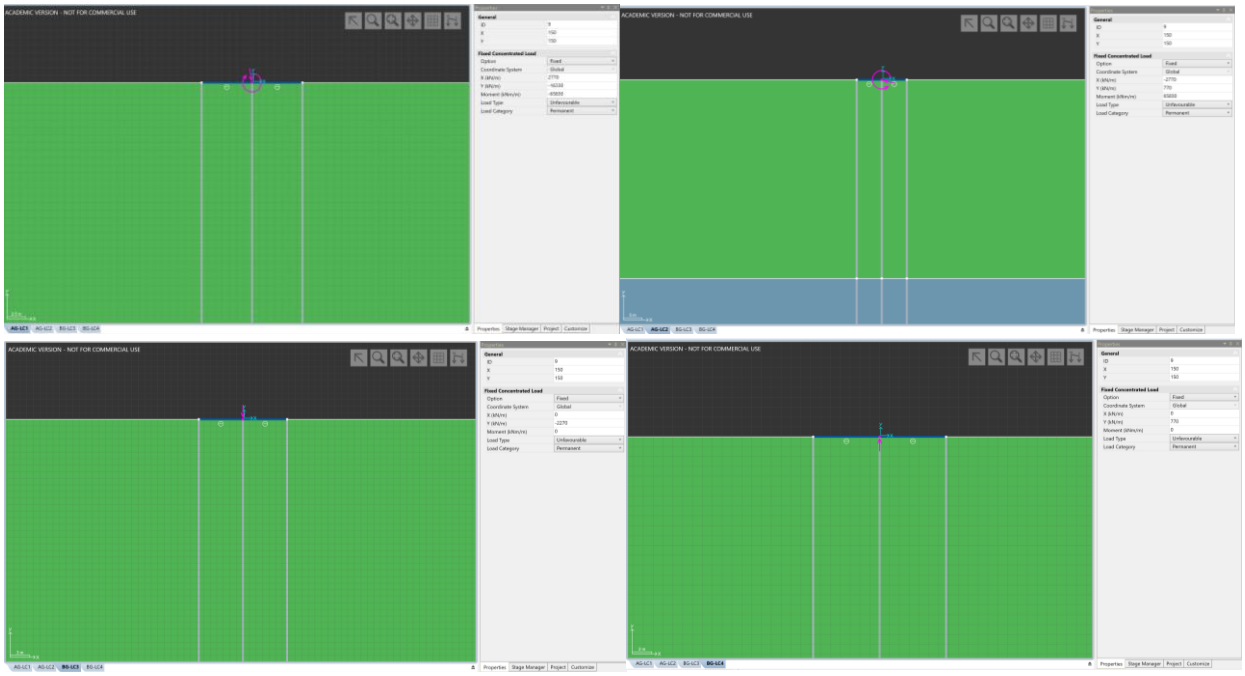

Figure 52. Loading cases: LC1, LC2, LC3 and LC4

## 10.4 ACCEPTANCE CRITERIA FOR PILES

It is considered that the loading conditions coming from design earthquake plus dead weight are higher than 2x the dead weight alone. For this reason, no dead-weight load alone is analyzed, and no factor of safety is included in the analyses. Note that the factor of safety over loading conditions that include the design earthquake are in the order of twice those for dead weight Normal Condition case[19].

Structural integrity against buckling and tension failure are checked for the piles. The maximum moment is defined at 65 MN·m, and the maximum compression load to avoid buckling, is conservatively defined at 200

MN. To meet this first requirement without hinge formation and load redistribution (to avoid buckling), a heavily reinforced pile section is needed. A 0.025 m thickness, 1.5 m diameter 60 ksi (about 410 MPa) stainless steel cylinder inserted in the concrete pile would suffice for providing a yielding moment higher than 65 MN·m. The maximum buckling load comes from a simplified and conservative calculation of the buckling load for a pile point loaded axially.

Shear loads and membrane tension stresses are not accounted for structural integrity, since they are expected to be fairly irrelevant in the layout analyzed. Membrane tension comes from friction forces piles-soil or pile-rock, which are capped.

The maximum displacements during earthquake to guarantee that no pipe breaks thanks to the bellowed penetrations is set at 0.3 m (serviceability criterion). To ensure that this requirement is fulfilled, no displacement in x or y directions on the basemat is allowed to be over 0.21 m.

## 10.5 ANALYSIS OF FOUNDATIONS

Figure 53 to Figure 64 show displacements in the x and y directions in piles and basemat, and normal force, shear and bending moments in the piles for the 4 load cases.

Figure 53 to Figure 55 show displacements in the x and y directions in piles and basemat, and normal force, shear and bending moments in the piles for AG- Loading Case 1. Figure 53 shows displacements in the x and y directions. The only displacements relevant for the design are the basemat ones. The maximum displacement in the x direction on the basemat is 9.35 cm and the maximum in the y direction, 7.16 cm. They are both below 21 cm, therefore the serviceability criterion is met. Figure 54 shows Normal and Shear forces. The maximum compression load is 63 MN, thus below 200 MN. The maximum shear load is 3.5 MN, an order of magnitude below the maximum compression obtained. Figure 55 shows the bending moments on the piles. The maximum moment is 20 MN·m, thus below 65 MN·m.

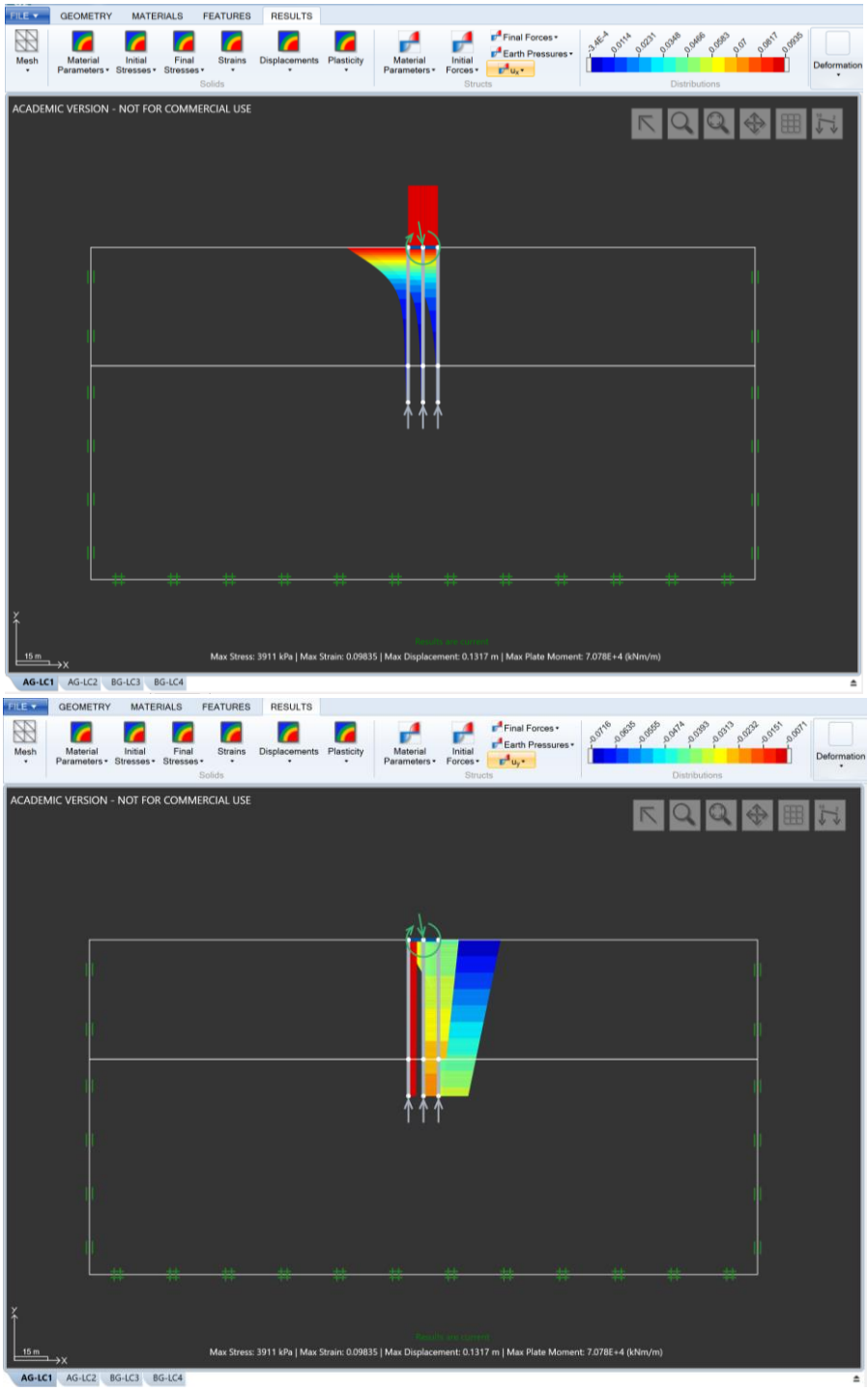


Figure 53. AG-Loading Case 1-displacements: x direction top/ y direction bottom

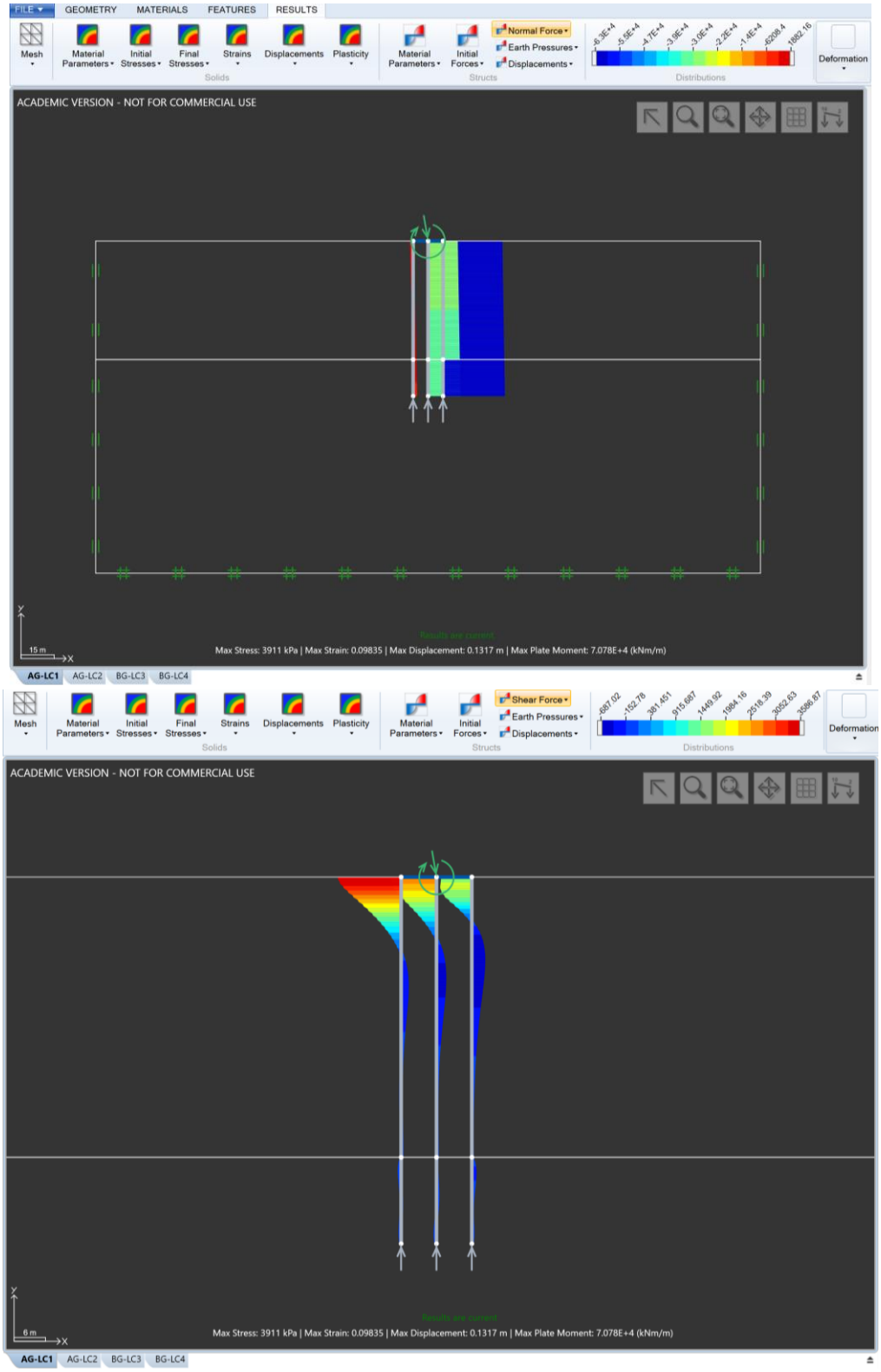


Figure 54. AG-Loading Case 1-Normal Force (top)/shear force(bottom)

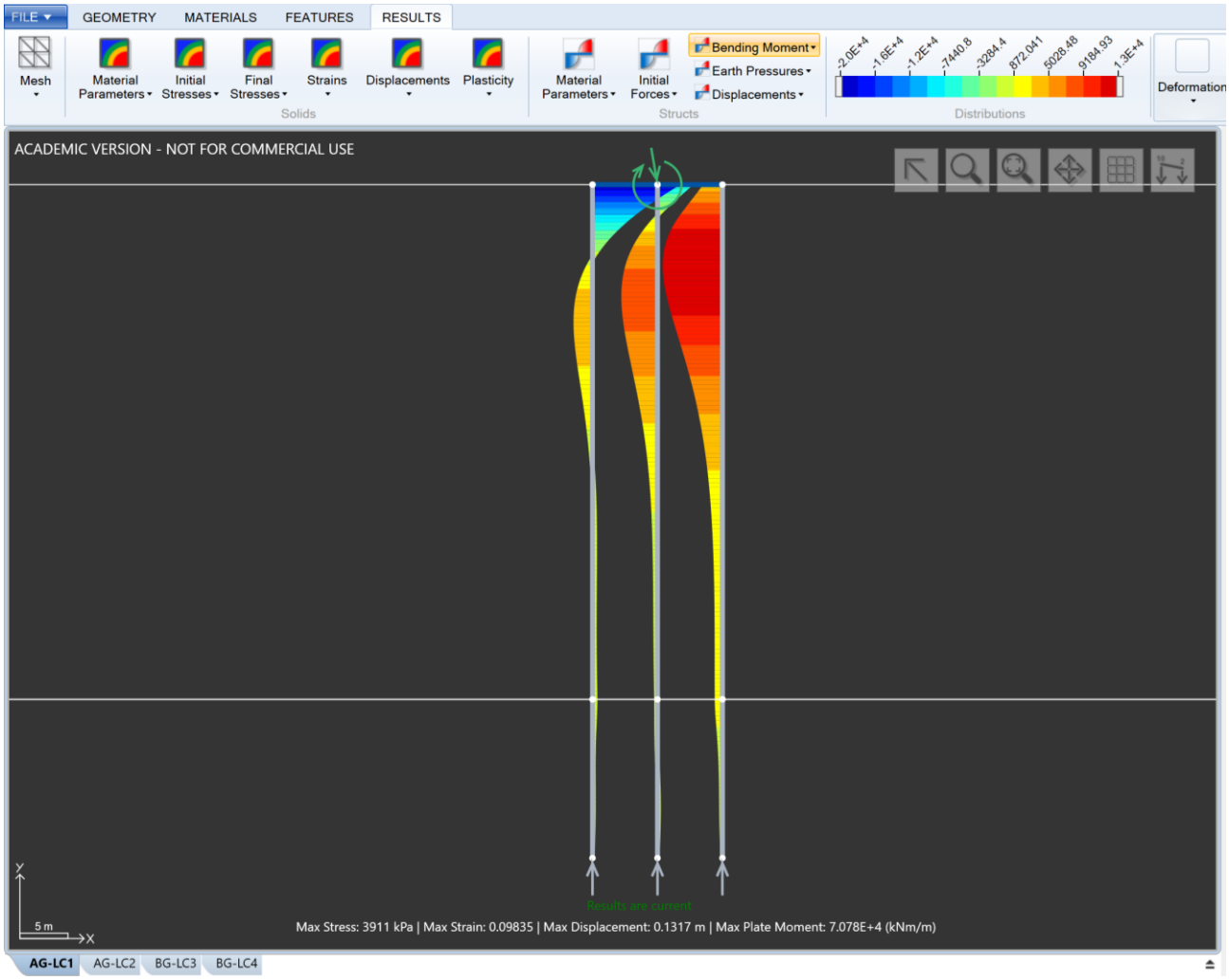


Figure 55. AG-Loading Case 1- Bending moment

Figure 56 to Figure 58 show displacements in the x and y directions in piles and basemat, and normal force, shear force and bending moments in the piles for AG- Loading Case 2. Figure 56 shows displacements in the x and y directions. The maximum displacement in the x direction on the basemat is 33 cm and the maximum in the y direction, 39 cm. They are both above 21 cm, therefore the serviceability criterion is not met. Figure 57 shows Normal and Shear force. The maximum compression load is 22 MN, thus below 200 MN. The maximum shear load is 3.3 MN, an order of magnitude below the maximum compression obtained. Figure 58 shows the bending moments on the piles. The maximum moment is 57 MN·m, thus below 65 MN·m.

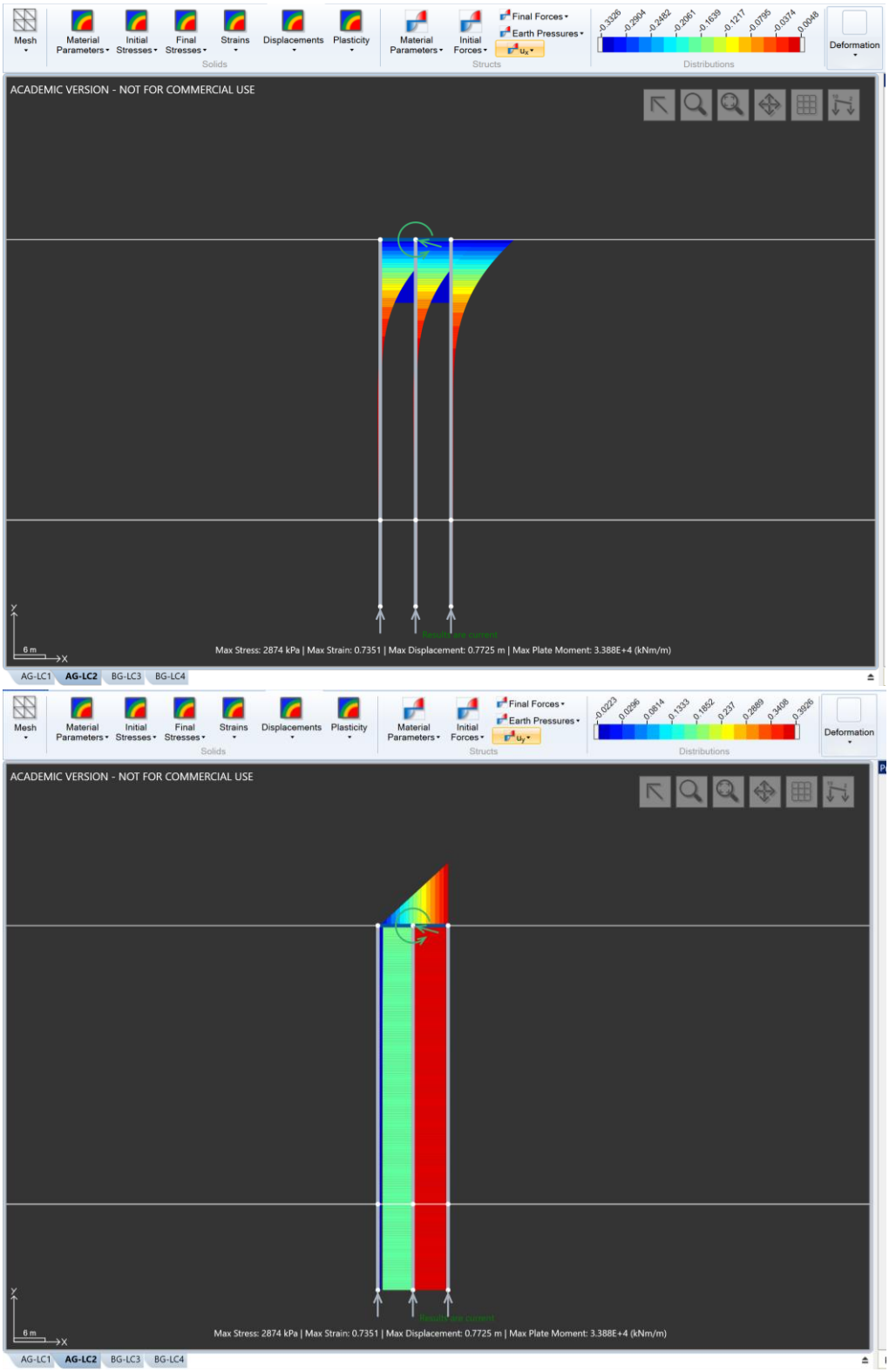


Figure 56. AG-Loading Case 2-displacements: x direction(top)/ y direction(bottom)

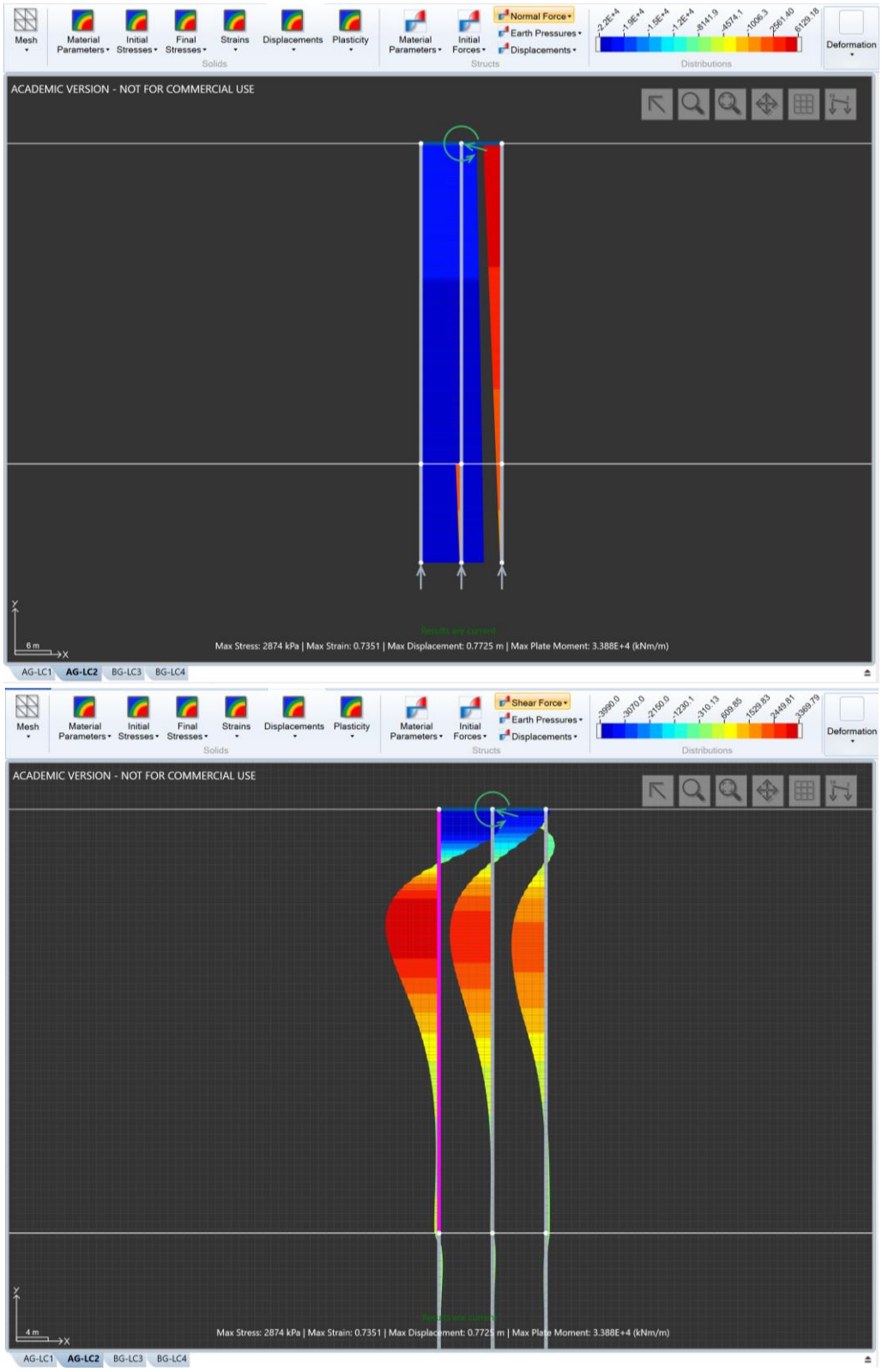


Figure 57. AG-Loading Case 2-Normal Force (top)/shear force(bottom)

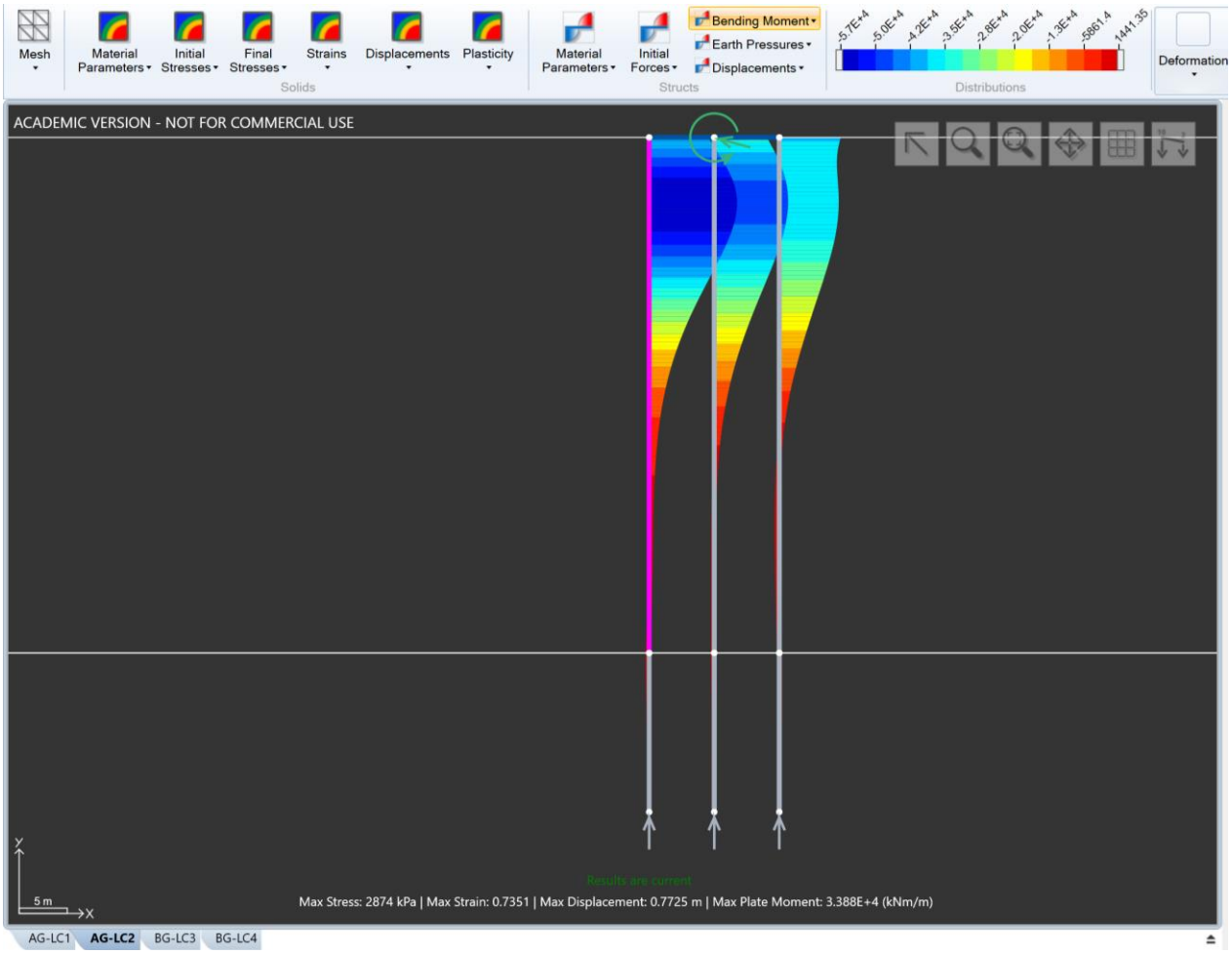


Figure 58. AG-Loading Case 2- Bending moment

Figure 59 to Figure 61 show displacements in the x and y directions in piles and basemat, and normal force, shear force and bending moments in the piles for BG- Loading Case 3. Figure 59 shows displacements in the x and y directions. The maximum displacement in the x direction on the basemat is practically 0 and the maximum in the y direction, 0.5 cm. They are both below 21 cm, therefore the serviceability criterion is met. Figure 60 shows Normal and Shear force. The maximum compression load is 4.8 MN, thus below 200 MN. The maximum shear load is 0.6 MN, an order of magnitude below the maximum compression obtained. Figure 61 shows the bending moments on the piles. The maximum moment is 11 MN·m, thus below 65 MN·m.

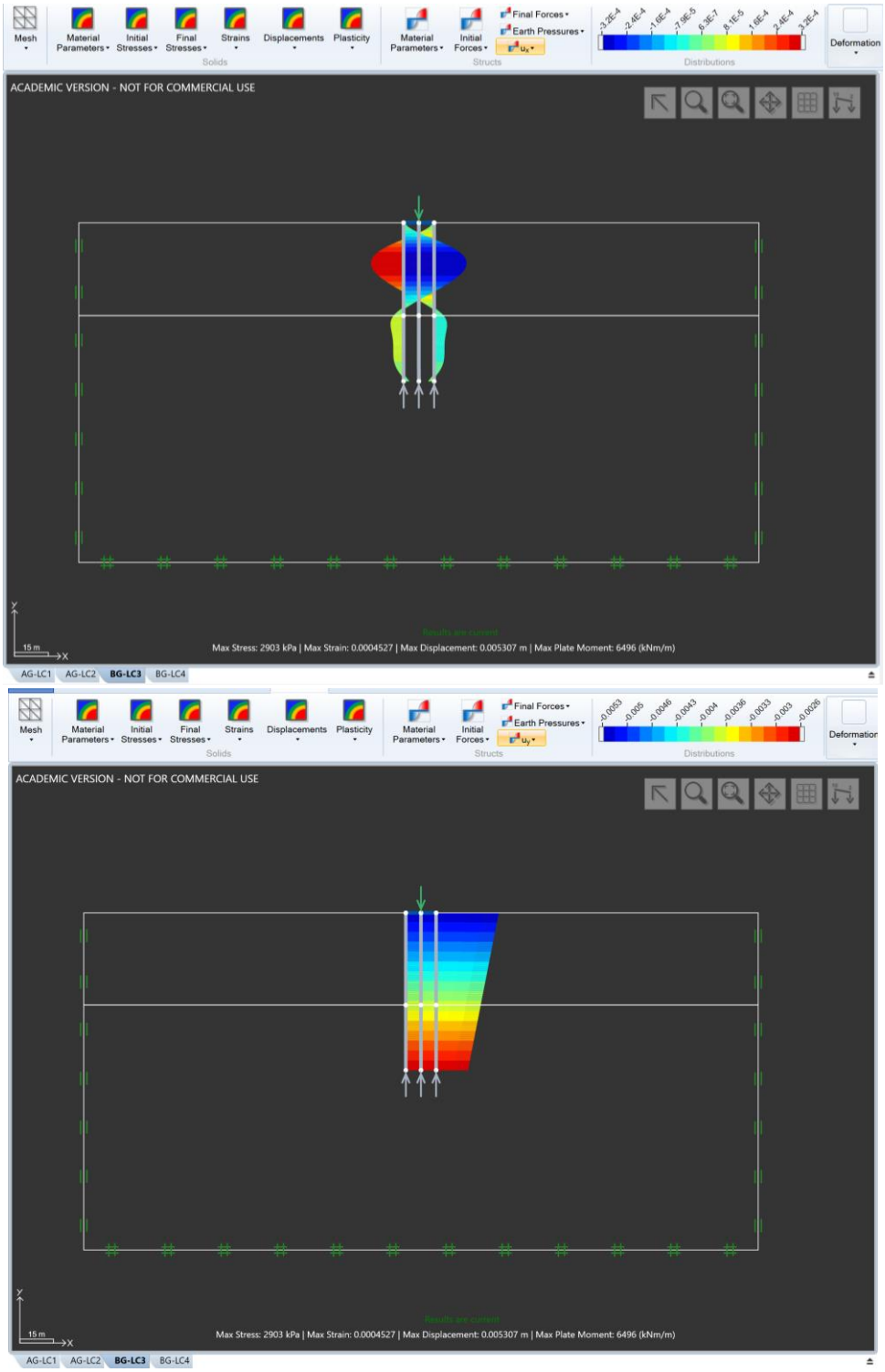


Figure 59. BG-Loading Case 3-displacements: x direction(top)/ y direction(bottom)

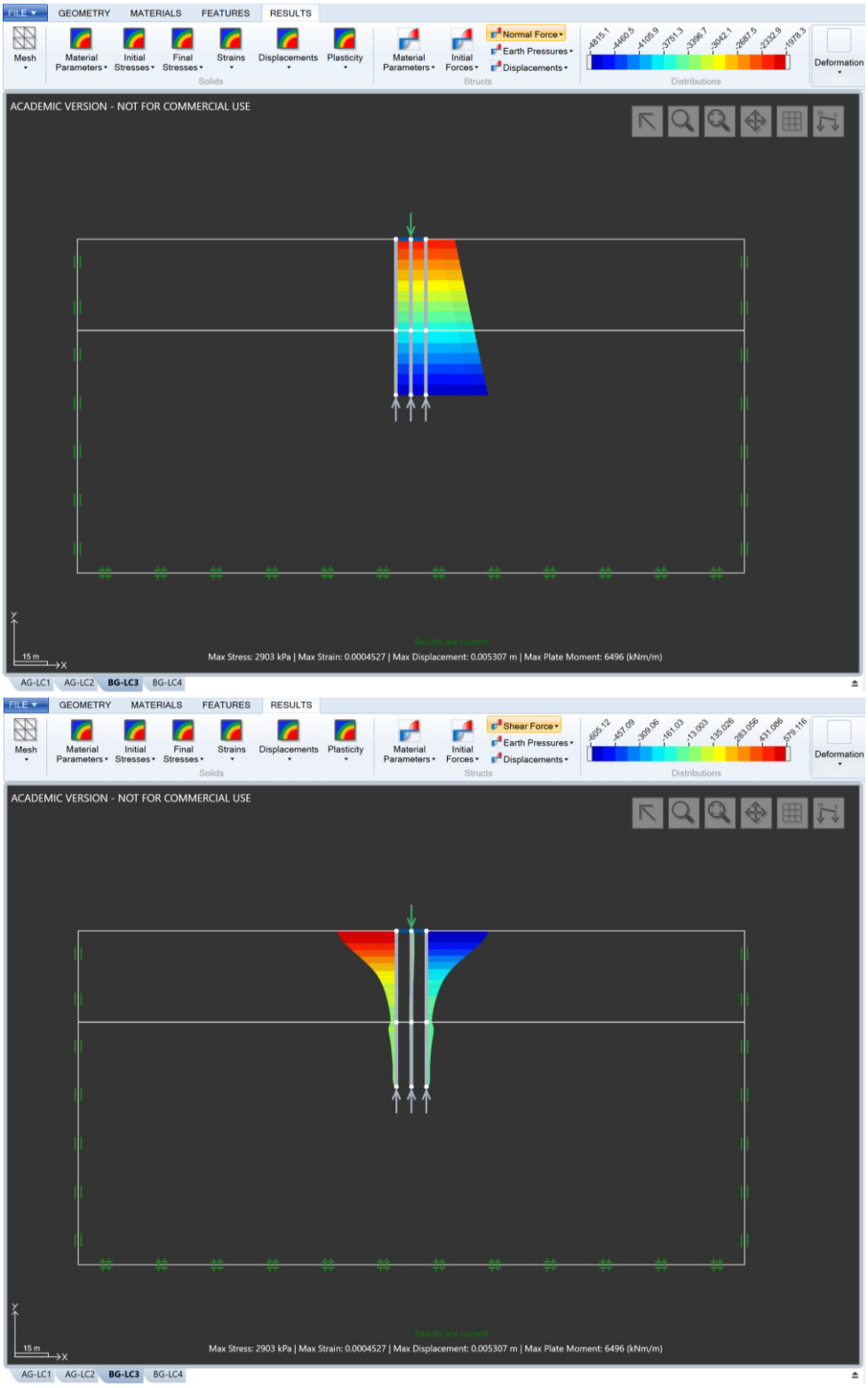


Figure 60. BG-Loading Case 3-Normal Force (top)/shear force(bottom)

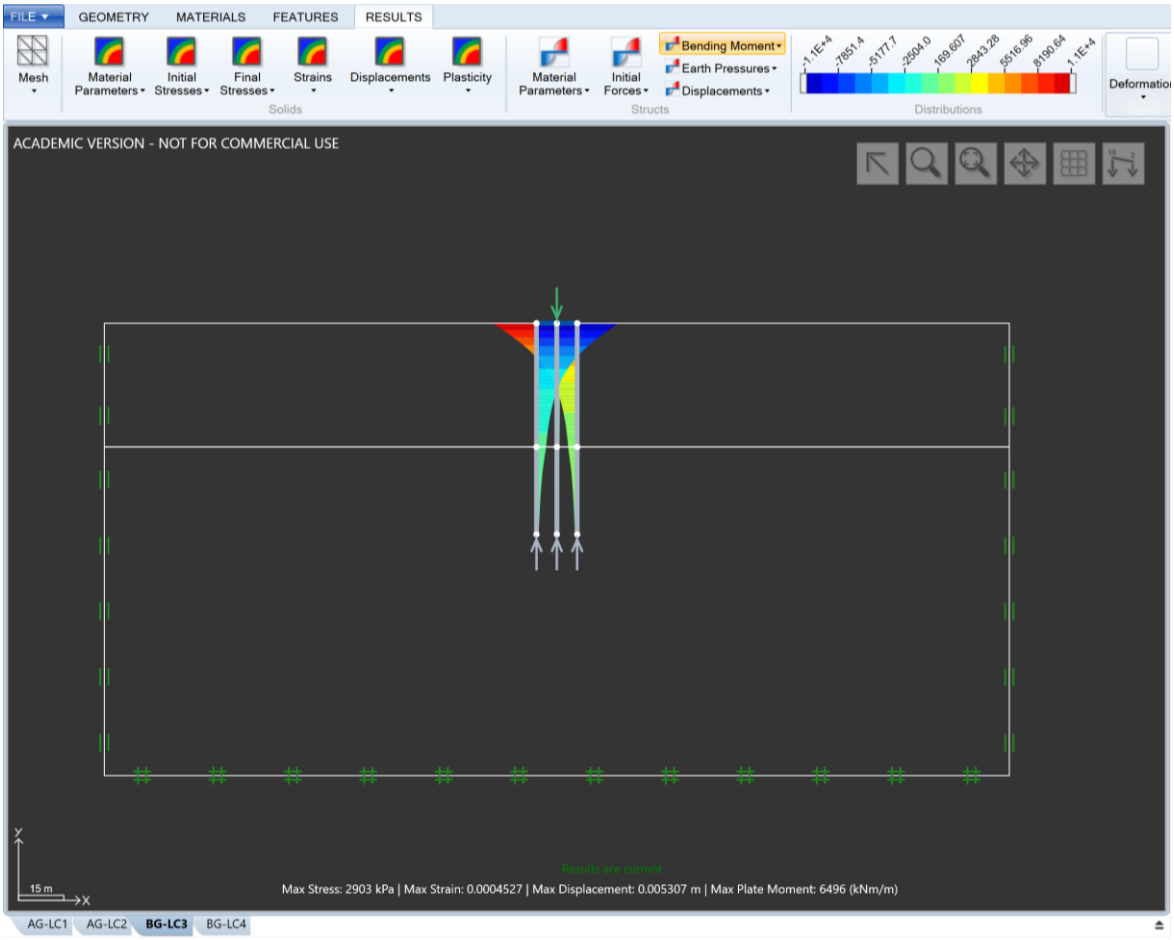


Figure 61. BG-Loading Case 3- Bending moment

Figure 62 to Figure 64 show displacements in the x and y directions in piles and basemat, and normal force, shear force and bending moments in the piles for BG- Loading Case 4. Figure 62 shows displacements in the x and y directions. The maximum displacement in the x direction on the basemat is practically 0 and the maximum in the y direction, 0.1 cm. They are both below 21 cm, therefore the serviceability criterion is met. Figure 63 shows Normal and Shear force. The maximum compression load is practically 0. The maximum shear load is 0.5 MN, which is very small for the size and morphology of these piles. Figure 64 shows the bending moments on the piles. The maximum moment is 11 MN·m, thus below 65 MN·m.

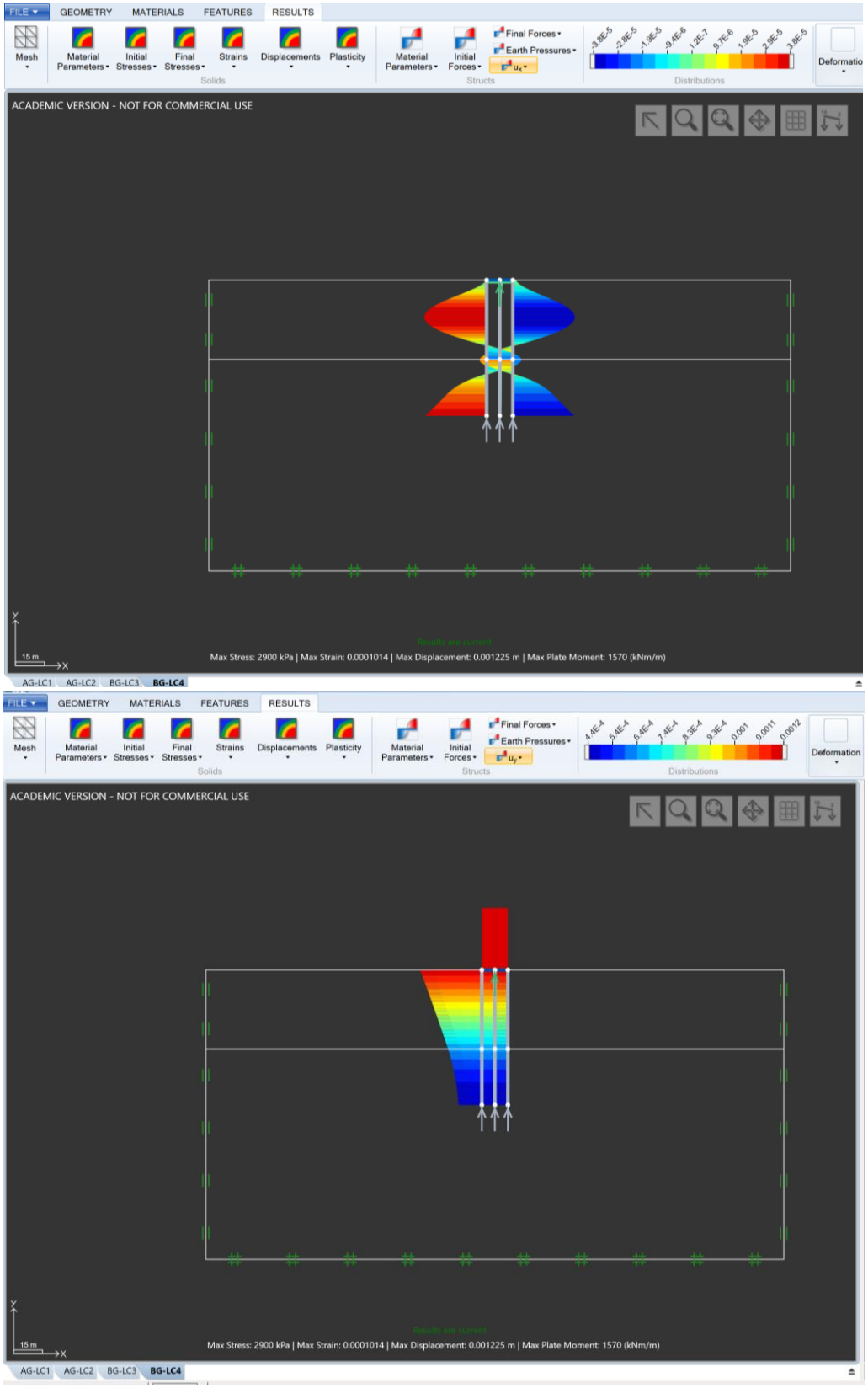


Figure 62. BG-Loading Case 4-displacements: x direction(top)/ y direction(bottom)

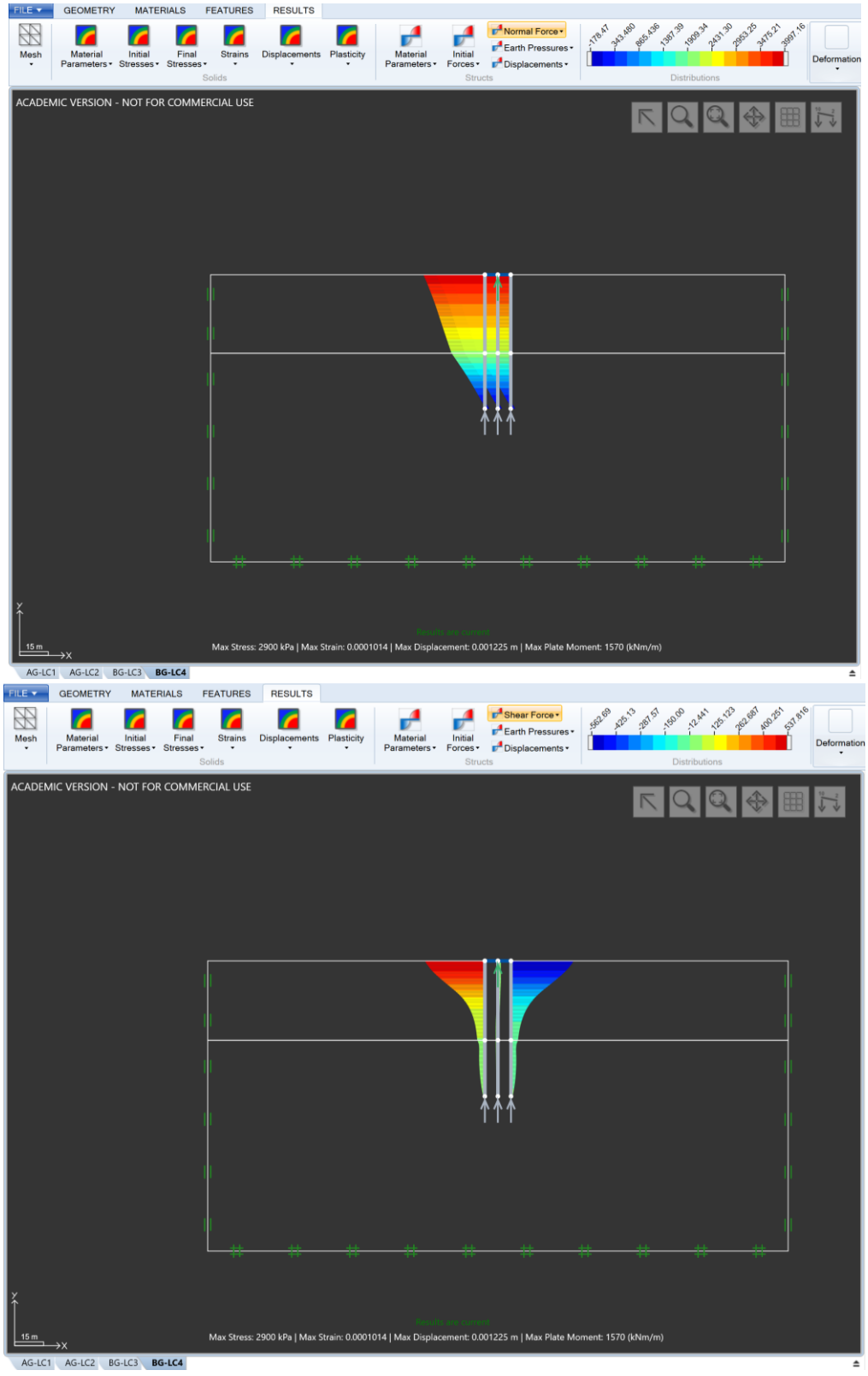


Figure 63. BG-Loading Case 4-Normal Force (top)/shear force(bottom)

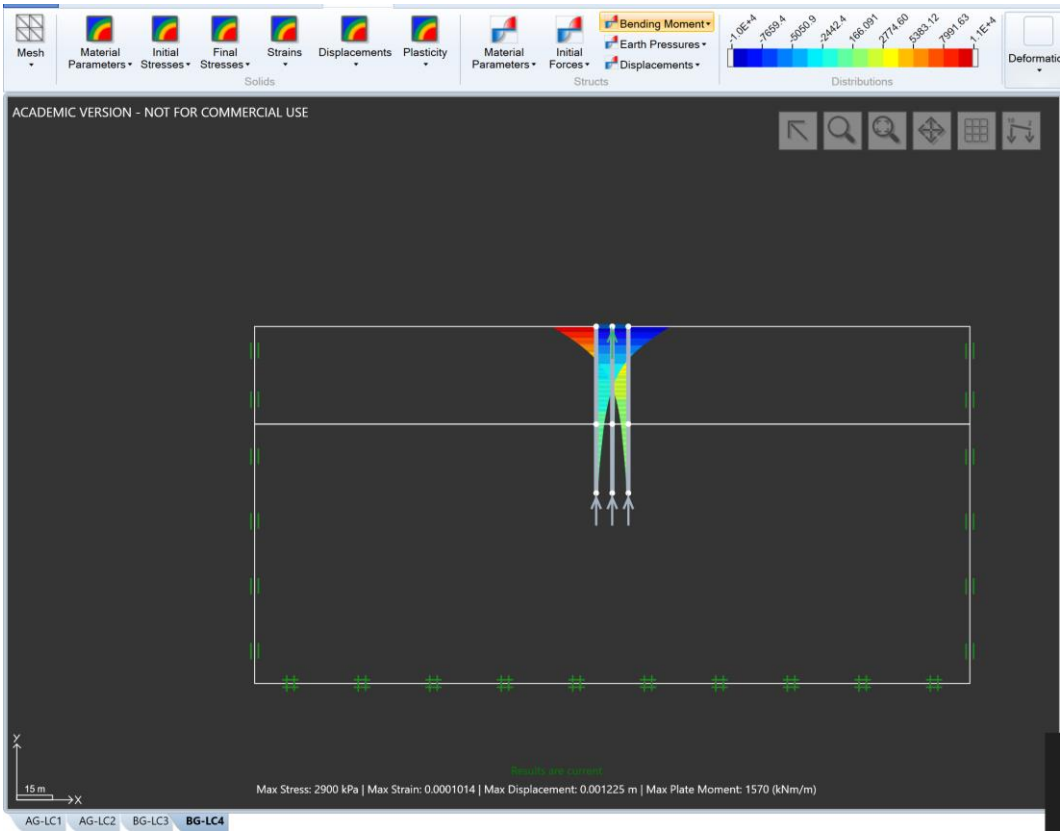


Figure 64. BG-Loading Case 4- Bending moment

The large displacements coming from the loading case 2 (with uplift force) are due to the full piles needing to be mobilized upwards caused by how limited the shear capacity of the pile-soil interaction is. The whole pile group and almost all the surface of each pile needs to provide friction downwards to counter the uplift force.

From the figures shown in this paragraph, it is clear that both, maximum compressive load and maximum bending moment requirements, are met. However, the maximum displacement requirements are not met in all cases.

## 10.6 CONCLUSIONS OF FOUNDATIONS DESIGN

Overall, the limiting factor is set by the necessity to take some of the load in tension to absorb the uplift earthquake load. This uplift load is similar in the AG and BG designs and requires both designs to have their piles penetrating bedrock. To design the actual pile foundations, we use the FEA calculation as a reference to size them, applying engineering judgement, without making use of the results obtained directly.

In fact, the design for the AG configuration did not meet the acceptance criteria due to large displacements. However, there is no rule that sets the aforementioned maximum allowable displacements. They stem from what the systems (mainly piping) penetrating the walls of the building can take. These could be reduced drastically by either:

- Making the piles longer in the AG case. In fact, we know that the friction coefficient in rock is higher than what we have modelled. Thus, probably shorter piles than those modeled would be able to take the whole load in friction, if we refined the modelling.
- Installing tension anchors (tie down).
- Anchoring the piles to bedrock in the vertical upwards direction

Based on these results it is possible to bound how much longer the set of piles for the AG would need to be compared to the BG ones. The addition of tension anchors(tie-backs) or anchorage of the current piles in the upwards direction, are possible solutions to cope with uplift force, inducing a negligible increment in concrete and steel volumes. In consequence, considering piles connecting the basemat to the bedrock at the top represents well the difference in cost.

The analyses show that after the excessive displacements are reduced, the most hazardous loads are bending moments. Bending moments are in fact limiting the design of the foundations. The limiting moment in each configuration is relatively close to the base in position, and close to the moment at the base in magnitude. Thus, if we designed considering how the piles cracked and/or yielded loads would redistribute [51], the maximum moments would not be much lower in magnitude than currently. Additionally, shear loads would increase. Consequently, the amount of material needed would not be much lower than if we consider absence of cracking/yielding. Hence, the current approach does not bring about much conservativism in judging the amount of material needed, in comparison to computing iteratively the appearance of every hinge.

Moreover, the fact that the piles are modelled penetrating bedrock considerably, does not change significantly the behavior of the site-piles interaction, with respect to the hypothesized system, i.e., piles penetrating bedrock a few meters. This conclusion stems from the low horizontal displacements, moments and shears that we can see in Figure 53 to Figure 64 below the water table, in rock and soil. These low horizontal displacements and loads make also irrelevant the effect of the undrained condition in which the soil is loaded during the earthquake load. We assume that the few meters needed to make the piles penetrate into bedrock cause a negligible difference in cost, thus this extra length is omitted from the cost comparison. For cost comparison purposes, it is considered that the piles end where the bedrock starts.

## 10.7 EXTRAPOLATION TO EARTHQUAKE SCENARIOS

Considering the pile layout described before, but instead 0.75 m radius carbon steel piles, the result from the OPTUMG2 analyses are extrapolated to obtain the thickness needed in each earthquake scenario. As justified before, we consider bending as the limiting load on the piles. Typically, we design considering how the piles crack or yield at the maximum bending location. Then the moments would redistribute, and the maximum

moments would appear at the pile's embedment in the basemat. As the maximum moments from the models are like the ones at the basemats, considering the formation of plastic/crack hinges would not result in a sizing very different from the current solution. Additionally, shears would increase. Consequently, the current approach is not excessively conservative in this regard.

## 10.8 BASEMAT

Basemats in NPP and in general in civil construction tend to be tick and rigid[32] [52]. In a soil site, where the bearing surface underneath the mat is flexible and weak, it is more necessary to have a rigid basemat than otherwise. Assuming thus that the basemat undergoes very limited deformations and given the configuration chosen for it, vertical loads are dominating in the definition of the thickness over horizontal ones. Horizontal loads, come from the cylindrical wall, and are transmitted directly to the ring of basemat where the piles are embedded. The added mass of water exerts inertial load due to horizontal earthquake, mainly on the cylindrical wall, but not so much on the basemat. However, vertical earthquake exerts additional water pressure and depression over the basemat, coming from the water column above it, as shown in Figure 65.

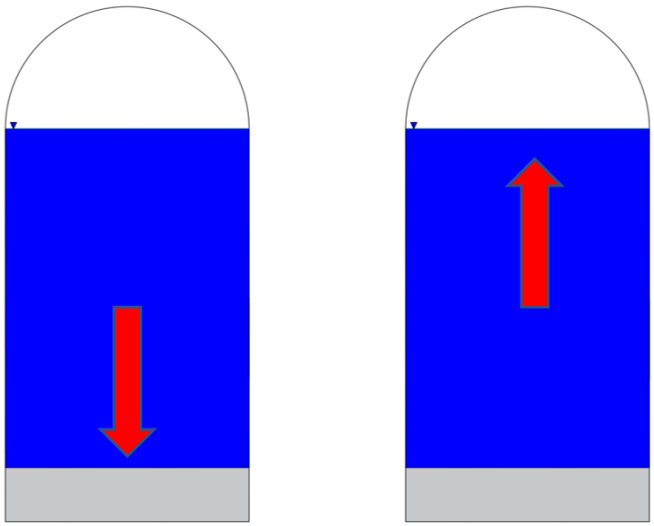

Figure 65. Left: Earthquake acceleration downwards. Right: earthquake acceleration upwards

Vertical loads over the basemat are assumed to be similar in both cases. The reactor module and its concrete support are assumed similar. The water flooding the building is similar. The connection of the basemat to bedrock through Stainless Steel piles, makes the system considerably stiff in the vertical direction, regardless whether it is embedded or semi-embedded (see Figure 3).

Therefore, the thickness and reinforcement of the basemat are similar in steel and concrete volumes for both configurations: embedded and semi-embedded.

# 11. COST COMPARISON FOR THE NUSCALE SCENARIO

Table 10 shows the excavation direct cost items[25] and the total cost. Excavation cost are calculated simply as the labor rate ($/man·h) multiplied by the estimated labor speed (manh/ft³).

Table 10. Excavation direct cost

| Labor | ($/man·h) | (man·h/ft³) | ($/ft³) | ($/m³) | m3 | total cost |
|---|---|---|---|---|---|---|
| AG | 50 | 0.1 | 5 | 176.6 | 4,199 | $741,387 |
| BG | 50 | 0.1 | 5 | 176.6 | 7,380 | $1,303,044 |

Table 11 leads to the final cost after including the difference in design of the foundations. It follows that in every scenario, the embedded silo type reactor is cheaper than the partially embedded reactor building. Note that the percent differences only refer to the sum of the components where a difference is foreseen, this is, cylindrical walls and piles. “Difference (AG-BG)” does not include the cost of excavation. “Savings: AG-BG/AG%” represents the fractions saved from the BG option with respect to the AG options. The basemat cost, cover, internals and penetrations are excluded from the analysis, since they are assumed to be similar, although not exactly equal, based on the previous sections. The given percentages could be reduced if one employed innovative fabrication technologies with cost reduction potential, such as steel plate composites. Given the significant number of assumptions and simplifications, such as

- not accounting for the fact that building underground is more complex, and therefore there might be increased cost, such as in assembling the cylindrical wall,

- neglecting the design of the cavity in which the main steam or feed water lines are hosted in the BG case,

these results cannot be considered directly applicable to the cost difference of a new built NPP. However, they serve the purpose of suggesting that under certain conditions, embedment siting might be cheaper than building above ground. Consequently, they are worth consideration. Furthermore, the results in Table 11 show direct cost and comparison of the parts analyzed, which are by no means the entire Reactor Building (since lid, basemat, internal concrete structures and basemat are excluded). Figure 66 represents visually the data in Table 11.

Table 11. Cost comparison for the NuScale scenario

| Cost | | Direct cost: Materials + labor | | | |
|---|---|---|---|---|---|
| | | Cylindrical wall (not including foundations) | | | Excavation |
| | | Lower bound | Enveloping FRS | Upper Bound | Excavation (Champlin)/2 |
| w/o foundations | AG | $ 1,811,622 | $ 4,287,478 | $ 14,499,722 | $ 370,694 |
| | BG | $ 1,218,143 | $ 1,463,346 | $ 7,774,141 | $ 651,522 |
| | Difference (AG-BG) | $ 593,479 | $ 2,824,132 | $ 6,725,581 | $ (280,828) |
| Excavation (Champlin)/2 | Dif. Including exc. | $ 312,650 | $ 2,543,304 | $ 6,444,753 | |
| | Savings: (AG-BG)/AG % | 14% | 55% | 43% | |
| | (AG-BG)/AG w/o exc. % | 33% | 66% | 46% | |
| | | Total (including foundations: piles) | | | Excavation piles (Champlin)/2 |
| total | AG | $ 4,350,216 | $ 11,540,605 | | $ 66,775 |
| | BG | $ 1,773,990 | $ 2,019,193 | | $ 51,173 |
| | Difference total (AG-BG) | $ 2,576,226 | $ 9,521,412 | absurd piles, need other solution | $ 15,602 |
| Excavation (Champlin)/2 | Dif. Including exc. | $ 2,310,999 | $ 9,256,186 | | |
| | Savings: (AG-BG)/AG % | 48% | 77% | | |
| | (AG-BG)/AG w/o exc. % | 59% | 83% | | |

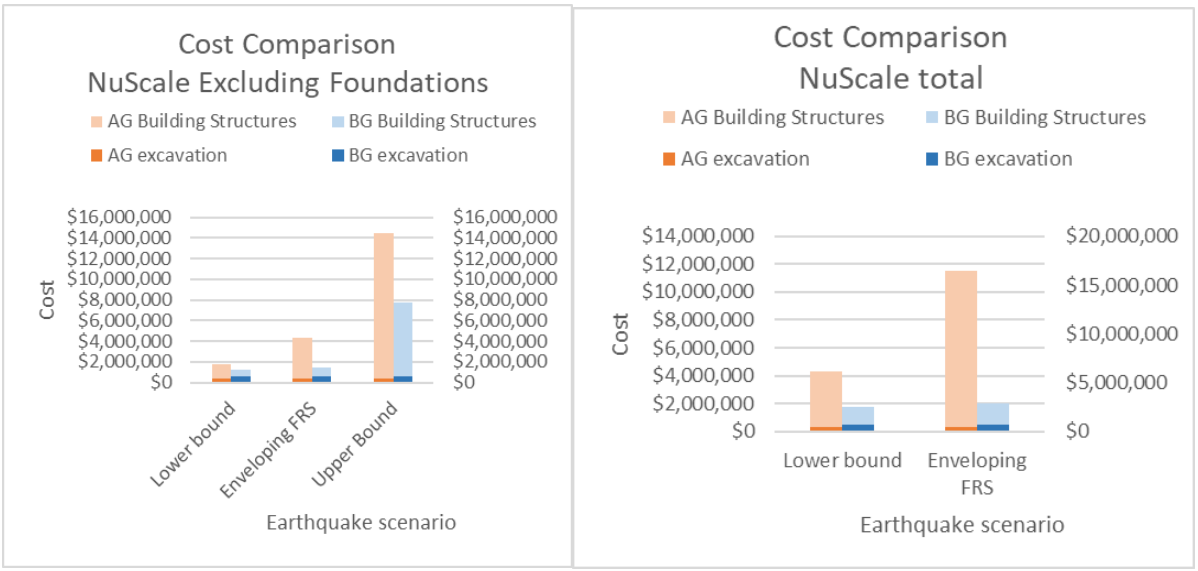


Figure 66. Cost comparison for the NuScale scenario

These results are conditional to being able to use the structural capacity of the weak soil around the reactor building, which general geotechnical engineering good practice discourages and Nuclear Codes, such as ASCE4-98 preclude. The contribution of the weak soil surrounding the reactor building was taken credit for to resist earthquake loads. Should this effect be excluded, the difference in excavation cost will be greater than the difference in added cost of concrete and steel at the exterior walls and the cost of piles foundations in every case. Thus, the comparison will be favorable for the semi-embedded option over the embedded one.

# 12. ASSUMPTIONS, CONSIDERATIONS AND HYPOTHESES MADE IN THE BWRX-300 ANALYSIS AND PRISMATIC EQUIVALENT

As in the NuScale case, there are 3 important groups of assumptions and simplifications: the set of loads, the influence of those loads on the design of the building, and the cost evaluation of this design.

General

- The building's internals and the external areas in the AG and BG designs are identical.
- The analysis is conservative regarding BG, since the goal of this work is to yield a cost comparison, not a cost assessment. Hence the supports of the internals, and the extra costs in the AG design with respect to the BG one for making internals earthquake resistant are not accounted for in the cost assessment.

Design

- The reactor vessel is considered rigidly attached to the interior wall. Components inside the buildings are considered rigidly attached to the floors where they are at.

Loads definition

- The same site and design earthquake accelerations at the buildings' basemats are considered.

Earthquake loads

- The horizontal earthquake loads stemming from the spectrum in [7]are multiplied by a factor 1.4. This factor accounts for horizontal bidirectionality.

Cost items

- The costing data do not consider the fact that building embedded structures is more complex (and hence more expensive) than building them above ground, especially, with respect to what relates to the penetrations and lines that are placed below ground.

Site conditions

- $\rho$(sand at the same elevation as the buildings)= 15KN/m$^3$≈1500 kg/m$^3$.
- same passive condition earth pressures as in NuScale.
- Soil and Rock do not fail under earthquake loads.

# 13. INPUT DATA FOR BWRX-300 AND PRISMATIC EQUIVALENT

## 13.1 GEOMETRY

The external diameter of the building is approximately 20 m and the total volume, including the maintenance building above, 15,500 m³[4]. If the building was only cylindrical, it would have a total height of 49 m, including the maintenance building. Based on this information, the reactor module is estimated to be 30 meters high. Based on Figure 4, it is assumed that that there is a concrete containment in the inside of the reactor module of half its diameter. This containment is assumed to be 500 mm thick based on the ESBWR design[52]. Four floor slabs are assumed to connect the external wall with the containment wall, at 10, 15, 20 and 25 m elevation with respect to the bottom of the reactor module.

## 13.2 LOADS DEFINITION

Following from the NuScale study, only earthquake loads, dead weight, airplane crash and earth pressures are considered in the design. Horizontal earthquake loads follow from Figure 67. The red (Hard Rock) case is considered for the rock site and the green one (Soft to medium soil) for the soil case. Vertical accelerations are assumed 1g for every frequency from 2Hz to 33Hz, based on the AP1000 control document [31].

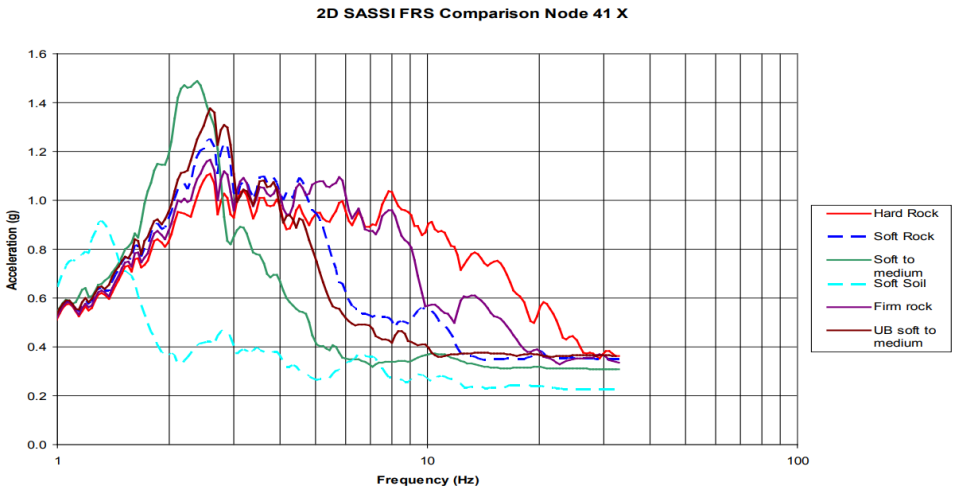


Figure 67. Response spectrum in horizontal direction

Airplane crash is defined in the same way as in the NuScale case (see 7.4.2). The same soil density and friction angle as in NuScale are considered in computing the earth pressures on the building (see 7.1).

# 14. BUILDINGS DESIGN ASSUMPTIONS AND SIMPLIFICATIONS IN THE ANALYSIS OF THE BWRX-300 BUILDING AND ITS PRISMATIC EQUIVALENT

- The mass of water atop the reactor module, assumedly 4.6 m deep, is added to the assumed 1m thickness reinforced concrete roof slab. A factor 3 in the mass of the containment wall and floor slabs account for the masses of the reactor vessel full of internals and other components inside the building that have not been modeled, nor defined yet. This mass amounts to about 4500 MT.

- Radial shear necessity is neglected since it is assumed to be only relevant in discontinuities, therefore, also assumed, will not having a major effect on final cost.

- Stresses at discontinuities can be mitigated by local thickening, hence, their effect in cost is negligible.

- Minimum reinforcement is not applied, as prescribed by some codes

- It is assumed that only what is inside the containment needs protection from an airplane impact for the comparison. It is assumed that nothing on the floors next to the containment, need protection from aircraft impact. Aircraft impact on the roof of the building is not postulated, since all configurations are susceptible to a crash there.

- Components inside the building are considered infinitely rigid.

- The dynamic degradation of soil properties is not considered in the analysis, i.e., the backbone curves.

## 14.1 LOADING CONDITIONS

As in the NuScale case, it is considered that the load combination that drives the design of the cylindrical wall of the Reactor Building is called the Abnormal/extreme environmental case in Table 6. This table shows this load combination marked in the table in the ASME III code [19] that indicates the load combinations to prove structural integrity against in the design of a concrete containment.

# 15. WALL SIZING FOR BWRX-300 AND PRISMATIC EQUIVALENT

The same material properties and material considerations as those of NuScale are considered in the sizing of the BWRX-300 building and its prismatic equivalent. FEA analyses of the airplane crash, earth pressures, vertical earthquake and horizontal earthquake are conducted. Figure 68 shows the meshes employed at one of the cylindrical building cases and at one of the prismatic building cases. The purple elements are those having their density increased for representing the mass of non-modelled parts, such as the water above the roof or the pressure vessel. Note that neither the purple colored areas nor the basemat are evaluated in this section. They are modelled only to accurately represent stiffness and mass in what concerns the external wall.

The iterative process is automated. An ANSYS APDL[31] script calculates the needs of reinforcement areas due to horizontal loads for a wall thickness and input acceleration. At the start of each iteration, the thickness of concrete in each wall between floors is set. Later, natural frequencies are computed by means of a modal analysis. Finally, stresses at the walls are calculated using FEA. These stresses are converted into reinforcement areas. Based on these reinforcement areas, the wall thicknesses and earthquake accelerations are reset for the next iteration, until convergence to a maximum reinforcement density of 8-10% or to a minimum wall thickness of 0.4 m. The nodal displacements in the three spatial directions are constrained at the lower surface of the model, i.e., the basemat. The displacements perpendicular to the walls' surfaces are constrained up to 6m below the surface, for all the modal analyses and the evaluation of stresses due to earthquake and dead weight. The airplane crash model and the earth pressures do not have degrees of freedom at the walls constrained. We assume that the containment vessel in the prismatic cases is robust enough to prevent any scabbing from damaging the reactor vessel. As in the NuScale case, the 0.4 m thickness of the wall together with the 0.5 m thickness of the inside wall is enough to prevent the reactor from undergoing damage from an airplane crash.

It follows that the 0.4 m wall thickness is just enough to take all the vertical compression loads, assuming a square biaxial interaction failure curve in the concrete in every case. The vertical compression loads come from vertical earthquake and dead weight. Earth pressures cause hoop compression in the case of the cylindrical BWRX-300 building. In the case of the prismatic wall, earth pressures cause in-plane shear, resulting in additional reinforcement needs. On the other hand, as vertical earthquake loads and dead weight together do not produce tension in the case of the BWRX-300 cylindrical building, the horizontal earthquake alone defines the areas of reinforcement.

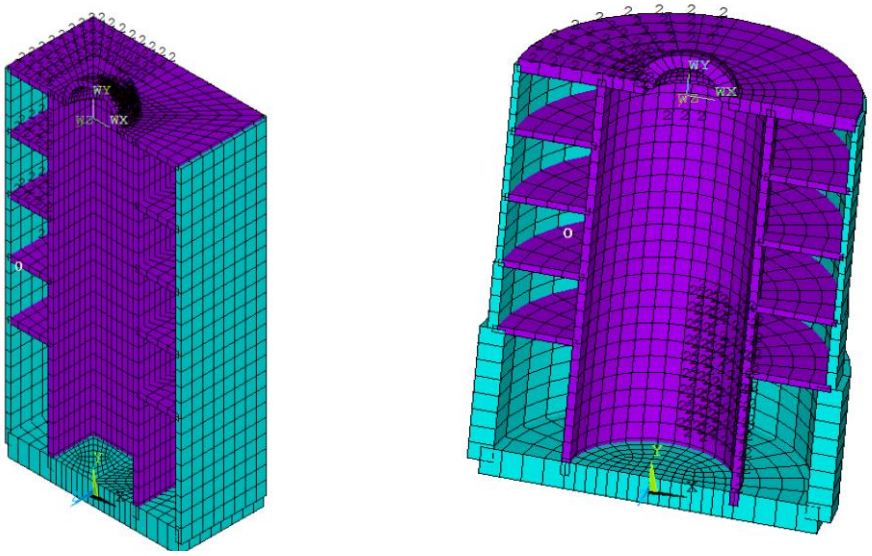

Figure 68. FE Models of prismatic building and Cylindric building

Figure 69 illustrates the general trends in thickness in the exterior walls after conducting the analysis. It follows that the effect of earth pressures on thickness is greater in the prismatic cases than in the cylindrical cases. An additional totally out case was examined for the rock cases. The totally out cases turn to be slightly less expensive than the semi-embedded ones, since the latter need to bear on the walls and the totally out ones does not .

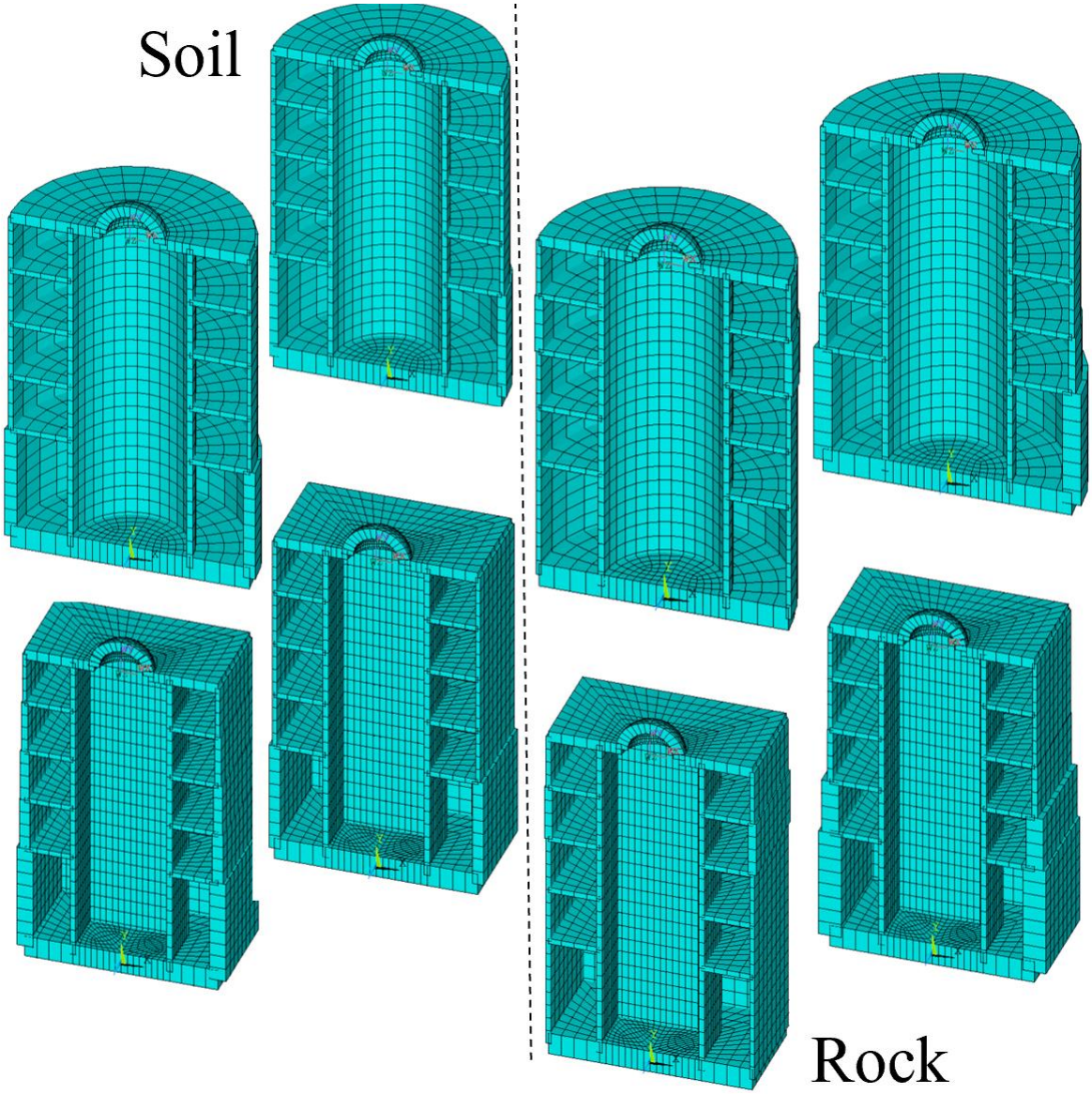


Figure 69. Embedded and semi-embedded cylindrical and prismatic-equal volume final

# 16. COST COMPARISON FOR THE BWRX-300 SCENARIOS AND ITS PRISMATIC EQUIVALENT

Figure 70 shows the cost for the different options. It shows in blue the cost of structures, including concrete and steel, and in orange the cost of excavation. It follows that the external walls of the reactor building are less costly to build if they are cylindrical than if they are prismatic, for the same internal volume. Furthermore, embedment is always cheaper than the alternatives, except if the building is prismatic and embedded in soil.

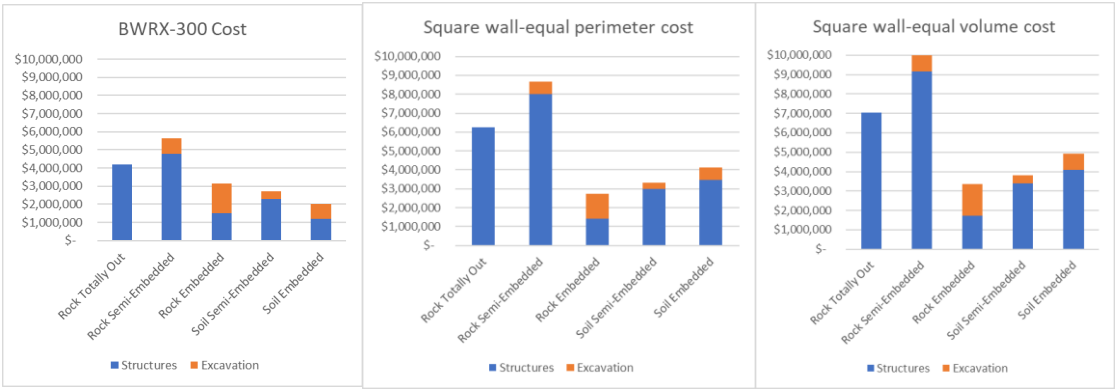


Figure 70. Cost comparison of external wall in alternative BWRX-300 building design

Table 12. Cost breakdown of external wall in alternative BWRX-300 building design

| Prismatic wall-equal perimeter | | Concrete (m³) | Steel (m³) | Excavation (m³) | Cost Concrete ($) | Cost steel ($) | Cost steel + concrete ($) | Cost excavation ($) | Steel + concrete + excavation ($) |
|---|---|---|---|---|---|---|---|---|---|
| Rock | Totally Out | 1587 | 145 | 0 | 1,030,432 | 5,214,437 | 6,244,868 | 0 | 6,244,868 |
| | Semi-Embedded | 1955 | 187 | 3720.9375 | 1,269,373 | 6,724,825 | 7,994,198 | 654,885 | 8,649,083 |
| | Embedded | 794 | 25 | 7441.875 | 515,541 | 899,041 | 1,414,581 | 1,309,770 | 2,724,351 |
| | dif. (SE-E) | | | | | | 6,579,616 | (654,885) | 5,924,731 |
| | Savings (SE-E)/SE% | | | | | | 82% | -100% | 69% |
| Soil | Semi-Embedded | 942 | 66 | 3720.9375 | 611,636 | 2,373,468 | 2,985,104 | 327,443 | 3,312,546 |
| | Embedded | 1505 | 69 | 7441.875 | 977,190 | 2,481,353 | 3,458,542 | 654,885 | 4,113,427 |
| | dif. (SE-E) | | | | | | (473,438) | (327,443) | (800,881) |
| | Savings (SE-E)/SE% | | | | | | -16% | -100% | -24% |
| Prismatic wall-equal volume | | Concrete (m³) | Steel (m³) | Excavation (m³) | Cost Concrete ($) | Cost steel ($) | Cost steel + concrete ($) | Cost excavation ($) | Steel + concrete + excavation ($) |
| Rock | Totally Out | 1788 | 163 | 0 | 1,160,940 | 5,861,746 | 7,022,686 | 0 | 7,022,686 |
| | Semi-Embedded | 2196 | 215 | 4715.2935 | 1,425,853 | 7,731,751 | 9,157,604 | 829,892 | 9,987,495 |
| | Embedded | 926 | 31 | 9430.587 | 601,248 | 1,114,811 | 1,716,058 | 1,659,783 | 3,375,841 |
| | dif. (SE-E) | | | | | | 7,441,545 | (829,892) | 6,611,654 |
| | Savings (SE-E)/SE% | | | | | | 81% | -100% | 66% |
| Soil | Semi-Embedded | 1200 | 73 | 4715.2935 | 779,155 | 2,625,199 | 3,404,354 | 414,946 | 3,819,299 |
| | Embedded | 1979 | 78 | 9430.587 | 1,284,956 | 2,805,007 | 4,089,963 | 829,892 | 4,919,855 |
| | dif. (SE-E) | | | | | | (685,609) | (414,946) | (1,100,555) |
| | Savings (SE-E)/SE% | | | | | | -20% | -100% | -29% |
| Cylindrical wall | | Concrete (m³) | Steel (m³) | Excavation (m³) | Cost Concrete ($) | Cost steel ($) | Cost steel + concrete ($) | Cost excavation ($) | Steel + concrete + excavation ($) |
| Rock | Totally out | 1353 | 92 | 4712.4 | 878,497 | 3,308,470 | 4,186,967 | 0 | 4,186,967 |
| | Semi-Embedded | 1400 | 108 | 4712.4 | 909,014 | 3,883,856 | 4,792,870 | 829,382 | 5,622,252 |
| | Embedded | 821 | 27 | 9424.8 | 533,072 | 970,964 | 1,504,036 | 1,658,765 | 3,162,800 |
| | dif. (SE-E) | | | | | | 3,288,834 | (829,382) | 2,459,452 |
| | Savings (SE-E)/SE% | | | | | | 69% | -100% | 44% |
| Soil | Semi-Embedded | 959 | 46.6 | 4712.4 | 622,674 | 1,675,812 | 2,298,486 | 414,691 | 2,713,178 |
| | Embedded | 1118 | 12.7 | 9424.8 | 725,912 | 456,713 | 1,182,625 | 829,382 | 2,012,007 |
| | dif. (SE-E) | | | | | | 1,115,861 | (414,691) | 701,170 |
| | Savings (SE-E)/SE% | | | | | | 49% | -100% | 26% |

Based on the results from Figure 70 it is possible to estimate whether embedment is a cost effective solution for the entire reactor building. There are two possible scenarios. In the first scenario, floors, basemats and tops depend mainly on vertical loads. They are thus similar for common site geologies, i.e., rock or soil. These loads are from vertical earthquake and gravity acceleration. They are independent of the degree of embedment. In the second scenario, horizontal loads have an influence on the cost of floors, basemats and tops. In this case an advantage in external wall cost from embedment in Figure 70 would also imply a cost reduction in civil structures overall. Thus, Figure 70 provides some indicative information on the effect of embedment on the overall cost of the reactor building at different sites.

The cost of the non-embedded case (Rock Totally Out case in Figure 70) is in every case lower than that of the semi-embedded case, stemming from the necessity in the latter to reinforce the load bearing walls. However, the basemat would be cheaper in the Rock SE case, since the soil around the bottom half of the building prevents it from tilting, so the cost of foundations for dealing with lateral loads would be lower.

The results in Figure 70 are not suitable, however, for comparing directly soil to rock sites, since basemats in soil sites would need to be thicker. Therefore, inclusion of the basemat in the analysis would favor the rock cases with respect to the soil cases.

All in all, there is infinity of ways to design the buildings, this is just one of them. As they are forced to have the same layouts, optimal solutions are not found, e.g., in prismatic embedded in soil cases we would use braces or ribs for stiffening the walls. This analysis stems from a code interpretation that is conservative. Another interpretation could make the comparison different.

It is worth to note that the lower bound for excavation cost used here, i.e., rock type, quality and excavation methods were set so the cost of excavation is minimum. An upper bound for granite would result in a factor 7x. In such case the cost of the cylindrical wall would be higher in the embedded configuration than in the semi-embedded or non-embedded one. Table 13 lists the variables that would favor or hinder the economic case for embedding in each of the cases analyzed.

Table 13. Economic case for embedment

| Hinder BG case | Favor BG case |
|---|---|
| Poor rock quality | High horizontal seismic loads |
| Unsuitable type of rock: not granite | Relatively low vertical seismic loads compared to horizontal loads |
| Liquefaction issues | |
| Building (to embed) size | |
| High water tables | |
| Non-competent soil: S-wave vel < 300 m/s | |

# 17. DISCUSSION OF THE RESULTS, FUTURE WORK AND FINAL REMARKS

Earth pressures were assumed to be conservatively high to evaluate the robustness of the economic case for the BG approach vs. the AG approach. Designers could set the earth pressures less conservatively for certain sites and construction methods. This would make the BG case even more appealing.

There are efforts being made to align ACI 359, ACI 349 and ACI 318[53]. Even though ACI 359 instead of ACI 349 or ACI 318 was used, and this might cause some deviations in cost with respect to using another code, the design was always consistent with the same code. Hence, given the robustness of the strongest trends detected in cost, i.e., from embedded to semiembedded in rock, it is deemed unlikely that they be changed by the use of another code. Additionally, a designer might deem it appropriate to use ACI 359, since the structural analysis considers that some parts have containment function, e.g., the basemat.

## 17.1 FUTURE WORK

One could calculate what cost of excavation in rock makes embedment not worthy based on the given results. Likewise, this study could serve as a starting point for assessing the effect of variations in labor or material cost of steel and concrete. On the other hand, similar analyses could be employed to evaluate different construction techniques, such as steel plate composites or high-performance concretes.

## 17.2 FINAL REMARKS

Several different layouts, at different sites and under different assumption were assessed. In most of them there is a clear potential on cost reduction through embedment. This potential would be clearer if one evaluated also the structural changes that embedding would yield in the floors and components inside the buildings. Yet, one needs to be cautious, as this study proves building cost to be also site and layout dependent.

Embedment could provide opportunities for simplifying the design of a plant, i.e., removal of some redundancies, and decrease in security measures as the area to protect is smaller. The cost savings induced by those would add to the structural argument for embedment.

# References


[1] J. Buongiorno, M. Corrandi, and J. Parsons, “The Future of Nuclear Energy in a Carbon-Constrained World,” *MIT Energy Initiative*. [Online]. Available: http://energy.mit.edu/research/future-nuclear-energy-carbon-constrained-world/. [Accessed: 16-Nov-2018].

[2] P. Duffaut and P. Vaskou, “Geological and Geographical Criteria for Underground Siting of Nuclear Reactors,” p. 10, 2014.

[3] W. Kröger, J. Altes, and K. Schwarzer, “Underground siting of nuclear power plants with emphasis on the ‘cut-and-cover’ technique,” *Nuclear Engineering and Design*, vol. 38, no. 2, pp. 207–227, Aug. 1976, doi: 10.1016/0029-5493(76)90097-2.

[4] John Ball, “BWR/X VSBWR,” Mar-2018.

[5] “Herrenknech online catalog https://www.herrenknecht.com/en/products/productdetail/vertical-shaft-sinking-machine-vsm/,” 2018.

[6] “Survey of Design and Regulatory Requirements for New Small Reactors,” *Final Report*, p. 144, 2014.

[7] Westinghouse, “AP1000 Design Control Document Rev. 19,” 2011.

[8] S. Pinto, “A survey of the underground siting of nuclear power plants,” Eidgenoessisches Inst. fuer Reaktorforschung, EIR--382, 1979.

[9] P. Duffaut, “Safe Nuclear Power Plants Shall Be Built Underground,” *Underground Space*, p. 6, 2007.

[10] H. Zhang, “China’s Stockpile of Military Plutonium: a New Estimate,” p. 10.

[11] W. M. Ned Elkins, “Underground Nuclear Parks and the Continental SuperGrid,” presented at the SuperGrid 2, Los Alamos National Laboratory, 2004.

[12] IAEA, “Cleanup and Decommissioning of A Nuclear Reactor After A Severe Accident,” 1992.

[13] X. Wang, Q. Zhou, K. Zhu, L. Shi, X. Li, and H. Wang, “Analysis of Seismic Soil-Structure Interaction for a Nuclear Power Plant (HTR-10),” *Science and Technology of Nuclear Installations*, 2017. [Online]. Available: https://www.hindawi.com/journals/stni/2017/2358403/. [Accessed: 19-Mar-2019].

[14] L. Tuñón-Sanjur, R. S. Orr, S. Tinic, and D. P. Ruiz, “Finite element modeling of the AP1000 nuclear island for seismic analyses at generic soil and rock sites,” *Nuclear Engineering and Design*, vol. 237, no. 12, pp. 1474–1485, Jul. 2007, doi: 10.1016/j.nucengdes.2006.10.006.

[15] F. F. Tajirian, “(7) (PDF) SEISMIC ANALYSIS OF THE MODULAR HIGH TEMPERATURE GAS COOLED REACTOR,” *ResearchGate*, Nov-1989. [Online]. Available: https://www.researchgate.net/publication/315496607_SEISMIC_ANALYSIS_OF_THE_MODULAR_HIGH_TEMPERATURE_GAS_COOLED_REACTOR. [Accessed: 16-Jul-2019].

[16] E. W. Klamerus, *Containment Performance of Prototypical Reactor Containments Subjected to Severe Accident Conditions*. DIANE Publishing, 2000.

[17] M. Amin, A. Curt Eberhardt, and B. A. Erler, “Design considerations for concrete containments under severe accident loads,” *Nuclear Engineering and Design*, vol. 145, no. 3, pp. 331–338, Dec. 1993, doi: 10.1016/0029-5493(93)90243-3.

[18] J. J. Ucciferro, “Effects of permissible shear stress on the design and construction of reinforced concrete containments,” *Nuclear Engineering and Design*, vol. 69, no. 2, pp. 195–203, May 1982, doi: 10.1016/0029-5493(82)90231-X.

[19] “ASME - STANDARDS - BPVC Section III-Rules for Construction of Nuclear Facility Components-Division 2-Code for Concrete Containments,” 2013. [Online]. Available: https://www.asme.org/products/codes-standards/bpvciii2-2015-bpvc-section-iiirules-construction. [Accessed: 05-Nov-2018].
[20] H. Ashar, B. Scott, J. F. Artuso, and J. D. Stevenson, “CODE FOR CONCRETE REACTOR VESSELS AND CONTAINMENTS,” p. 26, 2008.
[21] Y.-S. Choun and J. Park, “Evaluation of seismic shear capacity of prestressed concrete containment vessels with fiber reinforcement,” *Nuclear Engineering and Technology*, vol. 47, no. 6, pp. 756–765, Oct. 2015, doi: 10.1016/j.net.2015.06.006.
[22] O. Buyukozturk, J. J. Connor, and P. Leombruni, “Research on modeling shear transfer in reinforced concrete nuclear structures,” *Nuclear Engineering and Design*, vol. 59, no. 1, pp. 67–83, Jul. 1980, doi: 10.1016/0029-5493(80)90283-6.
[23] J. A. Smith, *Vessels with Prestressing Loss*. 2001.
[24] *ASCE 4-98, Seismic analysis of safety-related nuclear structures and commentary*. .
[25] Patrick A. Champlin, “TECHNO-ECONOMIC EVALUATION OF CROSS-CUTTING TECHNOLOGIES FOR COST REDUCTION IN NUCLEAR POWER PLANTS,” Jun. 2018.
[26] I. Němec, Š. Sychrová, I. Ševčík, J. Kabeláč, and L. Weis, “Study of a Nuclear Power Plant Containment Damage Caused by Impact of a Plane,” p. 6, 2011.
[27] ERIN Engineering & Research Inc., “NEI 07-13 Revision 8P, ‘Methodology for Performing Aircraft Impact Assessments for New Plant Designs.,’” 2011.
[28] J. Paul Stewart, “(15) (PDF) Nonlinear Site Response and Seismic Compression at Vertical Array Strongly Shaken by 2007 Niigata-ken Chuetsu-oki Earthquake,” *ResearchGate*, 2012. [Online]. Available: https://www.researchgate.net/publication/266340671_Nonlinear_Site_Response_and_Seismic_Compression_at_Vertical_Array_Strongly_Shaken_by_2007_Niigata-ken_Chuetsu-oki_Earthquake. [Accessed: 08-Nov-2018].
[29] K. Nagasawa and T. Narabayashi, “Seismic response and its analysis for components of Kashiwazaki-Kariwa Nuclear Power Plants in 2007 Niigata-ken Chuetsu-Oki Earthquake,” *Mechanical Engineering Journal*, vol. 4, no. 1, pp. 16-00482-16–00482, 2017, doi: 10.1299/mej.16-00482.
[30] “REGULATORY GUIDE 1.76. DESIGN-BASIS TORNADO AND TORNADO MISSILES FOR NUCLEAR POWER PLANTS, rev. 1,” 2007.
[31] “ANSYS 19.2 User’s guide.”
[32] Arthur H. Nilson, “Design of Concrete Structures 14th edition,” 2010. [Online]. Available: https://www.textbooks.com/Design-of-Concrete-Structures-14th-Edition/9780073293493/Arthur-H-Nilson.php. [Accessed: 16-Jul-2019].
[33] Saanio Timo, “Interview to Mr TIMO (Vice President at A-Insinöörit) on Cost of excavation in Finland,” Jul-2019.
[34] P. L. McCarthy, R. Livingstone, “Shaft or Decline? An Economic Comparison,” 1993.
[35] Stephen C. Plotner, et al., *Building Construction Costs with RSMeans Data,*. 2017.
[36] T. W. Lambe, T. W. Lambe, R. V. Whitman, and Whitma, *Soil Mechanics*. John Wiley & Sons, 1969.
[37] A. S. Vesic, “DESIGN OF PILE FOUNDATIONS,” *NCHRP Synthesis of Highway Practice*, no. 42, 1977.
[38] National Academies of Sciences, Engineering, and Medicine, *Rock-Socketed Shafts for Highway Structure Foundations*. Washington, DC, 2006.
[39] OPTUMG2, “OptumG2 users manual. Editor: K Krabbenhoft.” 2018.
[40] E. Hoek, “Practical Rock Engineering,” 2007. [Online]. Available: https://www.rocscience.com/learning/hoeks-corner/course-notes-books. [Accessed: 23-Mar-2019].

[41] E. Hoek and M. S. Diederichs, “Empirical estimation of rock mass modulus,” *International Journal of Rock Mechanics and Mining Sciences*, vol. 43, no. 2, pp. 203–215, Feb. 2006, doi: 10.1016/j.ijrmms.2005.06.005.
[42] “https://www.nuscalepower.com/.” .
[43] “REGULATORY GUIDE 1.92. COMBINING MODAL RESPONSES AND SPATIAL COMPONENTS IN SEISMIC RESPONSE ANALYSIS, rev 3,” Oct. 2012.
[44] *Eurocode 8: Design of structures for earthquake resistance – Part 4: Silos, tanks and pipelines. EN 1998-4:2006*. .
[45] James R. Roberts, Eduardo R. Basurto, and Pei-Ying Chen, *SLOSH DESIGN HANDBOOK I, NATIONAL AERONAUTICS AND SPACE ADMINISTRATION*. Washington, D. C, 1966.
[46] Ingo Brachmann, “The Riera Curve,” 2006.
[47] D. C. Ma, J. Gvildys, and Y. M. Chang, “Effects of Core Barrel on Vessel Seismic Loading,” *Argonne National Laboratory*.
[48] D. C. Ma, “Seismic Interaction Between Primary Tank and Core Barrel,” *Argonne National Laboratory*.
[49] ACI, “349-13 Code Requirements for Nuclear Safety-Related Concrete Structures and Commentary,” 2014. [Online]. Available: https://www.concrete.org/store/productdetail.aspx?ItemID=34913&Language=English&Units=US_Units. [Accessed: 16-Apr-2019].
[50] J. D. Riera, “On the stress analysis of structures subjected to aircraft impact forces,” *Nuclear Engineering and Design*, vol. 8, no. 4, pp. 415–426, Nov. 1968, doi: 10.1016/0029-5493(68)90039-3.
[51] B. B. Broms, “Lateral Resistance of Piles in Cohesive Soils,” *Journal of the Soil Mechanics and Foundations Division*, vol. 90, no. 2, pp. 27–64, 1964.
[52] GE-Hitachi, “ESBWR Design Control Document Tier, Revision 10,” 2014.
[53] National Institute of Standards and Technology, and Materials and Constructions Research Division, “Conccrete codes and standards for NPPs: recommendaitons for future developments,” Jun. 2011.

# APPENDIX A. JUSTIFICATION OF PILE FOUNDATIONS

The figure below shows the vertical displacements in an axisymmetric model of the site with the semiembedded NuScale reactor building atop in Normal operation conditions. Its purpose is to indicate whether the use of piles foundations is necessary. Since 60 mm settlement due to dead load is it too much, one would need pile foundations.